ABSOLUTE EXPERIMENTAL CROSS SECTIONS FOR THE IONIZATION OF SINGLY CHARGED BARIUM IONS BY ELECTRON IMPACT

A THESIS

Presented to

The Faculty of the Graduate Division

by

Robert King Feeney

In Partial Fulfillment

of the Requirements for the Degree

Doctor of Philosophy

in the School of Electrical Engineering

Georgia Institute of Technology

December, 1970

ABSOLUTE EXPERIMENTAL CROSS SECTIONS FOR THE

IONIZATION OF SINGLY CHARGED BARIUM IONS BY ELECTRON IMPACT

Approved:

Chairman

Date Approved by Chairman: 12/15/70

In presenting the dissertation as a partial fulfillment of the requirements for an advanced degree from the Georgia Institute of Technology, I agree that the Library of the Institute shall make it available for inspection and circulation in accordance with its regulations governing materials of this type. I agree that permission to copy from, or to publish from, this dissertation may be granted by the professor under whose direction it was written, or, in his absence, by the Dean of the Graduate Division when such copying or publication is solely for scholarly purposes and does not involve potential financial gain. It is understood that any copying from, or publication of, this dissertation which involves potential financial gain will not be allowed without written permission.

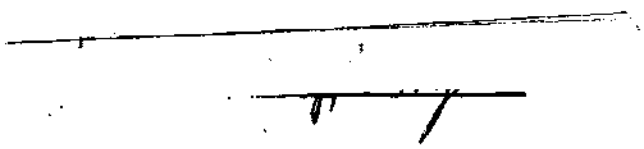

7/25/68

ACKNOWLEDGMENTS

It is with great pleasure that I extend my appreciation to my thesis advisor, Dr. J. W. Hooper, for his guidance and encouragement, not only during the prosecution of this research, but throughout the several years of our association. I also wish to thank Drs. E. W. McDaniel and D. C. Ray for their helpful comments while serving as members of the Reading Committee. Special thanks are due Dr. M. T. Elford of the Australian National University for his early work with the experimental apparatus.

This research was accomplished largely using the apparatus and techniques developed by Dr. W. C. Lineberger, and to him, I gratefully acknowledge my debt.

I would also like to express my gratitude to Dr. F. M. Bacon for his development of the prototype ion source, and to Dr. M. O. Pace for his helpful discussion and assistance during the developmental phases of the experiment.

I wish to thank the Controlled Thermonuclear Research Program, Division of Research, U. S. Atomic Energy Commission and the School of Electrical Engineering for their generous support of this research.

TABLE OF CONTENTS

Page

ACKNOWLEDGMENTS ii

LIST OF TABLES v

LIST OF ILLUSTRATIONS vi

SUMMARY vii

CHAPTER

I. INTRODUCTION 1

Phenomenological Description of the Ionization Process
Experimental Evidence of Structure in the Electron Impact Ionization Cross Sections of the Alkali Metals and Alkaline Earth Ions and Possible Theoretical Explanations for such Structure
Review of Applicable Theory
The Present Research

II. EXPERIMENTAL TECHNIQUE 29

Expression for the Cross Section in Terms of Experimental Parameters
Difficulties Associated with Charged Particle-Charged Particle Crossed Beam Experiments
Summary of the Requirements for a Valid Crossed Beam Charged Particle-Charged Particle Ionization Experiment

III. EXPERIMENTAL APPARATUS 47

Vacuum System
Ion Beam Source and Optics
Electron Source
Interaction Region
Electrostatic Analyzer
Ion Collection and Measurement System
Electron Collection and Measurement System
Pulsed Mode Operation

IV. EXPERIMENTAL PROCEDURES AND RESULTS 79

TABLE OF CONTENTS (Continued)

CHAPTER Page

Currents to the Ba^{2+} Detector
Measurement Procedures
Consistency Checks
Experimental Results
Discussion of Errors

V. COMPARISON WITH EXPERIMENT AND THEORY 107

Comparison with Previous Experimental Results
Comparison with Theory

VI. CONCLUSIONS 121

APPENDICES 124

I. DERIVATION OF σ_{12} IN TERMS OF EXPERIMENTAL PARAMETERS . 125

II. TYPICAL EXPERIMENTAL PARAMETERS AND DATA 130

BIBLIOGRAPHY 134

VITA 137

LIST OF TABLES

Table		Page
1.	Summary of Experimental and Theoretical Studies of Electron Impact Ionization of Heavy Alkali Metals	12
2.	Dependence of σ_{12} Upon Ion Energy at Selected Incident Electron Energies	
3.	Absolute Experimental Cross Sections for the Single Ionization of Ba^+ Ions by Electron Impact	95
4.	Comparison of Measurements Made by Pulsed and Continuous Methods at Selected Incident Electron Energies	101
5.	Typical Operating Parameters.	131
6.	Typical Form Factor Data Sheet	132
7.	Typical Cross Section Measurement Data	133

LIST OF ILLUSTRATIONS

Figure		Page
1.	Use of a Movable Slit Scanner to Determine Beam Profiles	32
2.	Schematic Diagram of the Experimental Apparatus	48
3.	Plan View of the Experimental Apparatus	49
4.	Overall View of the Experimental Apparatus	51
5.	Sketch of the Ion Source	54
6.	Typical Electron Beam Energy Distribution	63
7.	Interaction Region Seen from the Location of the Electron Beam Faraday Cup	65
8.	Typical Rate-of-Charge and Resistor Current Measurements with a Vibrating Reed Electrometer	72
9.	Dependence of the Measured Cross Section on Electron Current	90
10.	Dependence of the Measured Cross Section on Ion Current	92
11.	Dependence of the Measured Cross Section on Form Factor F	93
12.	Absolute Experimental Cross Sections for the Single Ionization of Ba^+ Ions by Electron Impact	98
13.	Low Energy Regime of Absolute Experimental Cross Sections	99
14.	Comparison with Previous Experimental Results	112
15.	Comparison with Classically Scaled Cs	116
16.	Comparison with Cross Sections Calculated Using the Classical Method Due to Gryzinski	119

SUMMARY

The absolute cross sections for the single ionization of Ba^+ ions by electron impact have been measured as a function of incident electron energy over the electron energy range from below threshold (10.001 eV) to approximately 1000 eV. It is found that the cross section increases from 1.94×10^{-16} cm^2 to 3.76×10^{-16} cm^2 between 15.5 and 18 eV actual incident electron energy. This rapid rise is interpreted as the onset of autoionization. Some evidence of structure occurring near the peak of the cross section curve such as found in the isoelectronic system of Cs is observed, but the relative magnitude of the apparent structure is of the same order as the 90 percent random error confidence limits and thus cannot conclusively be regarded as being present. The maximum total error in the measurements is estimated to have its greatest value of less than ±20 percent at 15.5 eV while ±12 percent is typical of other energies. Of the total error, ±7.0 percent is deemed to be systematic. At incident electron energies below threshold, the cross section is found to be zero to within one percent of the cross section at 48 eV. The present Ba^+ ionization data are compared with existing experimental and theoretical results.

These measurements were performed in an all metal ultrahigh vacuum crossed beam facility in which the nominal operating pressure was less than 5×10^{-9} Torr. In the experimental apparatus, approximately monoenergetic beams of Ba^+ ions and electrons are caused to intersect in a well defined collision volume. The charge state

composition of the emerging barium beam is determined by an inclined parallel plate electrostatic analyzer. The Ba^{2+} beam current is measured by means of a vibrating reed electrometer operating in the rate-of-charge mode. The ion source is a water cooled surface ionization type ion source while the electron source is a modified 6L6GC beam power tube. The two beam current density distributions are determined by means of a movable slit scanner driven from outside of the experimental chamber by a micrometer. The various particle currents, particle energies and beam current density distributions represent the experimental information from which the desired cross sections are determined.

Continuous beam techniques were used for the majority of the measurements, but modulated beam methods were employed as a check. Measurements made by the two techniques agreed to well within the allowable experimental error and showed no systematic variations. Numerous consistency checks were performed to evaluate possible sources of experimental error such as pressure modulation of the background gas, focusing of the ion beam by the electron beam, and errors in the beam profile determinations.

CHAPTER I

INTRODUCTION

This research presents a detailed experimental study of the single ionization of Ba^+ ions by electron impact over the range of incident electron energies from below threshold (10.001 eV) to approximately 1000 eV. The primary purpose of this study was to reveal possible structure in the cross section similar to that found in the isoelectronic system of Cs. Such structure is expected to appear between the threshold energy for the process and about ten times that value. The spacings of the experimental electron energies were chosen so as to obtain a maximum probability of detecting such structure consistent with the uncertainties in the incident electron energy.

In order to provide a basis for discussing the structure found in the electron impact ionization cross sections of the alkali metals and the alkaline earth ions, a phenomenological description of the several ionization processes is given. This is followed by a summary and evaluation of the experimental and theoretical investigations of ionization by electron impact in the alkali metals and their isoelectronic equivalents, the alkaline earth ions. A short synopsis of the theory applicable to the calculation of the ionization cross sections of ions by electron impact is then given. This discussion of necessity includes some analytical approaches to excitation processes, since it appears that autoionization, a decay process reached via excitation,

contributes to the total ionization cross section.

Finally, a brief discussion of the present research is presented.

Phenomenological Description of the Ionization Process

For the purpose of this discussion it is convenient to separate the mechanisms responsible for the production of positive ions into two categories. The first of these will be termed "ordinary" or "direct" ionization and is the conventional process whereby a valence electron or a loosely bound inner shell electron is removed in the ionizing encounter. The second category includes ionization events that are the result of an excitation process leading to a radiationless transition and the ejection of an electron.

Ordinary Ionization

Consider an encounter between a projectile electron and a target atom or ion. Energetically, the valence electron(s) is (are) most accessible to the perturbing field of the incident electron. It therefore follows that usually the greatest contribution to the total ionization cross section will come from the removal of the valence electron(s). It is also possible for the incident electron to remove an inner shell electron. This will leave the ion in an excited state. Such an excited ion may decay by spontaneous radiation and emit a photon of the appropriate energy, or if the energy of the excited state exceeds that of the next highest ionization potential, an Auger transition may occur further ionizing the ion. The Auger process is an example of a radiationless transition, a subject that is treated below.

Ionization via Radiationless Transitions

The Auger effect and autoionization are two names that are

associated with a class of radiationless transitions.[1] Auger processes usually refer to interactions in deep lying electronic shells accessible only to high energy particles or to x-rays, while the term autoionization* is concerned with the effects occurring in the outer shells that are observable in ultraviolet absorption spectra.[2] In the context of general use, however, there is a further difference between the two processes. One usually considers an Auger process to begin with the removal of an electron as, for example, in x-ray photoionization. An autoionizing event is generally associated with the excitation of one or more electrons. Both phenomena are, however, basically the same and may occur whenever the atomic configuration is changed so that one or more electrons occupy an energy state that lies above an ionization limit of the system. If the appropriate configuration interaction exists, i.e., the required selection rules are satisfied, the excited system may decay without the emission of radiation and the excess energy will be carried off by an ejected electron. Of course, it is not necessary that the final state reached by the radiationless transition be the ground state of the particular ion; it may be and often is an excited state of the residual ion.

Although the discovery of the Auger Effect antedates that of autoionization, the latter is of more importance in the present research and will be discussed first in some detail. A few of the interesting and applicable aspects of the Auger processes are then covered.

Autoionization. Consider the physical result of exciting an

---

*Autoionization is also called pre-ionization. The analogous phenomenon in molecules is called pre-dissociation.

inner shell electron, or possibly exciting two or more outer shell electrons simultaneously, by means of some process. The atomic system will now have assumed a new configuration and an entire new series of energy levels will exist. The excited electronic states in this new system may well have energies greater than that required to ionize the original system. Each of these new excited states can be properly characterized by its appropriate wave function. The existence of these new energy levels is experimentally verified by the use of absorption spectroscopy.

Lying above the ionization limit of the original atomic system is a continuum of energies each of which has associated with it a continuum of orbital angular momenta. Each of these continuum states is completely described by its appropriate wave function. If the matrix element connecting one of the highly excited states with an adjacent continuum state is non-zero, then each state assumes some of the characteristics of the other. The result is that after a very short time the electron in the highly excited state assumes the unstable orbit characteristic of continuum states; that is, it is unbound. This property of almost spontaneous ionization as the result of excitation to a highly excited state is known as autoionization. It is important to note that this is a lateral transition and emits no radiation. The atomic system undergoes a transition to an ionic ground state or to an excited state with no simultaneous emission of radiation, all of the excess energy being taken up by the electron as kinetic energy.

The ionized electron carries with it angular momentum about the center of mass and spin as well as energy. The residual ion is also

characterized by its proper set of quantum numbers. It is therefore logical that a set of selection rules must govern the process of autoionization since just as in ordinary de-excitation the initial and final states are designated by a set of quantum numbers. As usually formulated, the final state includes the ionized electron and the residual ion. The selection rules are therefore specified in terms of this formulation.

The selection rules for autoionization are derived by means of perturbation theory just as are the selection rules for radiative decay processes. The selection rules are therefore characteristic of the perturbation operator connecting the discrete and continuum states. In general, autoionization as referred to in the literature is the result of the electrostatic interaction between electrons. This interaction is the strongest and results in typical autoionizing state lifetimes of 10^{-13} to 10^{-15} seconds. As a consequence of the uncertainty principle, such autoionizing states, when observed in absorption spectroscopy, are characterized by very broad lines. If Russel-Saunders or LS coupling is assumed, the selection rules for autoionization via a Coulomb interaction are simply stated. The rules are,[3]

$$
\begin{aligned}
&(1)\ \Delta S = 0 \quad (S \text{ is the total spin angular momentum.})\\
&(2)\ \Delta L = 0 \quad (L \text{ is the total orbital angular momentum.})\\
&(3)\ \Delta J = 0 \quad (J \text{ is the total angular momentum, } J = L + S.)\\
&(4)\ \text{Parity } \pi \text{ is conserved, or even terms do not combine with odd terms.}
\end{aligned}
\tag{1}
$$

In the above formulation of the selection rules, the initial excited state is specified by L, S, J and π while the continuum state is

described by the configuration of the residual ion, the energy of the ejected electron, the angular momentum of the ejected electron and the overall configuration of the continuum state. This is best illustrated by an example. Let a Cs atom be excited to the possible autoionizing configuration, $(5p^5 6s5d)^2P^o_{3/2}$. Note that the last few electronic shells, where changes have occurred, are given followed by the term designation. (Often one finds that there is not enough information known to specify the term designation and only the electronic configuration is given.) The above state can decay via autoionization to the ground state of Cs^+. The reaction is given by

$$(5p^5 6s5d)^2P^o_{3/2} Cs \longrightarrow [(5p^6)^1S_0\ Cs^+ + \varepsilon\ p]^2P^o_{3/2} \ . \qquad (2)$$

The ejected electron has energy ε, one unit of spin angular momentum and one unit of orbital angular momentum. Observe that the selection rules are satisfied.

If the matrix element of the Coulomb interaction connecting the given discrete state to the continuum vanishes, then that state is metastable against autoionization. Such a state will either decay by a radiative transition or will autoionize due to a weaker magnetic interaction. It is very possible for a state to be metastable against both autoionization and radiative transitions. In general, the relative probability that a given state will autoionize as opposed to decaying by spontaneous radiation is given by

$$P = \frac{A_a}{A_s + A_a} \qquad (3)$$

where A_a and A_s are, respectively, the transition rates for autoionization and for spontaneous emission from the given state. If the state is not metastable against autoionization, then autoionization is almost certain to occur as a consequence of its much larger transition rate. Typical transition rates for autoionization are 10^{13} to 10^{15} per second. This compares with about 10^{8} to 10^{10} for the electric dipole radiative transition, which is the fastest type of radiative transition.

The above discussion briefly summarizes the process of autoionization as it applies to the present research. Autoionization is of great importance in other processes such as photoabsorption and elastic and inelastic scattering.[4] The process that is the inverse of autoionization, dielectronic recombination, is also of significance in astrophysics.[4]

Auger Effect. The Auger effect is initiated by producing a vacancy in one of the tightly bound filled shells of an atom. The energy required to remove such an electron is usually far more than the ionization potential of an electron in any of the remaining filled states above that shell containing the vacancy. The ion thus produced is therefore in a very highly excited state. The same situation then exists as in autoionization, and there is a possibility of a radiationless transition to the continuum. If such an event occurs, the inner vacancy is filled without the emission of radiation by an electron from a higher shell, and an electron, usually in the same higher shell, is ejected with great kinetic energy. The residual hole produced by the ejection of the Auger electron again leaves the atomic structure in a

highly excited state, and the process may cascade. Such cascading may lead to the eventual production of a highly ionized ion. For example, in vacancy cascading induced in Kr by K-shell photoionization, the mean charge of the residual ion is found to be +6 and ions having a charge of +12 are experimentally observed.[5]

Just as in the case of autoionization, the Auger process does not always occur since there is also a probability that a given state may decay via a radiative transition. The relative probability of Auger and radiative type transitions is called the Auger yield[6] and is defined as

$$a_J = \frac{N_A}{N_R + N_A} \tag{4}$$

where N_R and N_A are the numbers of radiative and Auger transitions, respectively, for an initial vacancy in the J^{th} shell. Note the similarity between Equations (3) and (4).

The Auger effect as distinguished from autoionization is relatively unimportant in the present research. The deeply lying atomic shells cannot be reached with the low energy (1 keV maximum) electrons used in the present experiment. If cascading effects initiated by a vacancy in some energetically accessible shell were to occur, they could not be observed because the charge state analyzer in the experiment allows only doubly charged ions to be detected. If the Auger process were very strong, however, there might be the possibility of a "resonance" effect at the energy corresponding to the Auger transition.

The next section presents a summary of experimental and

theoretical results relating to the existence of structure in the electron impact ionization cross sections of the heavy alkali metals and the alkaline earth ions. Before reviewing this body of data, it is helpful to restate the processes most responsible for ionization by electron impact in atomic systems.

If only single ionization events are considered, the mechanisms responsible for ionization by electron impact are listed below.

(1) Direct ionization of a valence electron.

(2) Direct ionization of an electron from one of the most loosely bound inner shells.

(3) Autoionization.

Each of the above processes has its individual cross section and characteristic threshold energy. The total ionization cross section will thus exhibit a variation which depends upon a summation of the cross sections for the several events. It is apparent, that if two or more processes can occur, each having different magnitudes and threshold energies, then this may be reflected as an unusual variation in the total cross section.

Experimental Evidence of Structure in the Electron Impact Ionization Cross Sections of the Alkali Metals and Alkaline Earth Ions and Possible Theoretical Explanations for such Structure

The electron impact ionization cross sections for alkali metals heavier than Na ($Z = 11$) exhibit well defined double maxima. This structure is quite prominent and has been observed by a number of investigators.[7-13] With the advent of modern crossed beam techniques it is possible to study the electron impact ionization cross sections of the

alkaline earth ions, which are isoelectronic to the alkali metals. These measurements will allow comparisons to be made between the behavior of the electron impact ionization cross sections for two members of each alkali metal isoelectronic sequence. Such comparisons should lead to a better theoretical understanding of the ionization processes and how they affect the shape of the cross section curve. The present research, which is directed toward this end, is primarily designed to examine the electron impact cross sections of Ba^+ for structure similar to that found in the cross sections of Cs.

Some experimental evidence of the existence of structure in electron impact cross sections and the theoretical explanations offered for such structure will now be summarized. The alkali metals will be considered first followed by the alkaline earth ions.

Ionization of the Alkali Metals

A number of experimental and theoretical studies of the heavier alkalis are summarized in Table 1. There appear to be no quantum mechanical calculations for the electron impact ionization of any of these heavy alkalis.[23] All of the theoretical calculations presented rely upon either classical or empirical approaches.

An analysis of the work summarized in Table 1, allows one to make, with a reasonable level of confidence, the following generalizations concerning the occurrence of structure in the electron impact ionization cross sections of the alkali metals.

(1) Several processes must contribute to the total cross section or there would be no structure.

(2) Valence electron ionization, inner shell ionization and

Table 1

Summary of Experimental and Theoretical Studies of Electron Impact Ionization of Heavy Alkali Metals

Heavy Alkalis (K, Rb, Cs) Studied	Investigator(s)	Explanation(s) for Structure	Calculations or other Supporting Data
(K, Rb, Cs)	Tate and Smith[7]	None	--
(K)	Kaneko[8]	None	--
(K, Rb)	Brink[9,10]	Autoionization	Cites autoionizing levels tabulated by Moore (Ref. 17) as corresponding to the observed locations of structure.
(K, Rb, Cs)	McFarland and Kinney[11]	None	--
(Cs)	Heil and Scott[12]	Autoionization	Cites autoionizing levels observed by Beutler and Guggenheimer (Ref. 18) as corresponding to the observed location of structure. Estimates magnitude of autoionization cross section. Calculates partial ionization cross sections using the methods of Gryzinski (Ref. 19) and Drawin (Ref. 20).

Table 1. (Continued)

Summary of Experimental and Theoretical Studies of Electron Impact Ionization of Heavy Alkali Metals

Heavy Alkalis (K, Rb, Cs) Studied	Investigator(s)	Explanation(s) for Structure	Calculations or Other Supporting Data
(Cs)	Nygaard[13]	Autoionization with possible contribution from inner shell ionization.	Cites work by Feldman and Novick (Ref. 21) on metastable autoionizing states in Cs and notes that their work suggests that a doublet state also exists with the autoionizing configuration proposed by Beutler and Guggenheimer (Ref. 18) Estimates the magnitude of the autoionization cross section; the value agrees well with that estimated by Heil and Scott (Ref. 12). Also calculates the cross section including inner shells using method of Gryzinski (Ref. 19), but concludes that this does not provide a complete explanation of the observed structure.
(K, Rb, Cs)*	McFarland[14]	Inner shell ionization and autoionization	Uses Gryzinski's method (Ref. 19) to calculate contributions from closed shells to the cross section. Notes that the double peaking may be explained qualitatively in this manner. Expects autoionization effects to be small.

Table 1. (Concluded)

Summary of Experimental and Theoretical Studies of Electron Impact Ionization of Heavy Alkali Metals

Heavy Alkalis (K, Rb, Cs) Studied	Investigator(s)	Explanation(s) for Structure	Calculations or Other Supporting Data
(K, Rb, Cs)*	Garcia[15]	Inner shell ionization	Calculates the ionization cross sections using Gryzinski's method (Ref. 19) with a delta function velocity distribution.
(K, Rb)*	Prasad[16]	None	Calculates electron impact cross sections using universal curve of Prasad and Prasad (Ref. 22) and the theory of Drawin (Ref. 20). Notes that McFarland's (Ref. 14) calculated double peak is the result of assuming a particular set of ionization energies.

*These are purely theoretical papers. All of the others are experimental, usually including some theoretical discussion.

autoionization are all likely to be present.

(3) The inner shell ionization is probably responsible for the somewhat "flat" appearance of the cross sections when appropriately compared (using the reduced cross section for example) with those of elements where inner shell processes are either absent or are insignificant. At higher energies, the major contribution to the total cross section is from the closed shells.

(4) Autoionization is probably responsible for the structure in the cross sections, producing a small abrupt change in the cross section at its onset. However, until better calculations are available, the possibility that the inner shell ionization at least contributes to the observed structure cannot be ignored.

Ionization of the Alkaline Earth Ions

The above conclusions give considerable insight into the processes responsible for producing the observed structure in the alkali metal electron impact ionization cross sections. The same processes should be expected to be active in the electron impact ionization of the alkaline earth ions, however, the manifestation of these processes in the form of structure in the cross sections might be expected to be slightly different due to the reasons tabulated below.

(1) The electronic binding energies of a given alkaline earth ion are larger than those of its isoelectronic neutral due to the net positive charge on the ion. This effect becomes of less importance as one progresses downward into the closed electronic shells.

(2) The threshold laws for the ionization of ions and neutrals by electron impact are probably slightly different.[24-26]

(3) The threshold laws for the excitation of atoms and ions by electron impact are apparently significantly different. This fact is of importance because any autoionizing states present must be reached by excitation. Both theoretical[25-27] and experimental[27-29] evidence leads to the conclusion that the excitation cross sections for ions are finite at threshold energy. This is not true for neutral atoms.[25-27]

At the present time there are only a few experimental and theoretical results for the ionization of the alkaline earth ions by electron impact. Cross sections for the electron impact ionization of Mg^+ have been measured by Martin et al.[30] and those for Ba^+ by Peart and Dolder.[31] Theoretical calculations are also rather limited. Bely[32] has predicted structure due to autoionization in the sodium-like isoelectronic sequence. Moores and Nussbaumer[33] have calculated the electron impact cross sections for the ionization of Mg^+ using the Coulomb-Born approximation. (The Coulomb-Born and some other quantum mechanical approximations are discussed elsewhere in this chapter.) Bely and Van Regemorter[26] indicate that there is an as yet unpublished calculation by Bely and Schwartz of the cross sections for the ionization of Ba^+ by electron impact. The above studies will now be examined in additional detail.

Bely has developed a theory that predicts the contribution of autoionization to the structure of the sodium-like ions.[32] He constructed the cross section curve by considering the autoionizing effect due to the excitation of the internal electrons with principal quantum number $n = 2$. The excitation of the closed shell electrons was computed using estimated Coulomb-Born cross sections. The cross section estimates

were made by scaling along the Fe XVI isoelectronic sequence. Bely's results indicate that the ionization cross sections for the ionization of Mg^+ by electron impact should have substantial discontinuities at approximately 57 and 101 eV energy. The experimental results of Martin et al.[30] do not show any significant discontinuities. Martin et al. estimated that an autoionization contribution as small as 3.0×10^{-18} cm^2 would have been detected.

Moores and Nussbaumer[33] have completed a more sophisticated calculation of the ionization of Mg^+ by electron impact. The Coulomb-Born (with exchange neglected) approximation was used, and both inner shell ionization and autoionization were included. The direct ionization component was taken to be the sum of the partial cross sections for the removal of the 3s valence electron and the 2p and 2s inner shell electrons. Excitation to the $1s^2 2s^2 2p^5 3snl$ levels for $n = 3, 4, 5$ and $l = 0, 1, 2$ were included in calculating the contribution to the ionization cross section due to autoionization. It was found that autoionization gave rise to a small amount of structure below the threshold (68 eV) for ionization of a 2p electron with a maximum jump of about 4.4×10^{-18} cm^2 occurring at about 57 eV incident electron energy. Extrapolation procedures were used to extend the range of the calculations to incident electron energies above 150 eV. The result of Moores and Nussbaumer shows clearly that inner shell contributions must be included when discussing the ionization of this alkaline earth ion. The autoionization contribution, although much less than Bely's[32] estimate, is still in conflict with experiment since Martin et al.[30] could have detected any discontinuity due to autoionization greater

than 3×10^{-18} cm^2. The total calculated cross section is 20 percent higher than the measured value at 150 eV electron energy decreasing to about 10 percent higher at 2000 eV.

It would appear, that in view of the various approximations used by Moores and Nussbaumer, their calculations indicate a reasonable degree of agreement with experiment. The authors discuss the limitations of their methods in detail.

Peart and Dolder have measured the cross sections for the single ionization of Ba^+ by electron impact from below threshold to approximately 2000 eV.[31] The authors present their experimental data in both tabular and graphical forms. While Peart and Dolder tabulate only three data points between threshold and 30 eV, and three points between 30 and 100 eV, their graphical data (Figures 3 and 5 in their paper) indicate that cross sections were measured for quite a few additional values of incident electron energy. It appears that the tabulated values were taken from a smooth curve drawn as some "best fit" through the experimental data values. This is a policy often followed by Dolder and his colleagues.[30,34,35]

The authors state in the text of their paper that an abrupt rise occurs in the cross section near 18 eV of incident electron energy which they attribute to autoionization via the $(5p^5 6s5d)P$ excited state of Ba^+. This structure is shown in detail by giving a recorder trace showing the cross section as a function of the electron energy from about 8 to 30

eV.* The trace was made by holding the electron beam current sensibly constant while sweeping the electron beam energy. The recorder trace shows a definite break that could represent the onset of autoionization. The slope of this break, which ideally should be infinite, is consistent with the authors' estimated electron beam energy distribution. Other features of the cross section shown qualitatively by the recorder traces are several small dips above about 20 eV of incident electron energy. The authors tentatively attribute these to be due to the onset of higher states of inner shell electron excitation. Peart and Dolder do not mention the possibility of direct inner shell ionization.

In the unpublished theoretical study of the ionization of Ba^+ done by Bely and Schwartz and cited by Bely and Van Regemorter,[26] the authors state the theoretical agreement with the experimental work of Peart and Dolder[31] is satisfactory so far as the position and magnitude of the autoionization process is concerned. No additional information is presently available concerning this study.

Review of Applicable Theory

Previous material in this chapter has presented both experimental results and some theoretical explanations for those results. It is now appropriate to examine the status of the available theory as it

---

*There are a number of significant inconsistencies in the paper by Peart and Dolder that complicate the interpretation of their low energy data. For example, the authors state in the text that the recorder trace shows the cross section to be increasing between 18 to 20 eV. Actually, the recorder trace shows the cross section to be decreasing from 18 to 20 eV. This and other inconsistencies are discussed in detail in Chapter V.

applies to the situation where both direct ionization and autoionization contribute to the total ionization cross section. Only a brief summary will be given here; the reader is referred to several review papers[24,26,27,36,37] for additional details and references.

Consider an ionizing event produced by an electron impact where both direct ionization and autoionization may be important. The total ionization cross section σ (total ionization) can be written as

$$\sigma(\text{total ioniz.}) = \sum_n \sigma_n(\text{direct ioniz.}) + \sum_i \frac{A_a(i)}{A_a(i)+A_s(i)} \sigma_i(\text{exc.}) \quad (5)$$

where the direct ionization is summed over the n contributing shells and the excitation cross section σ(exc.) is summed over i levels lying above the ionization limit of the target. The excitation cross sections are weighted by the branching ratio for radiationless and radiative transitions as previously defined in Equation (3). If as in the usual case of autoionization, $A_a \gg A_s$, Equation (5) becomes

$$\sigma(\text{total ioniz.}) = \sum_n \sigma_n(\text{direct ioniz.}) + \sum_i \sigma_i(\text{exc.}) \; . \quad (6)$$

If the positions of the autoionizing levels and the ionization energies of the various shells are known, the problem is reduced to calculating a set of ionization and excitation cross sections.

Unfortunately, at the present time, methods available for calculating the required cross sections are rather limited and usually give only approximate results. Even these approximate calculations,

except for some of the classical and empirical methods, involve a great deal of mathematical labor in their implementation.

The exact quantum mechanical collision problem involving excitation or ionization by electron impact is an example of the many-body problem and cannot be solved. In addition, in the usual formulation of the collision problem, the total wave function* is expanded in terms of the unperturbed wave functions of the target. Such an expansion leads to an infinite set of coupled partial differential equations. Since the solution of an infinite set of differential equations is mathematically impossible, approximations are always required. The approach usually followed is that of solving only those few equations as required to obtain an approximate solution and ignoring the remainder of the infinite set.

The available quantum mechanical approximations are relatively so crude and mathematically difficult that semiclassical, classical and even empirical methods are of significant importance. The following material discusses a few of the various approaches to the excitation and ionization problem that could be applied to the present research.

Excitation

Excitation is conceptually simpler than ionization since no electron is ejected and both the initial and final states of the atomic system are bound states. However, good agreement between experiment and theory is more often achieved in the case of ionization. Reasons

*The total wave function includes the target particle, the incident electron and, in the case of ionization, the ejected electron(s).

for this apparent inconsistency are discussed by Bely and Van Regemorter.[26]

Quantal Approximations. The simplest quantal approximation is the Born approximation. The Born approximation reduces the infinite set of differential equations to a single equation by assuming that the projectile electron is unaffected in the collision and that the only effect in the target is the coupling of that pair of eigenstates involved in the excitation. This is, in effect, a first-order perturbation-type calculation. In the Born approximation, the initial and final state wave functions are taken as the product of the unperturbed wave function for the state in question and a plane wave representing the incident or scattered electron.

The Coulomb-Born approximation for the excitation of positive ions is similar in concept to the Born, but Coulomb waves are used in lieu of plane waves to account for the distortion of the incident and scattered waves by the electric field of the ion.

The Bethe-Born approximation is the same as the Born, except that additional mathematical approximations are employed. These approximations restrict the validity of the Bethe approximation to energy regimes far removed from the process threshold. Although strictly valid only for neutral targets, the Bethe-Born method has been applied to ions by an empirical factor developed by Seaton.[38]

The close-coupling approximation is considerably more elaborate than the Born-type approximations. In the close coupling approximation one retains a few atomic states in the expansion and solves a finite set of coupled differential equations using numerical techniques. The

close-coupling method will be good only if the coupling with all neglected eigenstates is very weak. Additional information is needed to assess the applicability of the close-coupling method to the autoionizing levels in Ba^+.

The reader is referred elsewhere for a discussion of other quantal approximations.[26,27]

Semiclassical Approximations. In the semiclassical impact-parameter formulation the colliding electron is assumed to follow a classical path and the cross section is given in terms of the classical impact parameter. The impact parameter is in turn expressed as a function of the quantized angular momentum. A quantum mechanical perturbation technique is then used to evaluate the probability of excitation due to the interaction between the incident electron and a stationary target electron.

Other semiclassical methods are discussed in various review papers,[26,27,36,37] but any classical method is termed semiclassical, when in some manner, quantum mechanical properties are introduced into the classical treatment.

Classical Methods. Classical methods originate with Thomson[39] who regarded the collision as a classical binary impact between the incident electron and one of the atomic electrons initially at rest. Gryzinski[19,40-42] has developed a theory based on the assumption that the interaction between a charged projectile and an atom can be described classically by the Coulomb interaction between the projectile and atomic electrons. Gryzinski's method does not apply to ions, but should be approximately correct at high incident electron energies

where the effect of the Coulomb field is minimal.

Classical methods are reviewed in detail by Burgess and Percival[36] and also by Vriens.[37]

Ionization

The solution to the ionization problem is conceptually more difficult than that of the excitation problem. The main source of this difficulty is the extra electron removed from the target that must be included in the calculation. An additional complication is the necessity for integrating over the range of the final continuum states.

Quantal Approximations. The Born approximation for ionization is basically similar to that for excitation in that separable wave functions are used, and the effects of exchange are ignored. The charge seen by the ejected electron is taken to be $Z = 1$ while the scattered one moves in a neutral field. Thus inherent in the Born formulation is the approximation that the ejected electron completely screens the scattered electron from the nuclear field.

The Coulomb-Born approximation for the ionization of ions is generated by replacing the incident electron plane wave representation by a Coulomb wave representation. The ejected electron is, of course, always represented by a Coulomb wave.

The Bethe-Born approximation can also be applied to ionization. As in the case of excitation, its principal use is in indicating the functional dependence of the cross section at energies far removed from threshold. The Bethe approximation can be extended to include positive ions by the use of an empirical factor developed by Seaton.[38]

There are other variations of the Born-type approximations for ionization; for example, the Born-Oppenheimer and the Born-exchange approximations which attempt to include quantum mechanical exchange in the calculation. The reader is referred elsewhere for details on these and other quantal approximations.[24,26]

Classical and Semiclassical Approximations. Classical and semiclassical approximations have found more use in the estimation of ionization cross sections than excitation cross sections. Perhaps one reason for this is due to the fact that in ionization the final state lies in the continuum, a concept which is defined both classically and quantally.

The first classical approach to ionization was also due to Thomson.[39] Neglecting the interaction between the ionizing electron and the nucleus and assuming the atomic electron to be at rest, he derived an expression valid for a target having N electrons with binding energy I. The expression is given by

$$\sigma(x) = 4\pi\, a_0^2 N \left[\frac{I_H}{I}\right]^2 \frac{1}{x}\left(1 - \frac{1}{x}\right) \qquad (7)$$

where I_H is the ionization energy of hydrogen, a_0 is the radius of the first Bohr orbit and x is the reduced ionizing energy defined by

$$x = \frac{E}{I} \,. \qquad (8)$$

This theory is of value for it suggests that σ is a universal function of x. This is shown by defining a reduced cross section

$$\sigma_R(x) = \left[\frac{I}{I_H}\right]^2 \frac{1}{N}\sigma = 4\pi\, a_0^2\, \frac{1}{x}\left(1 - \frac{1}{x}\right) \qquad (9)$$

which is a function of x only. Thus, assuming that the reduced cross section for all atomic systems is the same, a scaling process can be used to convert from one system to another. This concept of classical scaling, has proven to be a useful one and is discussed again in Chapter V where classically scaled Cs cross sections are compared with the results of the present research.

Gryzinski[19,40-42] has developed a classical theory of ionization along the same lines as his excitation theory. He assumes that the cross section for ionization of an atom is given by the classical cross section for transfer of at least as much energy as the ionization energy of the electron treated as a free particle with a speed distribution appropriate to its bound state. Gryzinski first used a delta function speed distribution for the atomic electrons with the speed of the considered orbit as the argument.[40] Using the delta function velocity distribution, the asymptotic dependence of the cross section was found to be

$$\sigma \sim \frac{1}{E}\,, \qquad (10)$$

which is correct classically, but is not correct qualtally since the Bethe-Born approximation predicts the asymptotic variation

$$\sigma \sim \frac{\ln(E)}{E}\,. \qquad (11)$$

Gryzinski later[42] modified his assumed velocity distribution so as to obtain the correct asymptotic dependence of the cross section. The assumed velocity distribution is, however, not physically correct. Notwithstanding this apparent limitation, calculations using Gryzinski's method have often demonstrated remarkably good agreement with experimental data; for example, those detailed in this chapter.

The above classical theories are not strictly valid for positive ions since they do not account for the presence of the electric field of the ion. An empirical "focusing factor" is usually introduced to remedy this deficiency.[24,26,36] However, for large values of incident electron energy, the effect of the Coulomb field becomes negligible and the focusing factor approaches unity and is no longer necessary. Additional discussion of Gryzinski's method is found in Chapter V where calculations using his method are compared with the results of the present research.

Attempts have been made to improve Gryzinski's formulation by feeding in some quantum mechanical properties, either in the velocity distribution or by including exchange. The reader is referred elsewhere for details and additional references.[24,26,36,37]

There also exist a number of strictly empirical methods for predicting cross sections. Again, the interested reader is referred to the review papers.[24,26]

The Present Research

By means of a thorough discussion of the applicable theory and a series of critical reviews of the available experimental data,

previous sections of this chapter have demonstrated the importance of the autoionization and inner shell contributions to the total electron impact ionization cross section. This material provides the background for the present research, the primary goal of which was to complete a refined study of the absolute cross sections for the ionization of Ba^+ ions in the low energy regime, particularly near the peak of the cross section curve. This region was chosen for careful study since all of the structure present in the electron impact cross sections for the alkali metals is found near the peak of the cross section curve as is the calculated, but not experimentally verified structure in the cross sections for the ionization of Mg^+. The importance of inner shell ionization, at least as to how it affects the total ionization cross section, is well documented for the alkalis and for Mg^+. According to McFarland,[43] the estimated energies for ionizing a 5p and a 5s electron from a Ba^+ ion are, respectively, 29 and 53 eV. Thus any effects attributable to inner shell ionization would begin to occur near these threshold values and a careful study of the cross section in this region would be required to reveal any structure due to inner shell ionization. There are, of course, autoionizing states whose series limits are these ionization energies.

Although Peart and Dolder[31] apparently studied this energy range, their data presentation is not adequate to fully describe the behavior of the cross section in this regime. In the present research, the incident electron energy intervals were chosen so as to provide a maximum ability to resolve any possible structure consistent with the known energy spread of the electron beam and the likelihood of such structure

being present. This result was achieved by using 5 eV measurement intervals from 20 to 60 eV of incident electron energy and 10 eV intervals from 60 to 100 eV. Below 20 eV the measurement intervals were spaced so as to obtain maximum information with fewest points. Above 100 eV, where high resolution was not needed, 50 and 100 eV intervals were used.

CHAPTER II

EXPERIMENTAL TECHNIQUE

This chapter provides a detailed explanation of the experimental method used in this research. The experimental technique involves the use of a crossed beam apparatus in which approximately monoenergetic beams of Ba^+ ions and electrons are caused to intersect at right angles in a well defined collision region. The crossed beam technique, which probably originates with the work of Funk[44] has now achieved a measure of sophistication. Several papers[45-49] discussing the advantages and difficulties inherent in charged particle-charged particle crossed beam experiments have been written and most of the early work using this technique has been critically evaluated. Accordingly, it is not deemed profitable to review previous experimental work in the present chapter. However, experimental work directly related to the present research will be discussed in the appropriate chapter. The scope of the present chapter is confined to an explanation of the theoretical basis upon which the experimental apparatus described in Chapter III must operate. An expression for the cross section in terms of the experimental parameters is presented first. Then the difficulties expected to be encountered in obtaining those experimental parameters are discussed. This discussion leads directly to a set of criteria which the present experiment, or any similar experiment, must satisfy if it is to produce valid results.

Expression for the Cross Section in Terms of Experimental Parameters

In an electron-ion crossed beam experiment beams of ions and electrons are caused to intersect in a collision volume. Since the ions have much greater mass than do the electrons, momentum transfer to the ions will be such that the trajectories of ions which have undergone collisions do not appreciably deviate from the trajectories of the unreacted ions. It is thus possible in the case of ionizing events to separate the reacted ions from the unreacted ions by either electrostatic or magnetostatic analyzers. The electron current, the currents of the reacted and unreacted ions, the particle energies and the spatial distributions of the electron and ion beams provide the experimentally observed quantities from which the absolute cross sections can be calculated.

Consider a monoenergetic electron beam and a monoenergetic singly charged ion beam traveling parallel to the x and y axes, respectively, of a rectangular coordinate system. Let V_i and V_e be the ion and electron velocities. If both beams are sufficiently tenuous that multiple collisions can be neglected (thin target conditions) then the cross section for single ionization is shown* to be

$$\sigma_{12} = \frac{e\, V_i V_e}{2(V_i^2 + V_e^2)^{1/2}} \frac{I_{SIG}^{2+}}{\int_{z_{ie}} i(z)j(z)dz} \qquad (12)$$

*This expression is derived in Appendix I.

where $i(z)dz$ and $j(z)dz$ are the ion and electron currents passing through the region z to z + dz, I_{SIG}^{2+} is the total current of doubly charged ions produced by electron impact and e is the magnitude of the electronic charge. Equation (12) is usually written as

$$\sigma = \frac{I_{SIG}^{2+}}{JI} \frac{e\, V_i V_e}{2(V_i^2 + V_e^2)^{1/2}} F \tag{13}$$

where

$$F = \frac{I\,J}{\int_{z_{ie}} i(z)j(z)dz} = \frac{\int_{z_i} i(z)dz \int_{z_e} j(z)dz}{\int_{z_{ie}} i(z)j(z)dz} \tag{14}$$

and I and J are the total ion and electron currents. All of the currents in Equation (13) are directly measurable. The factor F, known as the form factor, is a functional defined on the ion and electron beam current density distributions. The form factor is usually approximated by simultaneously scanning both beams with an L-shaped probe having coplanar slits. This method, which is shown in Figure 1 has been employed by others.[34,46,50] Another method[50] of obtaining F is to use the top edge of the scanner to measure the integral of the current density distributions. Differentiation of the resultant data gives the functions i(z) and j(z) which are then used to evaluate Equation (14).

Difficulties Associated with Charged Particle-Charged Particle Crossed Beam Experiments

In principle, once the form factor is evaluated, it is simple to

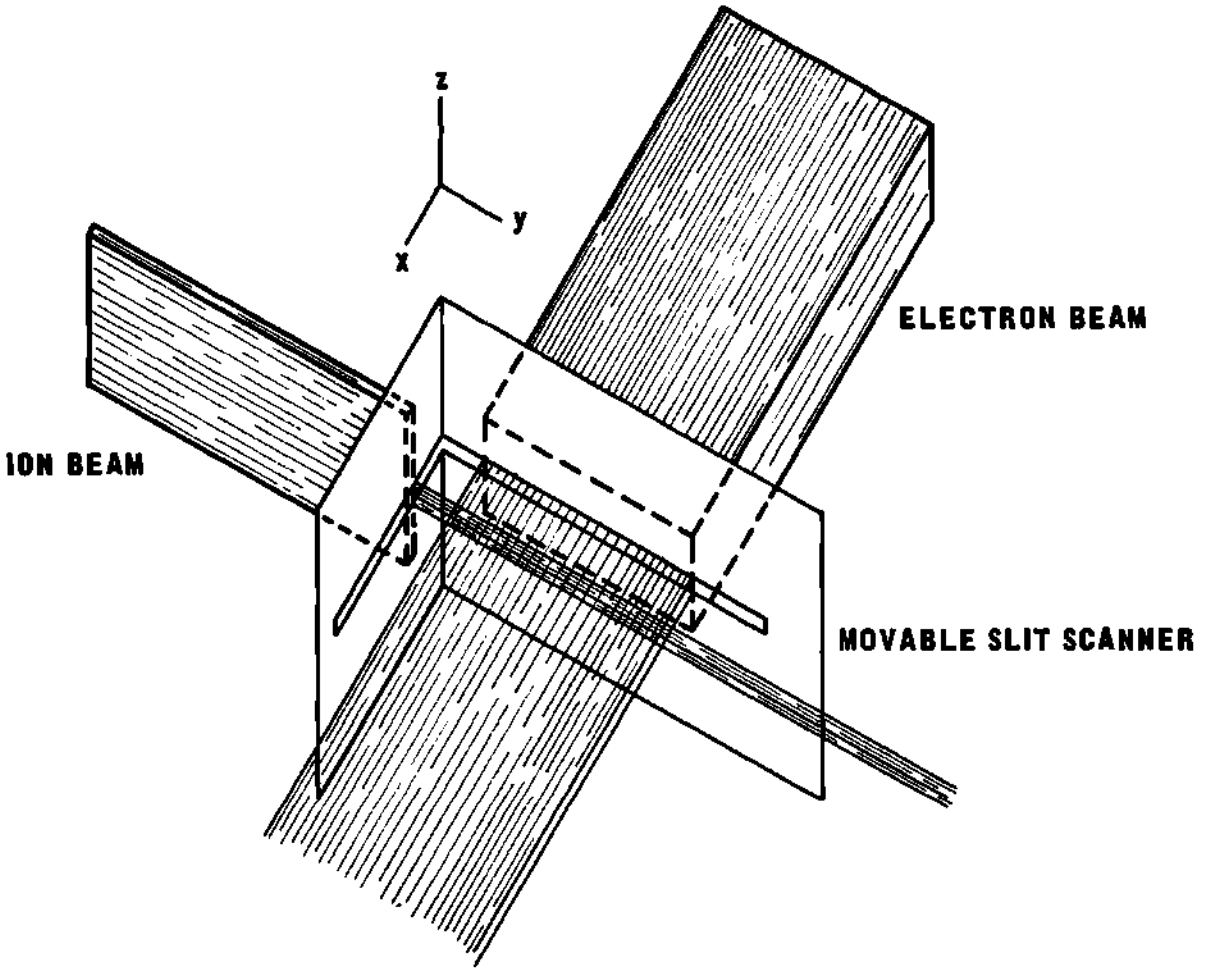

Figure 1. Use of a Movable Slit Scanner to Determine Beam Profiles.

calculate the cross sections; however, in practice serious difficulties are encountered in the measurements of I_{SIG}^{2+} and F. The other parameters in Equation (13) can be routinely evaluated assuming that proper precautions are taken in the apparatus design and accurate instrumentation is used. In contrast, the difficulties associated with the measurement of the electron impact ionization signal and the form factor are subtle in nature and require a somewhat detailed explanation.

Low Reaction Rates

The origin of one of the major difficulties associated with a crossed beam experiment is the small magnitude of the reaction component as compared with the primary beams. This fact necessitates careful precautions to ensure the recovery of the signal. The signal component obtained in a crossed beam experiment is far smaller than the usual signal levels encountered in a beam-gas experiment. For example, if one were investigating the charge stripping of He^+ on H_2, the H_2 pressure in the collision region could be adjusted to just below the point where multiple collisions of the ion beam became significant. The resulting He^{2+} signal might then be of the order of one percent of the magnitude of the primary beam. The signal available from a crossed beam experiment is far smaller because space charge and other considerations limit the permissible particle densities. An example of the low reaction rates typical of a crossed beam experiment is furnished by the present research. At an ion energy of 1 keV and with a 50 eV, 100 microampere electron beam about four Ba^+ ions in 10^8 are converted to Ba^{2+} ions. Thus the ion beam emerging from the collision volume con-

tains two components differing in intensity by about seven orders of magnitude. This difference in intensity requires that careful attention be given to ensure that stray particles from the primary beams or particles originating from some other source do not completely obscure the smaller reaction product.

Errors Introduced by Collisions with the Background Gas

Even at ultrahigh vacuum pressures (10^{-9} Torr) the number densities of the particles in the beams are comparable to the number density of the residual gases. In such cases the interaction of the primary ion beam with the residual gas cannot be ignored. In an electron impact ionization experiment, the most troublesome of the possible interactions is that of charge stripping:

$$X^+ + R \longrightarrow \begin{matrix} X^{2+} + R + e \\ X^{2+} + R + 2e \end{matrix} \qquad (15)$$

where X^+ is one of the primary ions and R is a residual gas molecule. Such stripping collisions produce only a very slight change in the trajectory of the primary ion beam. Thus if the stripping occurs in a field free region prior to the point of charge state separation, the charge stripped ions are indistinguishable from doubly ionized ions produced by electron impact. The charge stripped component thus constitutes a source of "noise" superimposed on the desired signal the intensity of which varies directly as the residual gas density and hence gas pressure. One is therefore not necessarily able to obtain the net electron impact ionization signal by a simple subtraction of

the doubly charged signal with the electron beam off from that with the electron beam on. If such a subtraction is to yield a valid measure of the electron impact component of the beam either,

(1) the vacuum chamber pressure is unaffected by the presence or absence of the electron beam, or

(2) the charge stripped component is sufficiently small relative to the electron impact ionization component that changes in the charged stripped component attendant with turning the electron beam on and off do not make a significant difference in the computation of the net electron impact ionization current.

Requirement (1) can be met by pulsing the electron beam. Under pulsed conditions, the magnitude of the gas density modulation will be filtered by the vacuum system in much the same way an electrical signal is filtered by an RC circuit.[45] The attenuation factor A is given by

$$A = [1 + (2\nu V/S)^2]^{-1/2} \qquad (16)$$

where ν is the modulation frequency, V is the volume of the chamber and S is the pumping speed. Thus by proper choice of ν the pressure variations can be made as small as desired. While pulsing just the electron beam will establish a steady state pressure, a frequently employed scheme[34,49] is to simultaneously pulse both the electron and ion beams. By a simple change of the relative phases of the two beams, the ions and electrons can be made to cross the interaction region either in time-coincidence or in time-anticoincidence. The difference between the coincidence and anticoincidence modes yields the electron

impact ionization current. One should note that during the pulse interval the beams travel a distance many times greater than the size of the vacuum chamber. Thus all of the difficulties inherent in any continuous beam experiment, except the problem of pressure modulation by the electron beam, exist in a modulated beam experiment. In addition, Dunn[45] notes that the simple assumptions leading to Equation (16) are sometimes invalid, and that each experiment must be evaluated on an individual basis.

If the experiment is to be operated in the continuous beam mode, requirement (2) must be shown to be satisfied. Since the pressure will certainly rise when the electron beam is turned on, due to the release of adsorbed gases caused by the electron bombardment, the difference between the I^{2+} current with both beams present and the I^{2+} current with only the ion beam present will be too large by an amount equal to the increase in the charge stripped current caused by the increased pressure. However, if the experiment is operated at an electron energy below the threshold for electron impact ionization, only the charge stripped current component will be present. Thus, assuming that no other sources of error are present, charge stripping is not a serious problem provided that the measured cross section below threshold is approximately zero when compared with that found well above threshold. This assumes that the ion and electron currents used below threshold are typical of those used above threshold. It is generally required to reduce the operating pressure to below 10^{-8} Torr before the charge stripped component

becomes small enough to accomplish the required measurement without the use of pulsing techniques.

Errors Caused by the Space Charge of the Beams

Other than producing errors in the measured form factor, a problem which will be treated separately, the space charge of the interacting beams can introduce errors since the space charge of one beam electrostatically deflects the other. The most significant sources of errors are listed below.

(1) The ion beam space charge causes variations in the background produced by the passage of the electron beam.

(2) The electron space charge causes variations in the background produced by the passage of the ion beam.

(3) The electron space charge causes losses or prevents losses from the ion beam due to deflection.

(4) The electron space charge causes an increase or decrease in any charge stripped component produced downstream from the interaction region by collisions of the primary ion beam with slit edges.

Variation of the Electron Beam Background. This difficulty is encountered only in experiments where electrons are detected or in excitation experiments where photons are detected close to the interaction volume. It therefore presents no source of error in the present experiment and the reader is referred elsewhere[47] for a detailed discussion.

Variation of the Ion Beam Background. This situation arises when a significant stripping background is produced prior to the

interaction region, for example on the edges of collimating slits. Assume that the divergence of this charge stripped component is great enough so that an appreciable portion misses the I^{2+} detector in the absence of the electron beam. When the electron beam is present its space charge creates an electric field which tends to converge the ion beam.* This convergence causes an increase in the charge stripped component and the concomitant error in determining the electron impact ionization signal component.

The difficulty discussed above is avoided in the present experiment by the expedient of a small deflection structure which removes all charge stripped ions produced prior to the interaction region.

Losses from the Ion Beam Due to Deflection. A common source of error in a crossed ion-electron beam experiment is the focusing of the ion beam under the influence of the electron beam space charge. Both increases and decreases in the apparent I^{2+}_{SIG} current can result from this cause. To show how such is possible first consider the case where the divergence of the ion beam is such that, with no electron beam present, a portion of the I^{2+} current is intercepted by an aperture prior to the I^{2+} detector. In such a situation, the application of the electron beam increases the convergence of the ion beam and thus adds an additional increment of signal to that present when the electron beam is off. If the density of the electron beam is further increased, it is possible for the ion beam to be focused to the extent that a

---

*Focusing action occurs in the z-direction; to first order, the electron beam space charge produces no focusing action in the x-direction.

crossover occurs in the ion beam trajectory. Once this condition is reached, additional increases in the electron beam density increase the divergence of the ion beam causing a loss of I^{2+} signal. The net effect of this on the cross section is to produce a measured value that is too large for small electron densities, and is too small for large electron densities. However, if the collection apertures are properly sized and the ion beam is properly focused the situation where the electron beam reduces losses by converging the ion beam will not normally arise. Extreme focusing of the ion beam leading to crossover and the attendant excessive losses can almost always be observed for some large value of electron density.

The presence of the above difficulties can be determined by a series of consistency checks. The converging action of the electron beam depends upon the electron number density which for a given electron energy is directly proportional to the electron current. Hence if the cross section measured at a fixed electron energy does not vary as a function of the electron current, it is reasonable to assume that the above focusing effects are absent. Another test for the above effects is obtained by varying the ion beam energy while measuring the cross section at a fixed electron energy and current. The deflection and hence focusing of the ion beam is inversely proportional to the ion beam velocity. Thus any systematic variation of the cross section as a function of ion energy indicates that the above or other sources of error are present. If the ion beam can be electrostatically focused a further check is possible. The cross section is measured with fixed particle energies and currents, but variations in the ion

beam profile are introduced by means of the focusing potential. If the cross section is independent of changes introduced in this way, then significant losses from the ion beam are unlikely.

Stripping of the Ion Beam on Slit Edges. In certain experimental geometries it is possible for ions which have lost energy or charge stripped on beam apertures to subsequently enter the I^{2+} collection system.* This condition produces another source of background which can be influenced by the electron beam space charge. If such a situation exists, the presence of the electron beam will converge the ion beam and reduce this slit edge produced component of the total I^{2+} signal. A variation in this manner will lead to a measured value of the I^{2+}_{SIG} which is too low since the noise component increases when the electron beam is off. The presence of this difficulty is detected by utilizing the methods discussed in the preceding section. The two problems can be separated, however, by noting the variation of the measured cross section as a function of the electron current with all other parameters held constant. If stripping or energy loss on an aperture edge is involved, the cross section will decrease as the elec- current is increased from a zero value, but will increase with increasing electron current when the problem of losses from the ion beam is encountered. Another sensitive test is to measure the cross section below the threshold for electron impact ionization. If the measured cross section below threshold is negative, this source of error may be present.

---

*The effects considered here occur after the ion beam passes through the interaction region.

Errors in the Determination of the Form Factor

The form factor determination is mainly subject to the following sources of error:

(1) the profile determinations are made a short distance away from the intersection of the beams rather than within the intersection and

(2) the beam profiles determined with the scanner are made under conditions of low space charge and may not reflect the actual situation when the scanner is not present.

The fact that the scanner is located away from the interaction region permits errors resulting from the space charge expansion of the beams, from the focusing of the beams in the interaction region and from possible tilt in the beams. The absence of excessive tilt can be demonstrated by the presence of an electron impact signal with the scanner lowered into the beams. If such a signal is present, the maximum tilt clearly must be less than h, the scanner slit width. Thus if the form factor is essentially constant under a relative profile shift of $\pm$ h, there is no appreciable error due to misalignment.

Both beams will expand as a result of their space charge, and can either expand or converge due to focusing action on the beams prior to their entering the interaction region. In most experiments the ion beam is nearly uniform over the short segment passing through the interaction region. Ion beam space charge will generally be too small to cause significant expansion and any nonuniformity is due to some focusing action. Any focusing conditions which produce significant nonuniformity over the short distance through the interaction region

will necessarily produce substantial divergence over the entire trajectory of the ion beam. Such divergence is easily detected and eliminated during initial checks of the apparatus.

The electron gun used in this experiment has no provision for electrostatic focusing, and consequently always produces a divergent beam. The electron beam height observed with the scanner will thus be somewhat less than the actual electron beam height in the interaction volume. In addition, the divergent electron trajectories increase the effective width of the ion beam in which interactions can occur. This requires a correction, appropriately averaged, in the measured form factor given by

$$\cos \alpha \tag{17}$$

where α is the angle between an electron trajectory and the x axis.

The above difficulties can be avoided if the ion beam is made as uniform as possible and taller than the ion beam and if the divergence angle α is limited to a maximum of a few degrees. If the ion beam is both reasonably uniform and taller than the electron beam, the measured form factor will be close to the actual form factor, namely that of a somewhat "spread out" electron beam. Since the space charge spread of the electron beam is directly proportional to the electron beam intensity, this condition can be checked experimentally by verifying that the measured cross section at a particular electron energy is independent of the electron beam intensity. Since $\cos \alpha$ varies slowly for small angles, a slight divergence of the electron beam causes but a trivial error. The maximum divergence of the electron beam

can be held to the desired value by observing the electron current to an aperture plate placed in front of the electron collector. If the aperture plate (properly sized) intercepts an insignificant fraction of the total electron current, the electron beam divergence will produce negligible error.

An additional error can be introduced because the space charge effects of both beams are altered when the scanner is lowered. When the electron beam is present it tends to converge the ion beams. That is, the ion beam tends to move to those regions where the electron beam is most dense. Since the beam scanner blocks off most of both beams, this space charge interaction is not reflected in the measured profiles. This difficulty is not eliminated by having the ion beam uniform and taller than the electron beam. Such a beam will still develop a more dense region in the vicinity of the electron beam. The ion deflection is not serious if it can be shown that the measured cross sections are independent of the ion energy. Since the ion deflection is reduced as the ion velocity increases, constancy of the measured cross sections as the ion energy is varied implies that deflection of the ion beam by the electron space charge is not significantly affecting the measured beam profiles. Another and very important test is to measure the cross section as function of the form factor. If the measured cross section is constant with the changing current distributions, which are reflected in the varying form factor, and is invariant under the previous tests, it is then reasonable to assume that the form

factor is being evaluated correctly.

A direct experimental check of the measured form factor is accomplished by comparing the value of the form factor measured in the differential mode with that measured in the integral mode. The integral mode measurement, made with the edge of the scanner, is made under conditions of varying space charge interaction. If the two measurements give the same value to within several percent, there is no significant error present due to the space charge interaction of the beams. Additional discussion of the difficulties associated with the measurement of the form factor is found elsewhere.[46-48]

Excitation State of the Ion Beam

In order for a crossed beam experiment to yield unambiguous results it is necessary to know the state of excitation of the ion beam. For this research the desired state of excitation is the ionic ground state. Since the ion source is removed from the interaction region, only metastable contamination is of any consequence because all ordinary excited states decay prior to reaching the interaction region. Ions excited to a metastable level have a larger cross section for ionization than ions in the ground state. The ionization threshold energy is lower for the metastably excited states than for the ionic ground state.

This last property allows an experimental assessment of the presence of metastable contamination. The ionization cross section is measured for an electron energy that lies above the threshold for the ionization of the metastable states, but below the threshold for ground state ionization. If the measured cross section is zero to

within the experimental error, there is no significant metastable contamination.

Summary of the Requirements for a Valid Crossed Beam Charged Particle-Charged Particle Ionization Experiment

The previous section has discussed in detail the major difficulties associated with charged particle-charged particle crossed beam experiments. A part of the discussion of each possible source of error was devoted to a description of experimental tests which could establish the presence of that difficulty. Unfortunately, few of the consistency checks so derived are unambiguous; several troubles can lead to a single symptom. The most obvious example of this is the existence of a non-zero cross section below threshold. However, by carefully evaluating all of the possible tests, one is usually able to achieve a satisfactory operating condition. These criteria which can be used to assess the validity of a crossed beam experiment are summarized below.

(1) The measured cross sections should ideally be zero, to within the experimental error, below the threshold energy for the process being studied. Since a variety of conditions can lead to a non-zero cross section, a series of measurements under varied operating conditions should always be made.

(2) The measured cross sections should be independent of the electron beam intensity.

(3) The measured cross sections should be independent of the ion beam intensity.

(4) The measured cross sections should be independent of changes in the beam profiles.

(5) The measured cross sections should be independent of the ion beam energy.

(6) If a beam pulsing technique is used, all of the above must be valid, and in addition, the particular modulation scheme used must not introduce other sources of error.

The results of the above consistency checks as applied to the present research are discussed in Chapter IV.

CHAPTER III

EXPERIMENTAL APPARATUS

The objective of this experiment was the measurement of the absolute ionization cross sections for the single ionization of Ba^+ ions by electron impact as a function of electron energy over the electron energy range from near threshold to approximately 100 eV. These measurements were made using the crossed beam technique discussed in the previous chapter with a modified version of the apparatus developed by Lineberger.[46]

A schematic diagram of the experimental apparatus is given in Figure 2 and a plan view photograph in Figure 3. Singly charged barium ions are produced by a water cooled surface ionization type ion source using a heated rhenium filament. Ions produced by the source pass through the several focusing, collimating and deflecting structures and then into the interaction volume. A rectangular electron beam intersects the ion beam in the interaction region. Just prior to entering the interaction region the two beams can be made to pass through a scanner which determines their spatial profiles. After undergoing collisions with the electrons in the interaction region, the ion beam which now contains several charge states, passes into the large parallel plate electrostatic analyzer. Here the Ba^+ and Ba^{2+} beam components are separated and directed into their respective Faraday cups. The schematic diagram does not show much of the ion

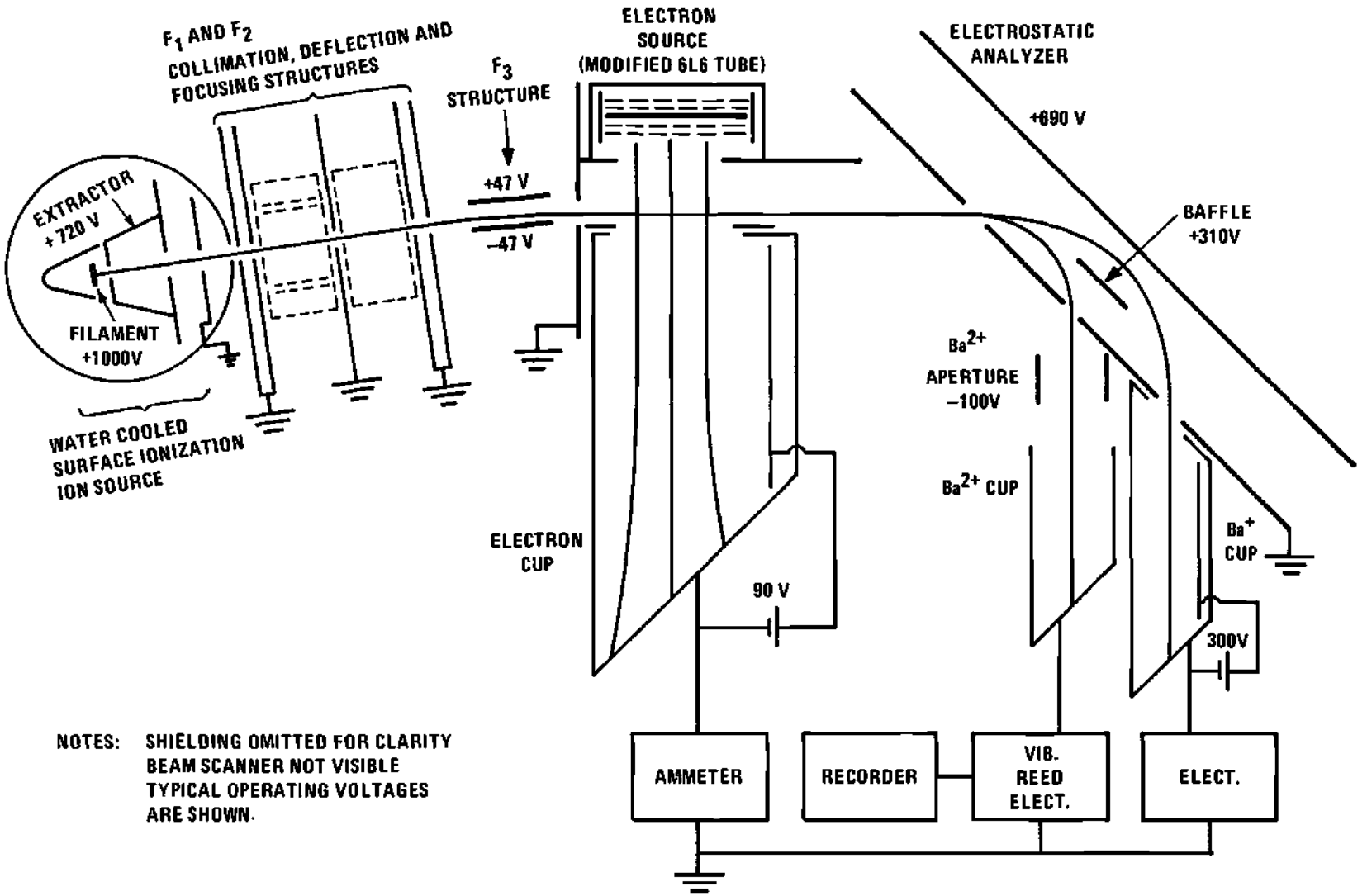

Figure 2. Schematic Diagram of the Experimental Apparatus.

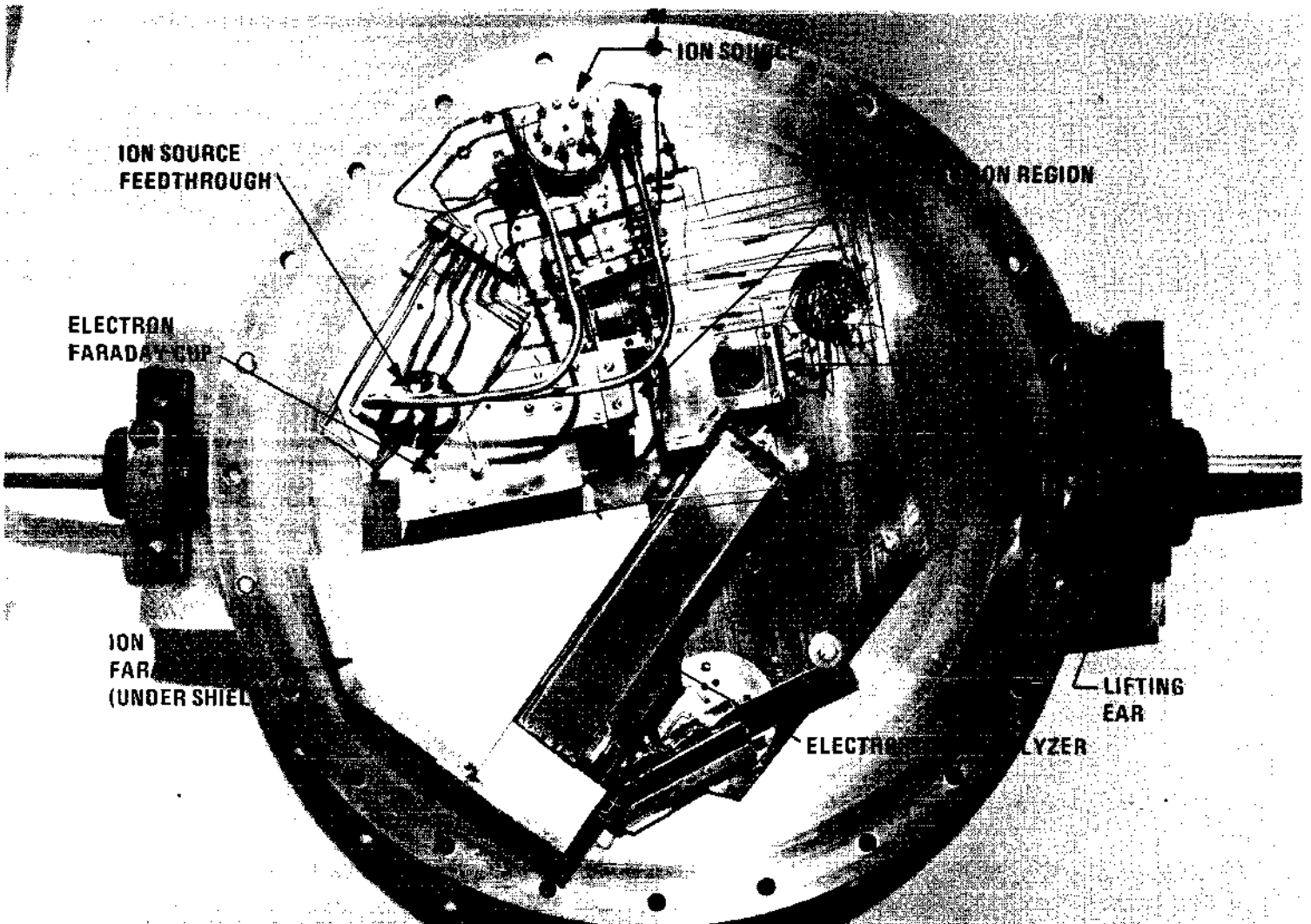

Figure 3. Plan View of the Experimental Apparatus.

source detail nor does it depict the extensive shielding around the Ba^{2+} Faraday cup which has been omitted for clarity.

An overall view of the entire experimental apparatus is shown in Figure 4. The vacuum system control instrumentation is on the right of the vacuum chamber, while the instrumentation for the actual experiment is on the left. The remainder of this chapter is concerned with a detailed description of the construction and operation of each of the major components of the experimental apparatus.

Vacuum System

The vacuum system is an all stainless steel bakable chamber 21.5 inches in diameter by 20 inches deep. The vacuum system was not designed specifically for the present experiment, but was engineered with sufficient flexibility to accommodate a variety of problems. For this reason, four Consolidated Vacuum Corporation four inch ports are welded into the chamber. The ion gauge tube mounting flange is fastened to one port; the other three are not used and are blanked off.

In keeping with ultrahigh vacuum practice, the interior of the chamber is polished to a nominal eight microinch finish in order to reduce outgassing. All welds are inert gas welds, made on the interior of the chamber and machined. The entire experiment proper is mounted on an experiment plate which is in turn suspended from the top cover of the chamber. This is done in such a manner so as to prevent any deformation in the top cover from being transmitted to the experiment and possibly causing misalignment of the beam optics.

No organic materials are used inside the vacuum chamber; only

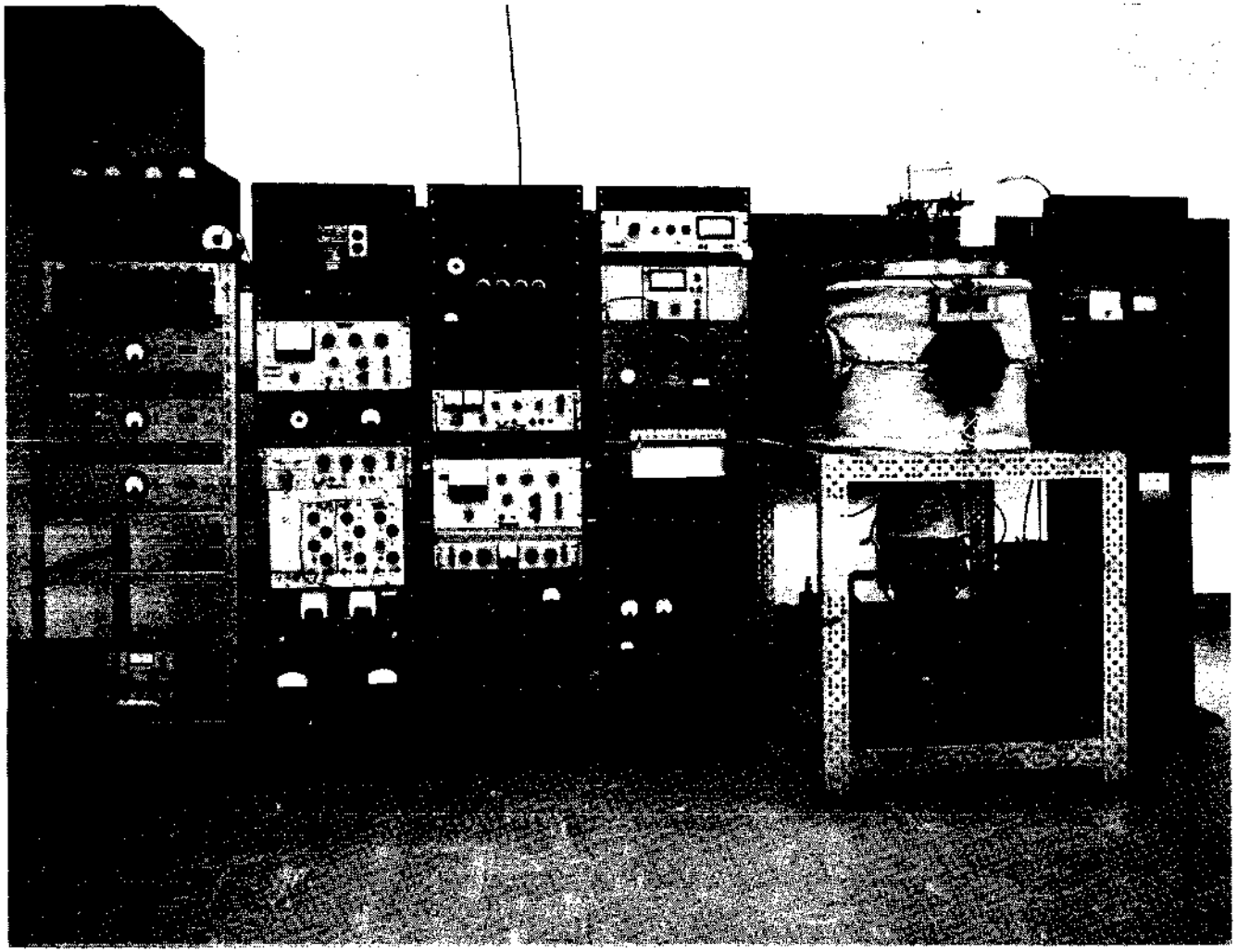

Figure 4. Overall View of the Experimental Apparatus.

metals and ceramics compatible with the ultrahigh vacuum environment are employed. The vacuum seals are of the metal o-ring compression type using gold or soft aluminum wire.

Pumping Apparatus

The pumping system consists of a six inch oil diffusion pump, Consolidated Vacuum Corporation type PMCU-6B, followed by a water cooled chevron baffle, type BCRU-60 and a zeolite molecular sieve trap, type TSMU-60. The diffusion pump is charged with Dow Corning Corporation type DC-705 silicone diffusion pump fluid.

The oxide cathode electron source is very sensitive to contamination, and thus provides a ready check on the backstreaming of diffusion pump fluid. In order to prevent cathode contamination, it was found advisable to replace the zeolite charge in the molecular sieve trap before every pumpdown.

Bakeout and Vacuum System Performance

The zeolite trap and vacuum chamber walls are heated to approximately 370°C and 200°C respectively for a period of 36 to 48 hours. During this period of time the ion source is heated to its operating temperature and the electron source is activated. Upon reaching room temperature after bakeout, with one milliampere of electron current and 10^{-7} amperes of ion beam current, the indicated pressure is 2-3 x 10^{-8} Torr. After several days of operation under these conditions the pressure continues to decrease to 3-5 x 10^{-9} Torr. No significant deterioration in this vacuum performance is evident over a period of at least one month. With both the electron and ion sources cold, the base pressure in the chamber is approximately 2 x 10^{-9} Torr.

Ion Beam Source and Optics

The ion source used in this experiment is a water cooled source of the surface ionization type. Once the ion beam has been produced it is shaped into the desired configuration by a combination of collimation, deflection and electrostatic focusing.

Ion Source

A surface ionization source was chosen because of the requirement that the ion beam be in its ground state. Since the $5^2D_{3/2}$ and $5^2D_{5/2}$ metastable electronic energy levels lie only 0.6 eV and 0.7 eV respectively above the $6^2S_{1/2}$ ground state, it was necessary that the ion source have a small probability of exciting these levels. Measurements made during this research have shown that the surface ionization barium ion source produces negligible metastable contamination of the ion beam.

The particular surface ionization ion source used in this experiment is a slightly modified version of that developed by Bacon,[51] and redesigned by Elford.* Details of the ion source are shown in Figure 5. Barium metal, contained within a molybdenum crucible, is heated to approximately 600°C by a tungsten heater embedded in a stainless steel heater block. A small rectangular jet of approximately 0.010 by 0.125 inch located at the top of the heater block directs the barium neutral beam through a guide tube and up onto the heated rhenium ionizing filament. The rhenium filament has the dimensions 0.002 inch by 0.125

---

*Dr. M. T. Elford was engaged in the redesign of the ion source and the design of some other aspects of the present experiment while he was a Visiting Professor in the School of Electrical Engineering at the Georgia Institute of Technology.

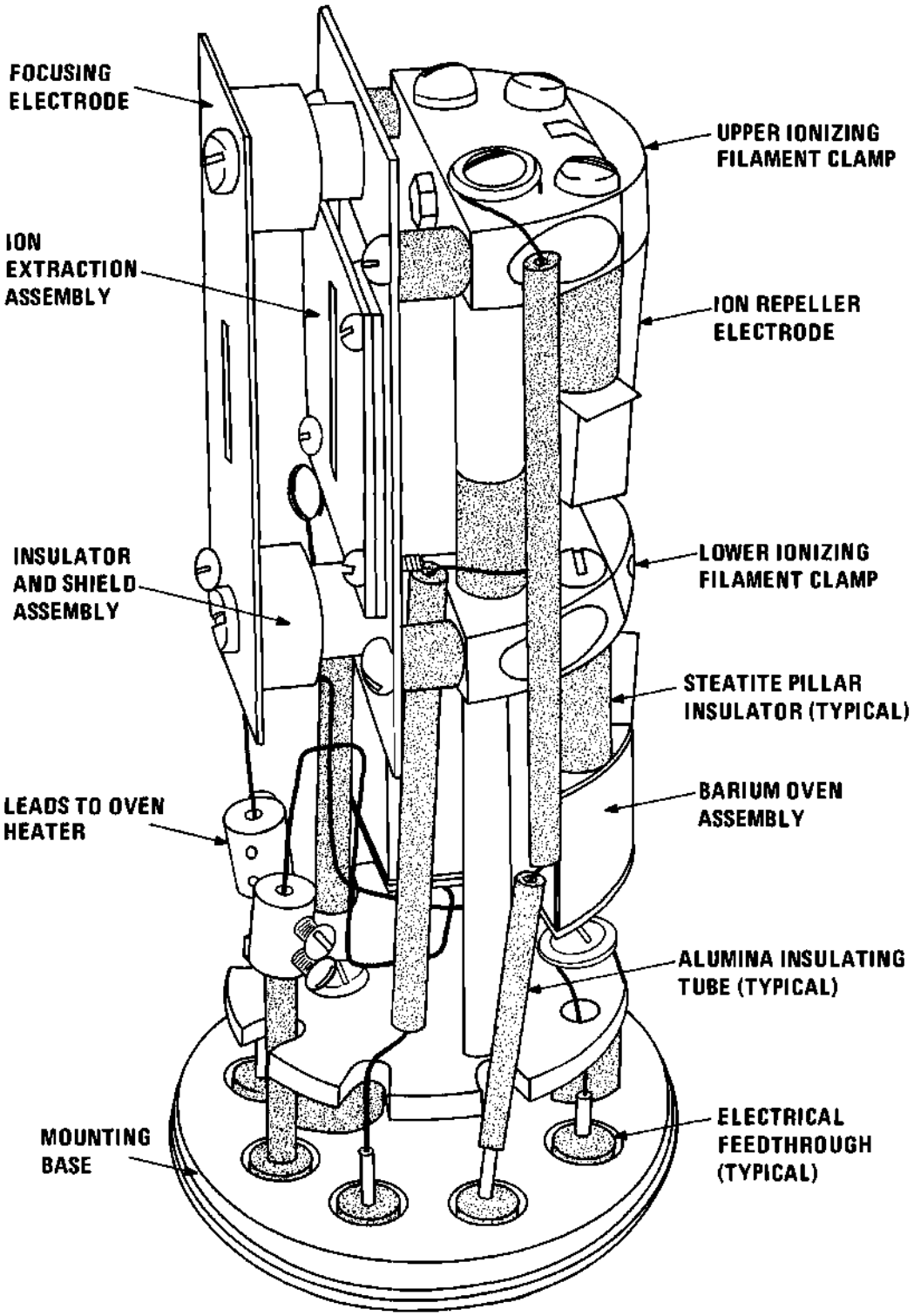

Figure 5. Schematic Drawing of the Ion Source.

inch by 1.2 inches long and is clamped between two stainless steel blocks. The ionizing filament is heated to approximately 1800°C by a direct current of 16 to 19 amperes. Direct current is employed to reduce the peak voltage drop across the filament (for a given power input) and to prevent amplitude modulation of the ion beam intensity. The guide tube is heated by conduction from both the heater block and the lower ionizing filament clamping block. This causes the temperature of the heater block to be higher near the exit nozzle and thus prevents stoppages due to melted barium plugging the jet. However, thermal conduction is sufficiently small that the ionizer and oven temperatures can be independently maintained at their optimum values. The entire ion source is housed in a three inch copper cylinder and is water cooled by a loop of 1/4 inch copper tubing which is clamped to the copper housing. Clamping is used in preference to welding since it allows the source housing to be easily removed thus providing access to the first collimating and deflecting assembly. The water cooling is efficient enough to allow chamber pressures of 3-4 x 10^{-9} Torr with the ion source operating.

The ion beam purity was established using an x-ray fluoresence unit and a magnetic sector mass spectrometer. An analysis of the barium metal used in the experiment made by means of an x-ray fluorescence unit revealed no detectable impurities other than strontium. The strontium content was established to be 0.7 ± 0.35 percent by volume. Since the first ionization potential of strontium is about 0.5 eV higher than that of barium, less than 0.01 percent of the emitted current could be Sr^+. The mass spectrometer showed that the rhenium

filament initially gave off Na^+ and K^+ ions. After eight or ten hours of operation, this contamination decreased to less than 0.2 percent and was still decreasing. Since the source was normally operated for a period of at least three days before any cross section data were taken, the Na^+ and K^+ contamination is estimated to be less than 0.1 percent. Since the cross sections for the ionization of Na^+ and K^+ ions are known to be smaller by factors of about ten and five,[49] respectively, than the final measured Ba^+ cross sections, the overall effect of this impurity ion contamination is seen to be negligible.

Water and electrical leads are passed through a five inch diameter stainless steel flange bolted to the chamber top. The electrical leads are number 12 copper wire which was vacuum brazed into seven Advac type 250-ES cable ends which were in turn heliarc welded into the flange. Water feedthrough is accomplished by two 1/4 inch diameter stainless steel tubes which were welded into the flange. The connection between the 1/4 inch stainless steel tubes welded into the flange and the copper cooling tube is made with two stainless steel fittings utilizing knife edge seals and copper gaskets. The copper tubing was vacuum brazed into one half of the fitting and the stainless steel tube heliarc welded into the other half.

The output current directly from the ion source is about ten microamperes. After collimation into a beam 1/32 inch wide by 1/4 inch high, currents of about 7×10^{-7} amperes can be obtained. The source has provided a collimated beam current of greater than 1×10^{-7} amperes for a continuous period of two months.

Ion Beam Optics

The successful completion of a crossed beam charged particle-charged particle experiment requires an ion beam which possesses a well defined geometry and is reasonably uniform. Three structures are employed in this experiment to form the ion beam into the desired configuration. The experimental apparatus originally used by Lineberger[46] had only two focusing and deflecting structures. A third structure is required in the present research in order to have sufficient versatility to collimate and focus the ion beam produced by the surface ionization ion source. This is because the uniformity and direction of the ion beam produced by the surface ionization source depends upon the orientation of the ionizing filament with respect to the extraction electrode and the neutral barium nozzle, which is a function of the thermal stresses within the filament. Thus, the position of the filament changes with its thermal history, necessitating some means of compensating for such changes.

To facilitate ready identification, each of the focusing structures and its accompanying deflecting plates has been assigned a symbolic designation. Starting from the ion source, the three structures are numbered, respectively, F_1, F_2 and F_3, as shown in Figure 2. Deflection plates parallel to the experiment base plate are assigned the designation "X" with the plate closer to the base plate being X_1. Plates perpendicular to the base plate are designated "Y" with the plates on the electron source side of the ion beam being Y_1 plates. Thus, for example, the complete designation F_1X_2 indicates that this is a plate in the structure nearest the ion source, it is a member

of the pair parallel to the experiment plate, and it is that member of the pair most distant from the base plate. Note that this system of notation is not in the coordinate system used to derive the cross section in terms of the experimental parameters.

Immediately upon exiting the ion source cooling jacket, the ion beam encounters the first collimating aperture which restricts the beam height to approximately 1/4 by 1/32 inch. This first slit forms one side of the F_1 focus structure. The F_1 structure contains four deflection plates for adjusting the ion beam direction. One of these plates, F_1Y_2, is ordinarily used to pulse the ion beam by moving it off the next slit. Under typical operating conditions, these plates are operated at only a few volts potential. Although the capability for doing so exists, the F_1 structure is not normally used for electrostati focusing of the beam. After leaving the F_1 structure, again through a 1/4 by 1/32 inch slit, the beam enters the F_2 structure. The F_2 structure is the main vertical (z-direction or 1/4 inch dimension) deflection and focusing structure. Potentials are set on the F_2 structure, which has only two plates, so as to minimize the losses from the ion beam. These plates, because they vary the height of the ion beam, can be used to control the form factor. As indicated previously, it is imperative that the measured cross sections are independent of modest variations in the form factor introduced in this manner. The F_2 plates are always operated with the minimum deflection and focusing potentials necessary to achieve the desired operating conditions.

As indicated in Figure 2 the ion beam enters the F_3 structure obliquely. The F_3 structure provides focusing action, but this is a

secondary function of the structure. The primary purpose of the F_3 deflection plates is to remove that small component of the ion beam which has either lost energy or been charge stripped in collisions with the knife edges of the previous ion optics. The horizontal deflector, F_3, introduces an eight degree bend into the main ion beam following the last slit edge that the ion beam is allowed to strike. The bend is sufficient to deflect the charge stripped and energy degraded component away from the last aperture before the interaction region, which removes it from the ion beam. The ion beam is not allowed to strike this aperture, which is 1/4 inch by 3/8 inch in size. The elimination of the ion beam noise produced prior to the interaction region improves the overall signal to noise ratio and at the same time precludes the possibility of the electron beam causing variations in the ion beam background. A third purpose of the F_3 structure is to prevent neutral atoms and photons produced by the ion source from entering the interaction region. Since the neutral atoms and photons are not deflected by the electric field, they strike the plate containing the last aperture and are prevented from entering the interaction region.

All focusing and deflecting potentials supplied to the experiment are derived from electronically regulated power supplies. Gaseous regulator tubes are used to obtain dual polarity outputs from a single electronically regulated power supply. The required polarity voltage for a given set of deflection plates is switch selected and its value set by means of a ten-turn potentiometer. The deflector plates are then floated at the required focus potential, which is obtained from a set of Lambda Electronics Corporation Model 71 Power Supplies.

Electron Source

The electron source is a modified 6L6GC beam power tube. A beam power tube was chosen for the source since it is designed to produce an approximately rectangular electron beam. The 6L6GC tube is prepared for use in the following manner. The tube basing and envelope are removed, and the plate structure is cut back exposing the cathode and grids. The remaining plate sections are bent into a position for spot welding to a mounting bracket. The mounting bracket holds the electron source and its associated connecting leads together as a complete unit. After the electron source has been welded into position, the entire bracket assembly is fastened into the electron source housing. The source leads, which are brought out through insulated feedthrough bushings on the end of the source bracket, are then attached with push-on connectors to the main 20-pin electrical feedthrough. The electron source is then carefully aligned with the ion beam. With proper care and the use of a telescopic alignment device, the position of the electron peak current density is repeatable to within ± 0.020 inch.

It was found that space charge expansion of the electron beam precluded the use of a single electron source configuration over the entire range of electron energies. Since the electron energy range below 100 eV was deemed most important in this experiment, the electron source was first optimized for this regime. To accomplish this, it was necessary to do the following: move the electron source housing

approximately 3/32 inch closer to the ion beam;* move the electron source approximately 3/32 inch closer to the electron source housing aperture, and remove most of the cant** from the electron emitter.

When first operating under these conditions it was noted that the electric field in the electron source penetrated into the interaction region. The origin of this field was established to be the beam forming plates of the 6L6GC tube, which with the cant removed were in a more exposed position. This field penetration was completely eliminated by decreasing the size of the exit aperture in the electron source mounting bracket. The electron beam still completely clears the aperture, which is now approximately the size of the spacing between the beam forming plates.

When operating in the 100 - 1000 eV regime, the cant is reimposed and the source is moved back 3/32 inch away from the electron source housing aperture; the size of the electron source bracket aperture is not disturbed and the electron source housing is not moved.

It has been shown that with these changes a satisfactory form factor can be obtained from 10 eV to 1000 eV of electron energy. There is a range of overlap from about 100 to 300 eV where either geometry can be used. Thus, when the geometry is changed, measurements in this

---

*The reference point is taken as the original position fixed by Lineberger, approximately 3/8 inch from the ion beam.

**The tilt or cant about the axis of the electron beam is placed in the electron source in order to increase the effective height of the electron beam. Such an increase in height is necessary at the higher electron energies (100 - 1000 eV) where the beam is highly peaked, if a good form factor measurement is to be obtained.

range serve as a transfer check on the performance of the electron source.

The energy spread of the electron beam is shown in Figure 6. This measurement was made by Bacon[51] on an electron source also constructed from a 6L6GC vacuum tube. Note that the energy spread of the electron beam at half of the maximum intensity is about 1.1 eV. Also observe that the electron energy is reduced by about two volts below that value set by the power supply due to the voltage drop within the oxide cathode. Retarding potential measurements, and the onset of autoionization in the present experiment appear to confirm the above measurements.

In operation, electrons are accelerated from the negative cathode to ground potential. The screen grid is normally set at ground potential and the control grid is employed to adjust the electron beam intensity. The electron acceleration potential is supplied by a Fluke Model 413C Power Supply and is monitored by a Fluke Model 871A DC Differential Voltmeter. The error in the electron beam energy due to the power supply is taken to be less than 0.25 percent. The control grid voltage is supplied from a ten-turn potentiometer connected across a gaseous regulator tube. The line voltage for these supplies as well as for all other critical equipment is stabilized by a Sorensen Model 2000S Line Voltage Regulator.

Interaction Region

The interaction region is designed to provide a field free space for the intersection of the ion and electron beams. The interaction

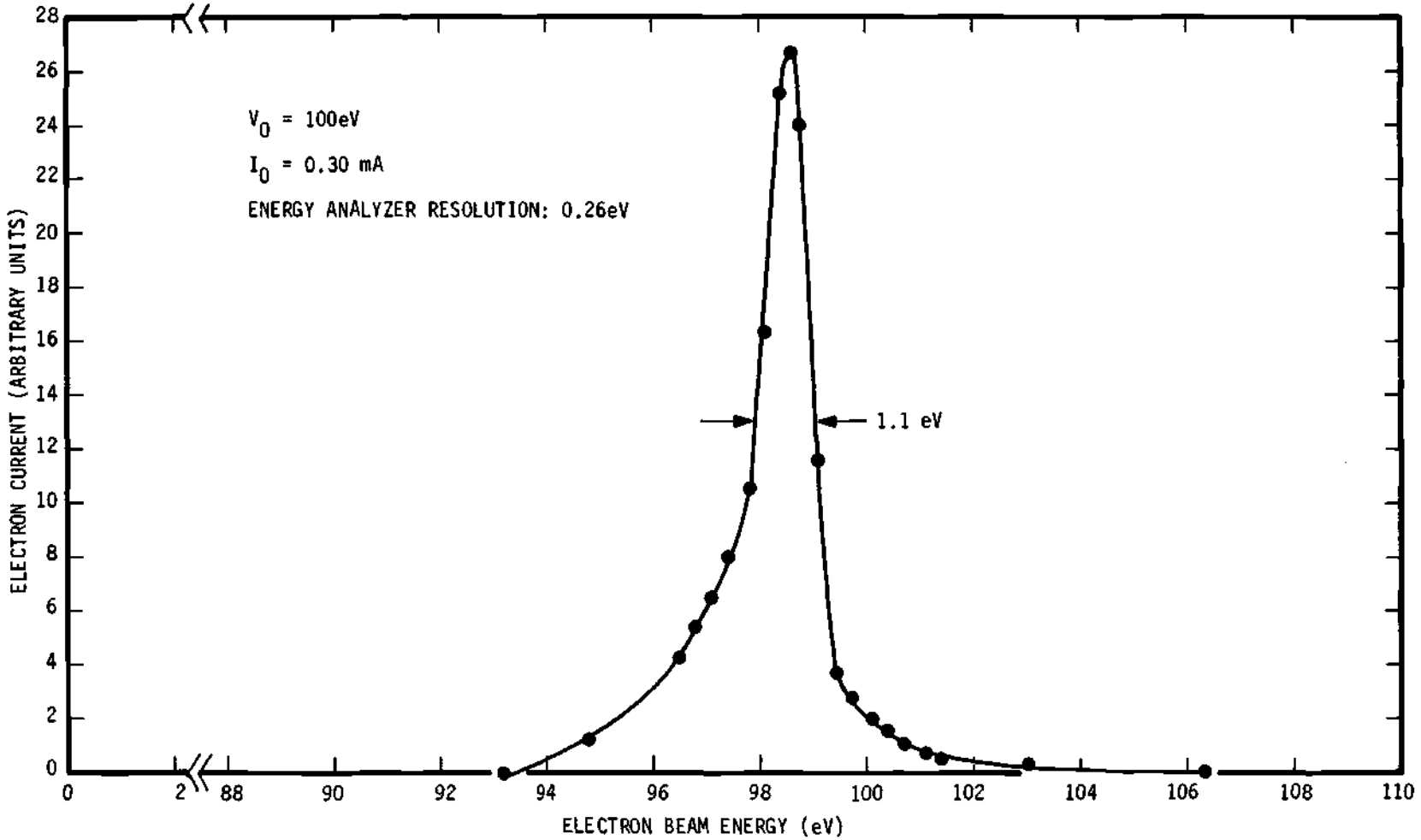

Figure 6. Typical Electron Beam Energy Distribution.

region is defined by the ion beam exit plate, the electron source housing and the electron cup aperture plate. The electron source housing and the ion beam exit plate also provide a guide for the movable slit scanner. A photograph of the interaction region, taken from behind the position normally occupied by the electron beam Faraday cup, is shown in Figure 7. Note that the feedthrough connections for the ion source are also visible in this view. In the figure, the slit scanner is positioned so as to allow the beams to pass through the interaction region without obstruction. The scanner intercepts the ion beam approximately 3/8 inch and the electron beam approximately 9/32 inch prior to their intersection. Notice that the scanner has two pairs of slits. One set has a height of 0.020 inch and while the other set is 0.010 inch high. This arrangement permits determination of the beam profiles with two significantly different slit sizes. In practice, the results obtained with the two slits agree to within several percent, and the larger slits are normally employed. The linear motion of the slit scanner is introduced by means of a metal bellows assembly positioned with a micrometer drive.

Electrostatic Analyzer

After interaction with the electron beam, the ion beam which now contains Ba^{+} and Ba^{2+} ions traveling with the same velocity must be separated into its various charge states. Since the Ba^{2+} beam component may be 10^{-8} times the size of the Ba^{+} beam, the separation must be performed very carefully in order to prevent stray particles from the Ba^{+} beam from completely obscuring the Ba^{2+} component. Either electrostatic or magnetostatic analyzers can be used to effect this

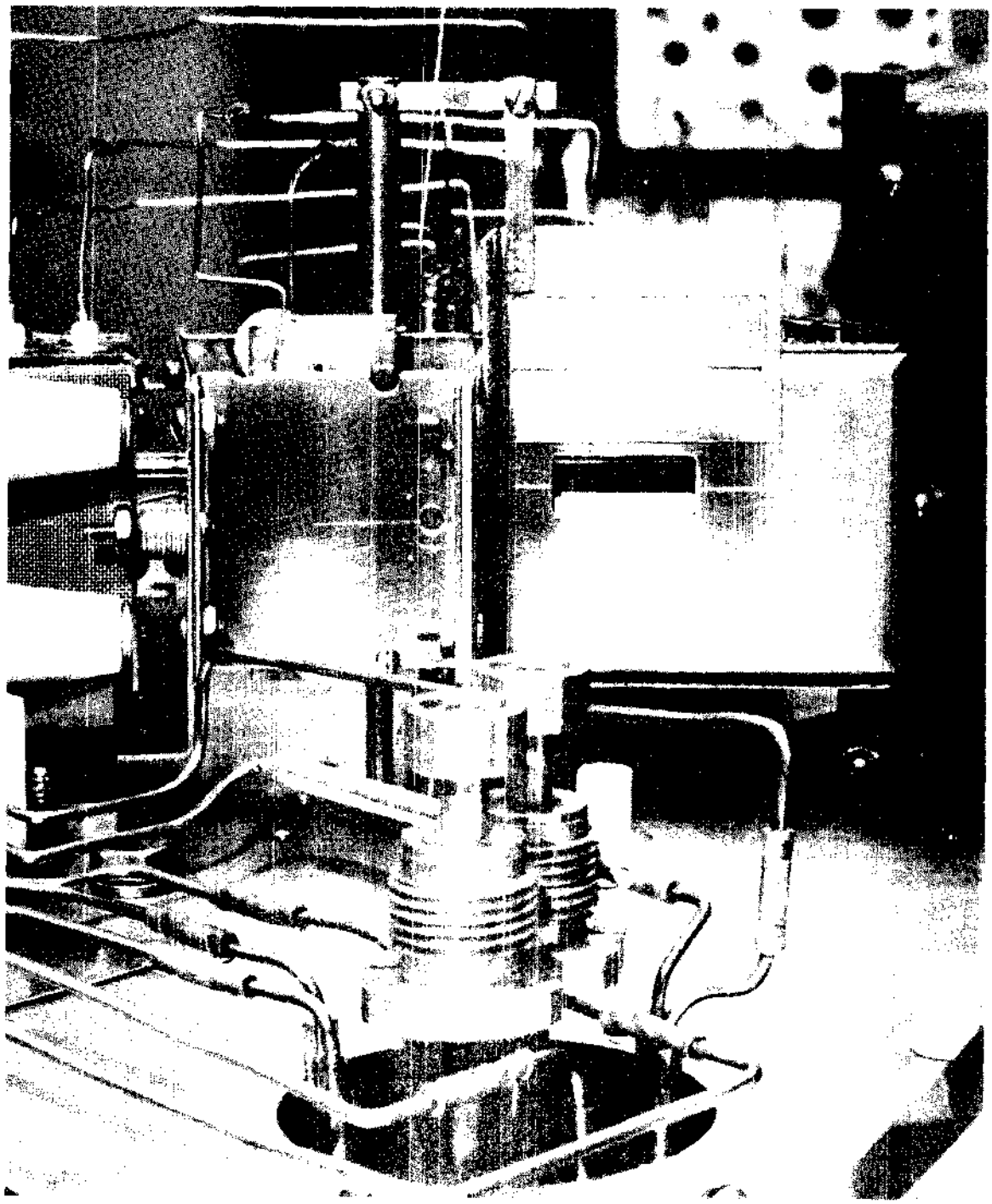

Figure 7. Interaction Region Seen from the Location of the Electron Beam Faraday Cup.

separation. Magnetic separation appears to offer superior rejection of unwanted charged particles,[48] however the electrostatic analyzer was chosen by Lineberger for this apparatus both from space considerations and the fact that the fringe fields of the electrostatic analyzer are more easily controllable. The present experiment employs the electrostatic analyzer assembly unchanged from Lineberger's design.[46]

Charge state separation is accomplished by an inclined parallel plate electrostatic analyzer as shown in Figure 2. The structure is a modification of an energy selector proposed by Yarnold and Bolton[52] and elaborated upon by Harrower.[53] The ion beam enters the analyzer at an angle of 45 degrees with respect to the plates. The singly and doubly charged ions are separated in the electric field of the analyzer and exit at angles of 45 degrees into their respective Faraday cups. The plates of the analyzer are separated by 1-5/16 inches, while the spacing between the adjacent apertures in the grounded plate of the analyzer is 2.0 inches. The Ba^{2+} exit aperture is approximately 3/8 by 3/4 inch while the Ba^{+} exit aperture is approximately 3/4 by 7/8 inch. Thus the size of both apertures is much greater than the nominal 1/16 by 1/4 inch size of the ion beam in this region. The analyzer plates are sufficiently large (5 inches by 7 inches) that the end field effects are well removed from the vicinity of the ion beams.

The baffle plate in the analyzer is held at the value of the local equipotential and does not seriously disturb the uniform electric field in the analyzer. The need for this plate can be seen from a consideration of the interactions of the primary ion beam with the

residual gas in the vacuum chamber. As the Ba^+ beam traverses the vacuum chamber, the following interactions with the residual gas are among those possible:

$$\text{ionization:}\quad Ba^+ + R \rightarrow Ba^+ + R^+ + e \tag{18}$$

$$\text{charge transfer:}\quad Ba^+ + R \rightarrow Ba + R^+ \tag{19}$$

where R is any residual gas molecule. In any of the above cases the R^+ ion formed will be a relatively slow ion. The Ba^+ beam thus produces a line of slow ions along its flight path. When this process occurs within the analyzer, the slow ions are accelerated toward the grounded plate of the analyzer. Any ions formed above the Ba^{2+} opening are thus accelerated into the cup and constitute a background signal. Experimental evidence indicates that this current is comparable to the Ba^{2+} electron impact signal current. The baffle plate intercepts these ions before they reach the Ba^{2+} beam opening and eliminates this background signal. The baffle plate is sufficiently small that both ion beams clear it by at least 3/8 inch.

Note also that the Ba^{2+} cup is set back from the grounded analyzer plate. This setback and the negatively charged Ba^{2+} aperture tend to augment the baffle plate in the removal of the slow ions.

Performance tests show that there is a broad plateau, approximately ± 5 percent, of analyzer voltage over which both components of the ion beam suffer no detectable losses in traversing the analyzer to their appropriate exit apertures. The baffle plate voltage which is derived from a voltage divider, is also noncritical.

Ion Collection and Measurement System

The collection of the Ba^+ beam component, which is of the order of 10^{-7} amperes, is routine and presents few problems. However, the magnitude of the Ba^{2+} beam current, about 10^{-14} amperes, requires that careful attention be given to the design of its collection system if meaningful measurements are to be made. Since the ion collection and measurement system was not altered from the original design of Lineberger, only the functional requirements and details are given here; the reader is referred elsewhere[46] for constructional details.

Ba^+ Collection and Measurement System

The Ba^+ Faraday cup is a deep cup geometrically constructed so as to minimize the tendency for secondary electrons and/or reflected ions to escape from the cup entrance. In addition, two plates parallel to the plane of the experiment plate produce an electric field which tends to retain the charged particles within the cup. These suppression electrodes are normally biased to 300 volts. However, it has been demonstrated that the cup is essentially 100 percent efficient without the suppression potential.

The Ba^+ beam current is measured by means of a Keithley Model 610R Electrometer. The calibration of this instrument is frequently checked with a Grya Model GS-57 Current Source. A Fluke Model 871A DC Differential Voltmeter and a one megohm 0.1 percent resistor is used as an additional calibration check. The accuracy of the Ba^+ instrumentation is taken to be better than ± 2.0 percent.

Ba^{2+} Collection and Measurement System

The Ba^{2+} collection system is shown diagrammatically in Figure 2.

The Ba^{2+} Faraday cup is set back slightly from the grounded analyzer plate, but its entrance aperture is still large with respect to the size of the ion beam. Interposed between the Ba^{2+} cup and the grounded analyzer plate is a box-shaped aperture electrode. This electrode, which is carried at about 100 to 150 volts negative with respect to ground, serves to suppress secondary electrons originating in the Ba^{2+} cup and also to prevent background electrons from entering the Ba^{2+} cup. The electron background arises from slow electrons which are attracted to the analyzer back plate, undergo elastic reflection from the back plate, and subsequently exit into the Ba^{2+} cup. These slow electrons originate from the electron "gas" that permeates the vacuum chamber when the electron source is operating. The density of this "gas" depends upon the electron energy and current, specifically the electron background increases with increasing electron energy and current. The dependence of this background upon electron energy and current is nonlinear; it increases more rapidly with current at the higher electron energies.

Above about 300 eV of electron energy, the extensive shielding and the Ba^{2+} cup aperture alone are not capable of reducing the electron background current to an acceptable value. Further reduction is accomplished by the placement of three permanent magnets outside of the vacuum chamber. The magnets are positioned so as to provide a magnetic field approximately perpendicular to the axis of the Ba^{2+} cup. This magnetic field serves as a barrier preventing the entrance of electrons. Properly located, these magnets produce a negligible field in the vicinity of the electron beam and interaction region. That

this externally produced magnetic field does not impair the performance of the experiment is assured through frequent checks as discussed in Chapter IV.

The magnitude of the Ba^{2+} beam current is too small and masked in noise to permit the observation of small changes in this current while the Ba^{2+} suppression is varied. Consequently, the collection efficiency of the Ba^{2+} cup was verified by indirect methods. These tests, the details of which are given by Lineberger,[46] showed that the Ba^{2+} ions are collected with essentially 100 percent efficiency.

The small magnitude of the Ba^{2+} signal current requires that the Ba^{2+} cup and its associated lead be carefully shielded from stray charged particles. It is also necessary to electrostatically shield all insulators from the Ba^{2+} collection structure. This precaution is necessary to eliminate polarization currents produced by the presence of electrically charged insulators.

Current collected by the Ba^{2+} cup is measured with a Cary Model 31 Vibrating Reed Electrometer. The electrometer preamplifier mounts directly above the Ba^{2+} cup vacuum feedthrough connector. The output of the vibrating reed electrometer is fed into a ten-inch Honeywell Electronik Model 15 Potentiometric Recorder having an accuracy of 0.25 percent. A recorder is necessary when the rate-of-charge mode of measurement is employed with the electrometer.

Two modes of operation are available for measuring currents with the vibrating reed electrometer. The first of these measures the voltage drop across a large value resistor. This method is convenient and provides a direct read-out of the magnitude of the ion current. In

the second method, known as the rate-of-charge mode, the instrument indicates the instantaneous voltage developed across a known precision capacitor by the beam current. If the beam current is constant, then

$$I = \frac{\Delta Q}{\Delta t} = \frac{\Delta V}{\Delta t} C \qquad (20)$$

where C is the capacitance of the capacitor being charged by the current I, and Δt is the time interval over which the voltage changed by ΔV volts. The beam current is thus determined by measuring the average time derivative of the output voltage of the vibrating reed electrometer and multiplying by the capacitance of the precision capacitor.

The superiority of the rate-of-charge mode over the more conventional resistor mode is demonstrated by Figure 8. This example shows two determinations of the same current, one using a 10^{12} ohm resistor and the other made using the rate-of-charge method. In both cases the dashed lines represent a ± 5 percent deviation from the mean. Since the slope of the voltage versus time curve can routinely be determined to within one percent, the improved precision attainable using the rate-of-charge measurement is quite apparent. Two additional advantages accruing from the use of the rate-of-charge mode are that

(1) it is not necessary to carefully zero the measuring instrument since only changes in voltage are significant, and

(2) the long term stability of the three-terminal guarded precision capacitor is much better than that of available high value resistors.

These advantages of the rate-of-charge mode far outweigh the additional

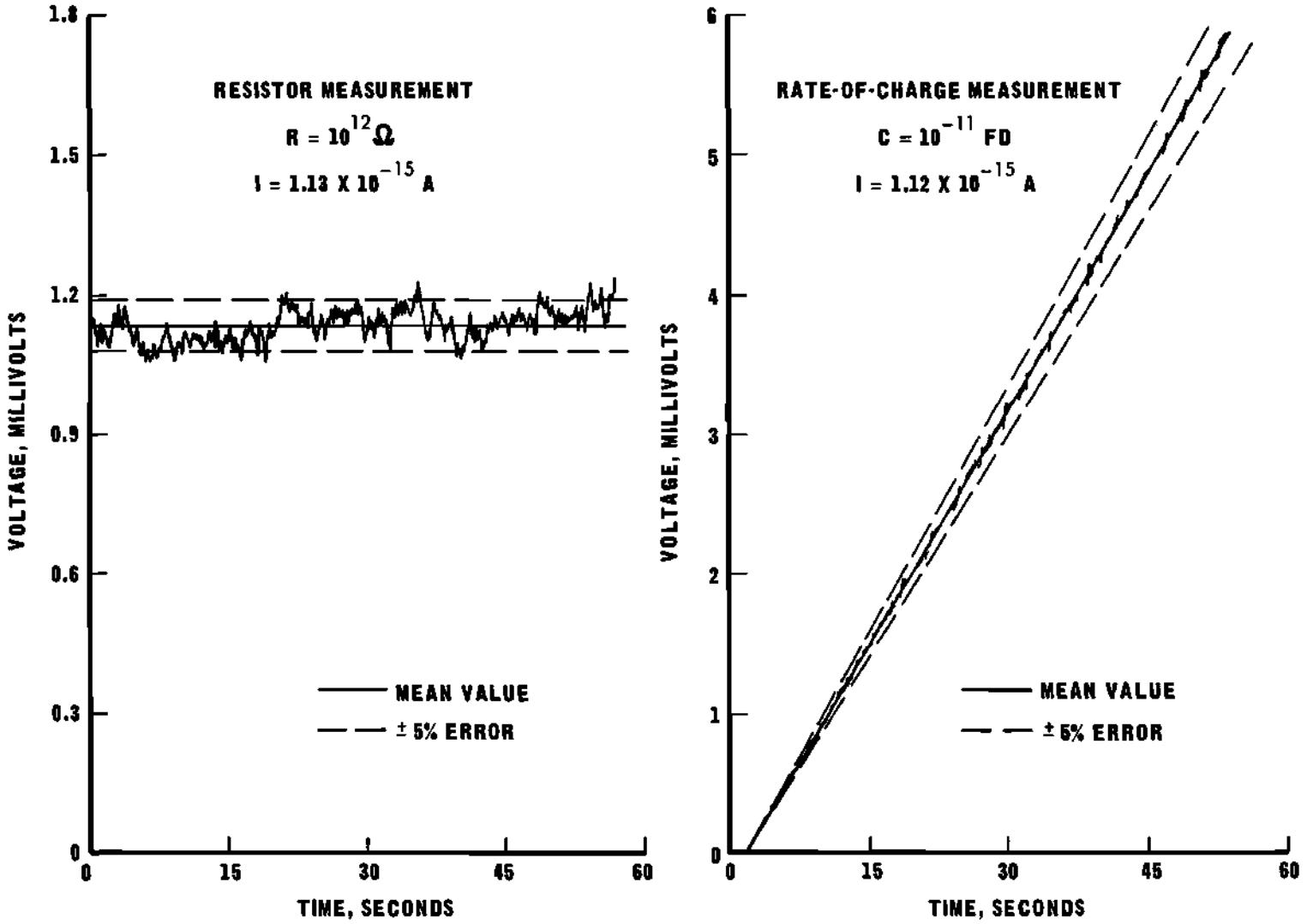

Figure 8. Typical Rate-of-Charge and Resistor Current Measurements with a Vibrating Reed Electrometer.

time and inconvenience required to determine the ion current that are associated with the method. The rate of charge mode was therefore used for all Ba^{2+} current measurements.

The accuracy of the rate-of-charge method depends upon the accuracy with which the time derivative of the voltage and the input capacitance are known. The input capacitance is specified by the manufacturer to have a nominal value of 1×10^{-11} farads. The actual value of the input capacitance was determined by measuring a known current from a Gyra Model GS-57 current source in the rate-of-charge mode; the resulting capacitance was $1.00 \pm 0.03 \times 10^{-11}$ farads. Since the accuracy with which the voltage derivative can be determined is usually better than one percent, the Ba^{2+} current measurements are taken to be accurate to within ± 3.0 percent.

Electron Collection and Measurement System

The electron cup is visible in the plan view of the apparatus, Figure 3, and in the schematic drawing, Figure 2. The shape of the electron cup was influenced primarily by the proximity of the water feedthrough and ion source leads. An L-shaped secondary electron suppression electrode (interior to the cup) extends across the top of the cup and down the side nearest the electrostatic analyzer. Shielding structures prevent the suppression field from entering the interaction region. The electron Faraday cup is 100 percent efficient with 90 volts applied between the suppression electrode and the cup, and is more than 98 percent efficient with no suppression voltage applied. The divergence of the electron beam is monitored by an aperture plate

placed in front of the electron cup. During data collection, the current to the aperture plate varies from less than 0.1 to about 2.0 percent of the total electron current. The electron aperture current is never allowed to exceed about 2.0 percent, even at the lowest electron energy.

The electron current is determined by measuring the voltage drop across a 1000 ohm, 0.1 percent resistor. A Fluke Model 845AB High Impedance Voltmeter-Null Detector is used in this measurement. The accuracy of this device is frequently checked with a Fluke Model 871A DC Differential Voltmeter. The estimated error in the electron current determination is taken to be ± 2.0 percent.

The electron current measurement circuit also incorporates a retarding voltage which can be applied in series with the cup to determine the "slow electron correction." The slow electron correction (SEC) compensates for the fraction of the total electron current that is due to "cold" electrons from the electron "gas" striking the electron cup. The magnitude of this current is determined by applying a few volts negative bias to the electron cup. Ths slow electron correction to the measured cross section is then given by

$$\text{SEC} = \frac{J}{J'} \tag{21}$$

where J is the electron current without bias and J' is the electron current with sufficient retarding bias supplied to plateau the change in the electron current. In the present experiment, a typical SEC is about one percent.

The retarding voltage is also applied to the electron cup when

form factor measurements are being made. If this were not done, the electron "gas" could sometimes cause substantial error in the form factor determinations. The magnitude of this retarding potential is only a few volts even when the electron energy is 1000 eV. The aperture plate is always grounded when retarding potentials are applied to the electron cup.

Pulsed Mode Operation

While it was believed that the present experiment could be operated in the continuous beam mode, provision was made for pulsed operation. Pulsed operation could thereby be used as a check for any errors caused by the electron beam modulating the gas pressure in the vacuum system. This was considered to be a potential problem at the higher electron energies. Actually, it was possible to operate the experiment below 10^{-6} Torr for all electron energies and the error introduced by the pressure modulation was negligible.

The pulsing scheme used is similar to that originally developed by Dolder et al.,[34] except that the electron beam is pulsed with the larger duty factor. It has been shown that pulsing the electron beam with the larger duty factor can result in an improvement in the signal-to-noise ratio.[49]

Pulses of variable period T are derived from a Tektronix Series 160 Pulse Generator and integrated circuit logic followed by transistor and vacuum tube pulse amplifiers. The result is an ion beam pulse that can be varied in phase delay φ and width τ with respect to the electron beam pulse. The duty cycle of the electron beam pulse is

precisely fixed at 50 percent since it is derived from a flip-flop. The ion beam duty cycle is continuously variable from zero to 50 percent. The system is changed from time-coincidence to time-anticoincidence by switching the output digital state connection of the electron beam flip-flop. Amplifiers boost the electron pulse amplitude to 55 volts and the ion beam pulse to 300 volts.

The electron pulse is applied by means of a clamping circuit to the control grid of the electron source. The output of the electron beam pulser is sufficient to cut off the electron beam at the highest electron energy of 1000 eV.

The ion beam is pulsed by moving the ion beam off a collimating slit with the F_1Y_2 deflection plate. This method of applying the pulsing signal was chosen after careful consideration of the possible alternatives. The ion beam could be pulsed in the following ways: by pulsing the ion acceleration voltage, by pulsing the ion beam extraction voltages, or by moving the ion beam off a collimating slit. The acceleration voltage was not pulsed because no method could be readily devised that would supply the required leakage current of five to ten milliamperes and at the same time ensure that the acceleration voltage amplitude was precisely established. The extraction voltage could not be used to pulse the beam as a result of it being impossible to completely cutoff the ion beam with zero extraction voltage. The ion source could be cutoff by making the extraction electrode positive with respect to the ionizing filament, but this would attract electrons to the extraction electrode. Unfortunately, the resulting electron flow would cause electron impact ionization of the barium gas within

the ion source, possibly resulting in the production of metastably excited states. The requirement that the ion beam be in its ionic ground state precluded the use of this method.

The only remaining possibility was to deflect the ion beam off a collimation slit. This method also has inherent disadvantages. The deflection plate spacing and length in the F_1 assembly is such that with a 300 volt pulse the rise and fall times of the ion beam are about 0.2 milliseconds. This is a significant fraction of the typical one to 12 milliseconds duration of the ion beam pulse. Two deleterious effects may result from the slow ion beam rise time; the ion beam and electron beam might not be in correct time phase, and the ion beam focusing properties could change during the rise and/or fall period. The first of these potential troubles is easily avoided by using the variable phase delay φ and pulse length τ controls for the ion beam pulse. By observing the actual electron and ion current waveforms on an oscilloscope, φ and τ are adjusted for proper operation.

The possibility of unusual focusing conditions introduced by pulsing was investigated in two ways. The cross section at a fixed electron energy was measured as a function of the pulse period for an ion beam with constant amplitude and duty cycle. Since the fractional time when the ion beam is changing configurations varies with the pulse length, significant changes in focusing occurring during the rise and fall periods should result in an apparent cross section which depends upon the pulse period. No such dependence was observed for pulse periods from five to 40 milliseconds having an ion beam duty cycle of about 35 percent. The second

test employed was to change the pulsing electrode from the F_1X_2 plate to the F_1X_1 plate. This caused the ion beam to be pushed in the opposite direction and thus had a different effect upon the beam focusing. When this test was performed, it was noted that the measured values of the cross sections tended to be about four percent higher than when the F_1X_2 plate was used. When the various consistency checks were applied to these data, it was found that measurements made with the F_1X_2 plate satisfied the checks to a greater degree than did those made with the F_1X_1 plate. Accordingly, the F_1X_2 plate was adopted as the pulsing electrode.

CHAPTER IV

EXPERIMENTAL PROCEDURES AND RESULTS

This chapter is concerned with the application of the theory presented in Chapter II to the practical task of obtaining the experimental electron impact cross sections with the apparatus described in Chapter III. A cross section is not derived from a single observation, but is obtained from a series of measurements including the various currents to the Ba^{2+} detector, the ion and electron currents, and the form factor. If the measured cross sections are to be as accurate as practicable with the available experimental apparatus, sufficient operational and consistency checks must be made so as to ensure that the problems associated with a charged particle-charged particle crossed beam experiment are not present.

An explanation of how the electron impact ionization signal is extracted from the several currents measured at the Ba^{2+} detector will be considered first, followed by a detailed description of the measurement procedures. A summary of the consistency checks which establish the validity of the experimental data will then be presented. Finally, the experimental results will be given together with an assessment of their probable errors.

Currents to the Ba^{2+} Detector

Currents measured at the Ba^{2+} detector include components produced by spurious collection of Ba^{+} ions and electrons from the two

crossed beams; by charge stripping and electron impact ionization of the Ba^{+} beam and by contact and thermal potentials present in the Ba^{2+} detector assembly. Notation will now be introduced to describe these components concisely. The following definitions are employed.

(1) I^{2+}_{SIG} (I, J) is that current of electron impact produced Ba^{2+} ions present when an ion beam of I amperes and an electron beam of J amperes are present in the interaction region. This current is not directly observable, but is a component of I^{2+} (I, J).

(2) I^{2+}(I, J) is that current measured at the Ba^{2+} detector with a Ba^{+} beam of I amperes and an electron beam of J amperes present in the interaction region.

(3) I^{2+}(I,0) is that current measured at the Ba^{2+} detector with only a Ba^{+} current of I amperes present.

(4) I^{2+}(0, J) is that current measured at the Ba^{2+} detector with only an electron current of J amperes present.

(5) I^{2+}(0,0) is the small background current measured at the Ba^{2+} detector with no beams present.

If the experimental apparatus is operating properly, the electron impact ionization signal, I^{2+}_{SIG} (I, J), can be extracted from the other currents enumerated above. The expression for I^{2+}_{SIG} (I, J) is obtained by noting that the signal to the Ba^{2+} collection system with both beams on is composed to the following components.

(1) I^{2+}(0, 0), a steady background current whose magnitude is unaffected by the presence or absence of the interacting beams.

(2) The noise component, $[I^{2+}(I, 0) - I^{2+}(0, 0)]$, which originates from the ion beam and is independent of the presence or

absence of the electron beam.

(3) The electron noise component $[I^{2+}(0, J) - I^{2+}(0, 0)]$, which is independent of the presence or absence of the ion beam.

(4) $I^{2+}_{SIG}(I, J)$, the electron impact ionization signal. By summing the above currents one can formally obtain the equation

$$I^{2+}(I, J) = I^{2+}_{SIG}(I, J) + [I^{2+}(I, 0) - I^{2+}(0, 0)] + [I^{2+}(0, j) - I^{2+}(0, 0)] + I^{2+}(0, 0) . \quad (22)$$

This relation, upon simplification, yields as the expression for the electron impact ionization current in terms of the observable currents to the Ba^{2+} detector

$$I^{2+}_{SIG}(I, J) = [I^{2+}(I, J) - I^{2+}(I, 0)] - [I^{2+}(0, j) - I^{2+}(0, 0)] . \quad (23)$$

From Equation (A-14) developed in Appendix I, the equation for the electron impact cross section in terms of the experimental parameters is given by

$$\sigma_{12} = \frac{I^{2+}_{SIG}}{JI} \frac{e V_i V_e}{2(V_i^2 + V_e^2)^{1/2}} F , \quad (24)$$

Equation (24) may be simplified slightly by noting that the electron velocity is always much greater than the velocity of the Ba^{+} ion, even at the lowest electron energy. Under this assumption and including the practical difficulty in the measurement of the electron current represented by the slow electron correction (SEC), the equation for the

electron impact cross section becomes

$$\sigma_{12} = \frac{e\, V_i}{2} \frac{I^{2+}_{SIG}}{J\, I} F(SEC) \ . \qquad (25)$$

This expression along with equation (14) gives the cross section in terms of the experimentally obtainable quantities. The validity of equation (25) depends upon the absence of errors in the determination of the electron impact ionization signal and the form factor. Assurance that the experiment is operating according to the theory presented in Chapter II, and that no such errors are present is obtained by subjecting the experimental data to a series of extensive consistency checks.

These consistency checks will be applied to the data derived from the present experiment after discussing the measurement procedures by which the data were procured.

Measurement Procedures

Before cross section measurements are initiated, a number of preliminary adjustments of the apparatus are necessary. These preliminary adjustments serve to eliminate sources of gross experimental error and to establish a "nominal" operating situation. Once this condition of nominal operation is established, a set of preliminary cross sections are determined and subjected to the required consistency checks. Only when such consistency checks reveal that the experiment is operating according to the requisite theory does the actual data gathering process begin.

Preliminary Adjustments

Following completion of the vacuum chamber bakeout it is necessary to wait approximately 48 hours for the background current, I^{2+} (0, 0), to decay and stabilize. Before that time, the background current is too large and unstable to permit accurate measurements. The primary sources of this current are thermal gradients, contact potentials, and stressed insulators. Once the background current has stabilized, the preliminary adjustments are made. These preliminary adjustments are listed below together with a short explanation of each.

(1) The stray electron current to the Ba^{2+} detector is minimized by means of the external magnets. The absence of appreciable stray magnetic fields in the interaction region is assured by observing the electron current to the electron cup aperture plate while operating the electron source at 10 eV indicated energy. If this current does not change appreciably as the magnets are slightly displaced from their nominal positions, the effect of the external magnets in the interaction region is small.

(2) The voltages of the electrostatic analyzer and the F_3 deflection structure are adjusted such that both the Ba^{+} and Ba^{2+} ion beams are centered on their respective exit apertures of the electrostatic analyzer. Particle losses in the analyzer are checked by doubling the analyzer voltage, thus deflecting the Ba^{+} beam into the Ba^{2+} detector. A 10^7 ohm resistor installed in the vibrating reed electrometer allows this test to be made with considerable ease. The electrostatic analyzer and F_3 deflection structure voltages are always

adjusted such that the Ba^+ currents measured at these two detectors agree to within the accuracy of the instrumentation.

(3) The Ba^+ beam is focused so as to restrict losses from the beam to less than 1.0 percent. Particle losses in the 1/32 inch dimension of the ion beam have not been encountered, but their possible presence can be determined by varying the electrostatic analyzer and the F_3 deflection structure voltages. Particle losses in the 1/4 inch dimension are measured by noting the increase in ion beam intensity resulting from application of the electron beam. The increase in ion beam intensity usually saturates at a few milliamperes electron beam intensity. Further increases in electron intensity cause a rapid drop in the ion beam intensity due to crossover in the ion beam trajectory. The ion beam loss is taken to be the fractional increase in ion beam intensity at the point of saturation.

(4) The ion beam profile is adjusted by means of the F_2 structure so as to obtain a satisfactory form factor.

(5) A check is made to assure that none of the currents to the Ba^{2+} detector are rapidly varying functions of the analyzer voltage. Such a condition may exist if the ion beam passes too close to the edge of an aperture.

(6) It has been found that the ion source extraction voltage has a significant focusing effect upon the ion beam and influences the attainability of the previous five conditions. This fact requires optimization of the extraction voltage for best performance. Usually, there is about a 20 percent plateau of extraction voltage over which the above requirements can be satisfied.

The above adjustments are interrelated and it is necessary to recheck all of them after the initial adjustment. On several occasions it has been impossible to meet all of these requirements. One of the difficulties most frequently encountered was that of obtaining a satisfactory form factor without introducing unacceptable losses in the ion beam. When this situation occurs, it is due to an unusual focusing condition in the ion source caused by a thermal "bowing" of the ionizing filament. The only remedy for this condition is to disassemble the apparatus, remove the ion source and replace the ionizing filament.

It is of importance to note that the preceeding checks are repeated each day and/or every time any operating parameter of the ion beam is changed.

Cross Section Measurements

Once the preliminary adjustments are completed, the cross section measurements can proceed. The following is the step-by-step procedure employed to obtain the ionization cross section at a particular electron energy.

(1) The electron energy, ion beam intensity, and electron beam intensity to be used in the measurement are selected.*

---

*It will be recalled that the ion beam extraction voltage influences the ion beam focusing. Therefore, the ion beam intensity is not controlled with the extraction voltage, but it is adjusted by varying the barium crucible heater power. Since the barium heater assembly has a long thermal time constant, no attempt is made to hold the ion current to an exact value. Instead, the barium ion current is allowed to vary about a nominal value. This variation is of no practical consequence, however, since it takes several days of operation for a drift of a percent or two to occur. As mentioned previously, line voltage regulation prevents short term drift.

(2) The slit scanner is lowered across the beams to provide data for the calculation of the form factor. The differential mode of measurement is normally used, but the integral mode is employed occasionally as a check. The usual scanner increment is 0.020 inch.

(3) The quantities $I^{2+}(I, J)$ and $I^{2+}(I, 0)$ are measured sequentially. Normally three measurements of each are made using the rate-of-charge mode. The length of time utilized for each determination is approximately 60 seconds. Occasionally, when making these measurements, the electrostatic analyzer voltage is varied a few percent. If the measured Ba^{2+} currents are found to be functions of the analyzer voltage, a condition of poor focusing is indicated and the preliminary adjustments must be repeated.

(4) The quantities $I^{2+}(0, J)$ and $I^{2+}(0, 0)$ are measured at least twice.

(5) Average values of $[I^{2+}(I, J) - I^{2+}(I, 0)]$ and $[I^{2+}(0, J) - I^{2+}(0, 0)]$ are calculated from (3) and (4) above, respectively. An average value of the electron impact ionization signal is then computed using equation (23).

When the above calculations are completed, the ionization cross section is obtained by substitution into equation (25). The raw data and calculated results of a typical cross section measurement are presented in Appendix II. The data are always taken at randomly varied electron energies. In addition, the electron and ion beam intensities are periodically varied to assure that the measured cross sections are independent of these parameters. Several electron energies are taken as check points and are frequently remeasured under varying conditions

to provide consistency checks. The electron energies most frequently used as check points are an energy below threshold, usually 8.0 eV, and an energy well above threshold near the peak of the cross section curve 48 eV. In addition, the 98, 198, and 298 eV points are frequently monitored so as to provide a transfer check when changing the electron source configuration. When the electron source is operated in the high energy configuration, 498 eV is the main check point. Approximately one out of five measurements is a repetition of one of these check points; this procedure facilitates close monitoring of the apparatus performance.

Consistency Checks

A consistency check is a test that establishes whether the experimental apparatus is performing in a manner predicted by the appropriate theory. A consistency test is to be distinguished from a performance check in that the latter only shows that the apparatus is operating in some nominal manner. The consistency checks for crossed beam charged particle-charged particle experiments have been discussed in Chapter II. The results of these consistency checks as applied to the present apparatus will now be given.

Cross Section Below Threshold

The measured cross section below threshold is zero to within ± 3 percent of the 48 eV value. The ± 3 percent interval includes the scatter which results from the cross section computation. Since the determination of the measured cross sections below threshold involves the arithmetic manipulation of numbers having nearly the same value, small random errors in the signal component

determinations can produce a substantial departure from the nominal zero value. Typically, the random scatter is several times larger than the mean value of cross sections measured below threshold. The average value of the measured cross section below threshold is less than one percent of the 48 eV cross section and the ensemble of values from which it is obtained shows no systematic trend; that is, positive and negative values occur with approximately equal frequency.

The measured cross sections below threshold were found to be independent of electron current, electron background, ion current and ion energy. The electron background was varied by changing the location of, or by removing the external magnets.* The lack of dependence upon any of the above quantities establishes the validity of the measurements below threshold.

The zero cross section below threshold leads to the following conclusions:

(1) The metastable $5^2D_{1/2}$ and $5^2D_{3/2}$ levels are not populated to any appreciable extent. If these levels were populated a consistently positive cross section would have been noted at the 9 eV energy value since the "tail" of the electron energy distribution overlaps the ionization energy of these metastable states.

(2) The ion beam is sufficiently well focused that there

---

*Above electron energies of about 300 eV the external magnets are required to reduce the electron background to an acceptable value. At lower energies, the magnets provide a convenient method for varying the electron background. The measured cross sections are not affected by the presence or absence of the magnets.

are no significant changes in the measured electron impact ionization signal due to the additional focusing action of the electron beam.

(3) There is no appreciable increase in the charge stripped signal component due to the pressure modulation of the chamber pressure by the electron beam and thus the continuous beam technique is valid.

While the measurement of the cross section below threshold is probably the most important check on the apparatus performance, it gives information only as to the sources of error in the determination of I_{SIG}^{2+}. A study of the variation of the cross sections above threshold as a function of the experimental parameters serves to reinforce the conclusions reached from the below threshold measurements and in addition reveals any error in the determination of the form factor.

Dependence of the Cross Section upon Electron Current

The dependence of the measured 48 eV cross section upon electron current is given in Figure 9. The ion energy is 1000 eV and the nominal ion current is 1×10^{-7} amperes. The size of the data points is chosen to represent the typical short-term random error in the measurements. The variation of the cross section with electron current is well within the acceptable error for this experiment.

An analysis of the 498 eV data shows a similar lack of dependence upon electron current and is not presented.

Dependence of the Cross Section upon Ion Current

The dependence of the measured 48 eV cross section upon the

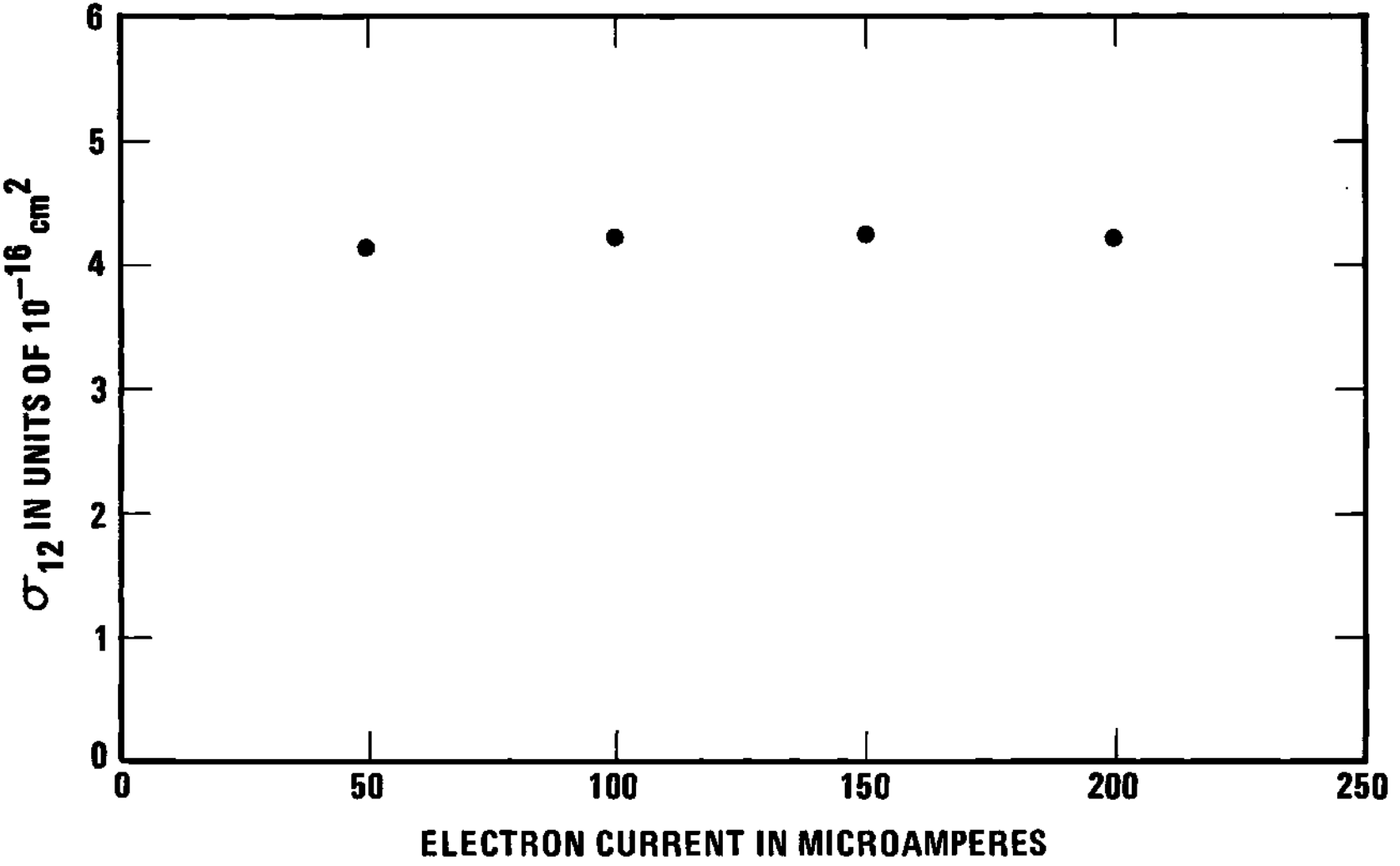

Figure 9. Dependence of the Measured Cross Section on Electron Current.

ion current if given in Figure 10. The ion energy is 1000 eV and the electron current is 100 microamperes. Again there is no systematic dependence upon the test variable.

Dependence of the Cross Section Upon the Form Factor

It is necessary that the measured cross sections be independent of changes in the beam profiles and hence of changes in the form factor. As discussed in Chapter II, this check is necessary to assure that the form factor measurement does not introduce any appreciable error in the cross section determination.

Figure 11 shows the variation of the cross section at 48 eV as a function of the form factor with all other parameters being held constant. The cross section is seen to be essentially independent of changes in the form factor except for the rolloff below about $F = 0.47$. This rolloff is shown to illustrate the effect of having a form factor which is too small. Physically, the rolloff represents the result of the ion beam becoming incapable of accommodating the space charge expansion of the electron beam. If the experiment were operated with a form factor smaller than the critical value, the measured cross sections would vary inversely with the electron current reflecting the direct dependence of the electron beam space charge blowup upon the electron beam intensity. As evident from Figure 11 such is clearly not the case when measurements are made with a value of F which is on the plateau portion of the curve. Accordingly, all data were taken with form factors in the plateau region of the curve.

Dependence of the Cross Sections upon Ion Energy

Table 2 shows the dependence of the measured cross section upon

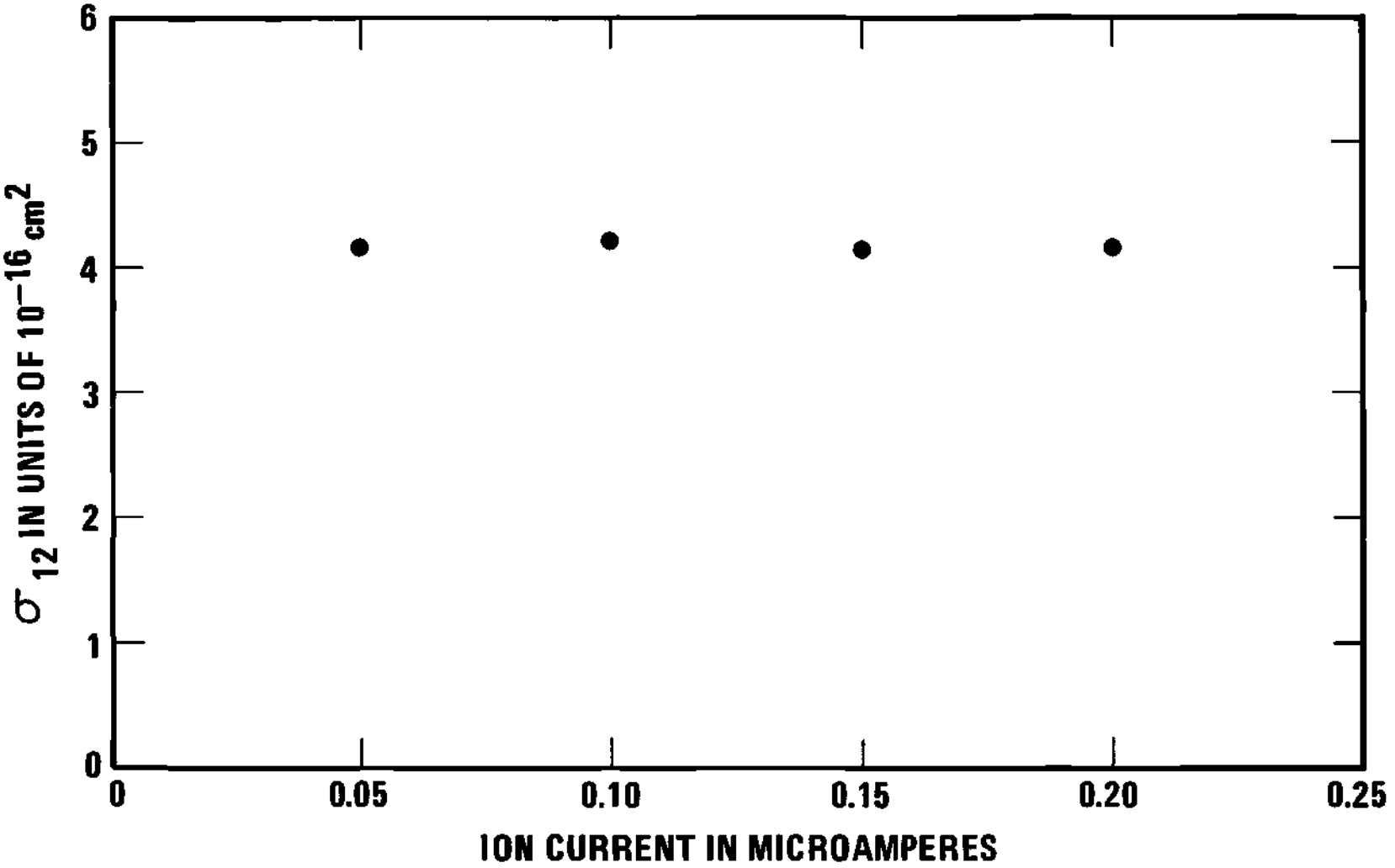

Figure 10. Dependence of the Measured Cross Section on Ion Current.

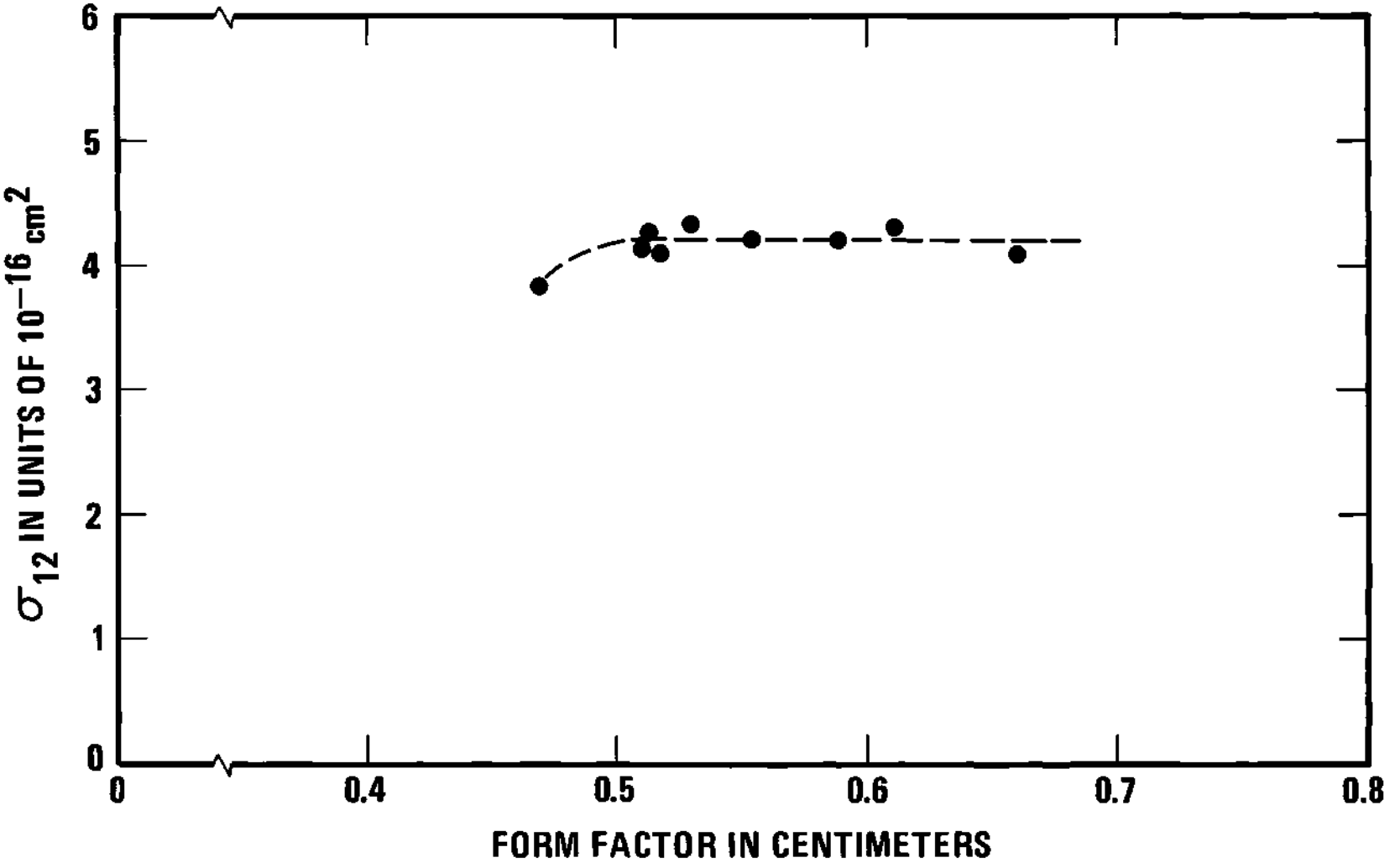

Figure 11. Dependence of the Measured Cross Section on Form Factor F.

Table 2

Dependence of σ_{12} Upon Ion Energy at Selected Incident Electron Energies

Indicated Electron Energy (eV)	Actual Electron Energy (eV)	Measured Cross Sections Units of 10^{-16} cm^2	
		1.0 keV Ions	1.4 keV Ions
50	48 ± 1	4.22	4.21
500	498 ± 2	1.64	1.66
700	698 ± 3	1.36	1.36

ion energy for several values of incident electron energy. Note that there is no systematic variation in the cross sections when the ion beam energy is increased from the usual value of 1.0 keV to 1.4 keV. This indicates that the deflection of the ion beam by the electron beam space charge is not a problem of any significance. Therefore, the electron beam space charge is not adversely affecting the measurement of the form factor.

Since the consistency checks as discussed in Chapter II have been shown to be satisfied, it is concluded that the apparatus is operating according to theory and is producing valid results.

Experimental Results

The experimentally determined absolute cross sections obtained utilizing the apparatus described in Chapter III, operating in the continuous beam mode, are given in Table 3, Figure 12 and Figure 13. Table 3, the most complete presentation, gives the uncertainty in

Table 3. Absolute Experimental Cross Sections for the Single Ionization of Ba^+ Ions by Electron Impact

Indicated Electron Energy, eV	Actual Electron Energy, eV	Cross Section Units 10^{-16} cm^2	90 Percent Confidence Limits, Percent	Maximum Experimental Scatter, Percent	Maximum Systematic Error, Percent	Maximum Total Error, Percent
10	8 ± 1	0.0	-	-	-	-
11	9 ± 1	0.0	-	-	-	-
15	13 ± 1	0.66	±8	+5 -9	±7	+12 -16
17.5	15.5 ± 1	1.94	±6	+12 -9	±7	+19 -16
20	18 ± 1	3.76	±6	+8 -9	±7	+15 -16
22	20 ± 1	4.12	±2	±2	±7	±9
25	23 ± 1	4.02	±2	+3 -5	±7	+10 -12
30	28 ± 1	4.24	±2	±3	±7	±10
35	33 ± 1	4.29	±3	+5 -4	±7	+12 -11
40	38 ± 1	4.26	±2	±3	±7	±10
45	43 ± 1	4.20	±3	+6 -5	±7	+13 -12

Table 3. Absolute Experimental Cross Sections for the Single Ionization of Ba^+ Ions by Electron Impact (Continued)

Indicated Electron Energy, eV	Actual Electron Energy, eV	Cross Section Units 10^{-16} cm^2	90 Percent Confidence Limits, Percent	Maximum Experimental Scatter, Percent	Maximum Systematic Error, Percent	Maximum Total Error, Percent
50	48 ± 1	4.22	±1	±3	±7	±10
55	53 ± 1	4.29	±3	+7 -6	±7	+14 -13
60	58 ± 1	4.09	±2	+3 -4	±7	+10 -11
70	68 ± 1	4.10	±1	±2	±7	±9
80	78 ± 1	3.97	±3	+4 -2	±7	+11 -9
90	88 ± 1	3.94	±2	±3	±7	±10
100	98 ± 1	3.72	±2	+4 -5	±7	+11 -12
150	148 ± 1	3.28	±2	+2 -4	±7	+9 -11
200	198 ± 2	2.69	±3	+4 -3	±7	+11 -10
300	298 ± 2	2.20	±1	±2	±7	±9

Table 3. Absolute Experimental Cross Sections for the Single Ionization of Ba^+ Ions by Electron Impact (Continued)

Indicated Electron Energy, eV	Actual Electron Energy, eV	Cross Section Units 10^{-16} cm^2	90 Percent Confidence Limits, Percent	Maximum Experimental Scatter, Percent	Maximum Systematic Error, Percent	Maximum Total Error, Percent
400	398 ± 2	1.87	±2	±2	±7	±9
500	498 ± 2	1.64	±1	±4	±7	±11
600	598 ± 3	1.49	±1	±3	±7	±10
700	698 ± 3	1.36	±2	+3 -5	±7	+10 -12
800	798 ± 3	1.27	±1	+2	±7	±9
900	898 ± 3	1.23	±3	+2 -4	±7	+9 -11
1000	998 ± 4	1.08	±5	+6 -5	±7	+13 -12

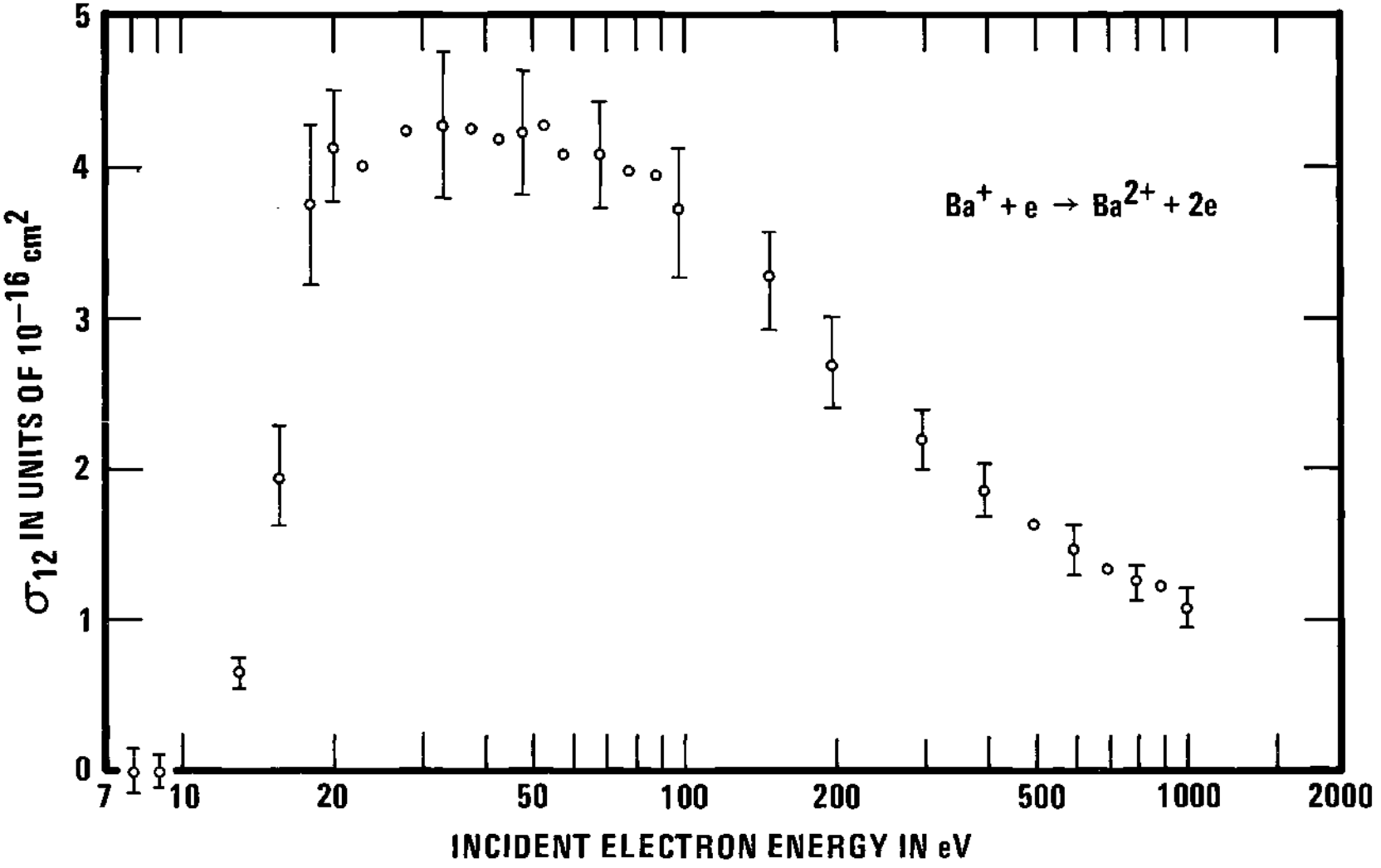

Figure 12. Absolute Experimental Cross Sections for the Single Ionization of Ba^+ Ions by Electron Impact.

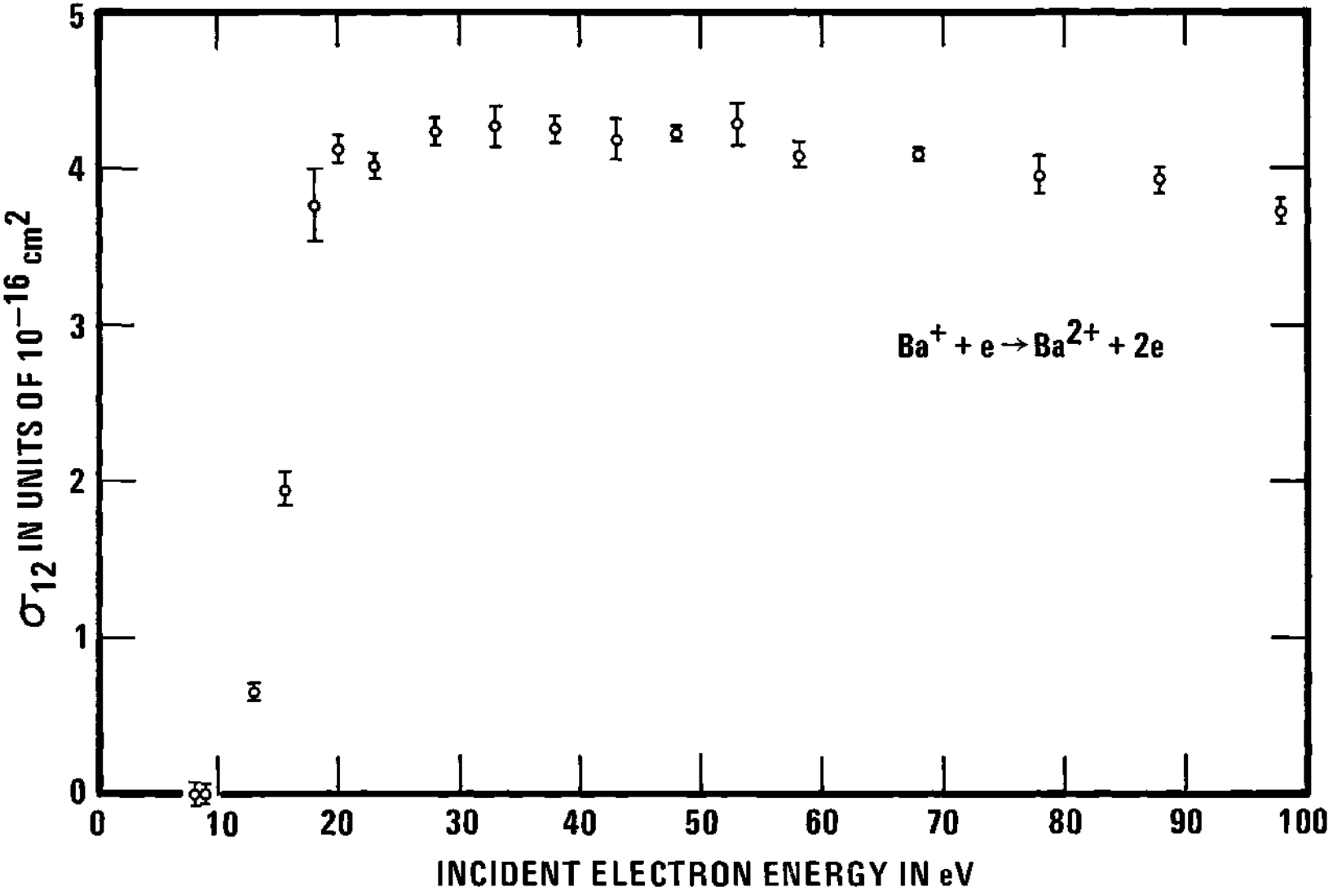

Figure 13. Low Energy Regime of Absolute Experimental Cross Sections.

the electron energy, the experimental results and a detailed breakdown of the experimental errors. Figure 12 presents all of the experimental errors. Figure 12 presents all of the experimental data graphically, with the error bars reflecting the "Maximum Total Error" as given in Table 3. Figure 13 gives the measured cross section data from below threshold to approximately 100 eV, with the error bars indicating the 90 percent confidence limits. This latter graphical presentation is useful in discussing the possible existence of structure in the cross section curve. Such a discussion is given in Chapter VI.

Some additional comments relating to the experimental data are listed below.

(1) In all cases the actual measured values of the data are given; the data do not represent points derived from a smooth curve drawn as some "best fit" to the experimental points.

(2) All of the data presented were taken with 1.0 keV ions. Additional data taken with 1.4 keV ions was used only as a check; the results of this check were given previously in Table 2.

(3) At least five valid measurements were taken at all energies with six to eight being typical. Many more measurements were taken at the various check points.

(4) The data represents only measurements made utilizing the continuous beam mode of operation. However, a comparison of measurements made by pulsed and continuous methods at selected incident electron energies is given in Table 4. The good agreement between the results obtained by these two methods demonstrates the effectiveness of the value of the cross section below threshold as an indicator of

the validity of the continuous beam technique.

Table 4

Comparison of Measurements Made by Pulsed and Continuous Methods at Selected Incident Electron Energies

Indicated Electron Energy (eV)	Actual Electron Energy (eV)	Measured Cross Sections Units of 10^{-16} cm^2	
		Continuous	Pulsed
10	8 ± 1	0.0	0.0
25	23 ± 1	4.02	4.00
50	48 ± 1	4.22	4.32
150	148 ± 1	3.28	3.26
500	498 ± 2	1.64	1.63
700	698 ± 3	1.36	1.37
1000	998 ± 4	1.08	1.04

Discussion of Errors

The total error in an experimental result is made up of the sum of the systematic errors and the random errors. Systematic errors are those which cause all measured values to be in error by the same amount or by an amount that has a definite functional dependence upon some experimental parameter. Typical sources of systematic errors are instrument calibrations and changing experimental conditions. When an experiment is repeated under unchanging conditions, the resulting data, in general, do not agree exactly. The causes of the disagreement between the individual values must also be causes of their differing from the "true" value. Errors resulting from these causes are called random

errors. Typical sources of random errors are small short-term fluctuations in some experimental condition and fluctuations due to the statistics of the process being studied.

Systematic Errors

The function of the consistency checks in the present experiment is to eliminate systematic errors in the operation of the experimental apparatus. While the consistency checks man not eliminate all of the error in the operation of the experimental apparatus, they reduce the size of the error to a level where the source of the error cannot be determined. This residual error, which probably fluctuates slightly, is then treated as a random error.

Sources of possible systematic errors that are not eliminated by the consistency checks are those due to the electron beam energy error, the ion beam energy error, and the calibration of the measuring instruments. The total systematic error is estimated to be ± 7 percent.

Electron Energy Error. An unusual error in the present experiment is that due to the energy spread and energy loss of electrons emitted by the oxide cathode of the electron source. As indicated in Chapter III, measurements indicate that the mean energy of the emitted electrons is about 2 ± 1 eV below the indicated electron acceleration energy. It was also determined that the electron energy distribution is about 1.1 eV wide at 1/2 maximum and about 4.0 eV wide at 1/10 maximum. This error is, at least in principle, a systematic error. The exact electron energy distribution could be determined and the appropriate mathematical methods used to eliminate this source of error in the measurements. Practical difficulties, however, preclude the ready

implementation of the above procedure. Accordingly, the expedient used in the present and other similar experiments[31,46] is to simply subtract the estimated cathode voltage drop from the acceleration power supply voltage to get the estimated actual electron energy. The oxide cathode voltage drop determination is then added to the electron energy power supply calibration uncertainty and is not stated as an explicit error in the cross section at some nominal electron energy. Both the energy loss in the oxide cathode and the electron energy power supply calibration error are reflected in the "Actual Electron Energy" as given in Table 3.

The problem of the finite electron energy spread is accounted for in a more qualitative fashion. The electron beam constitutes, in effect, a sampling function that is applied to the cross section during the measurement process. The width of this sampling function determines the minimum size, in energy, of any structure that can be resolved in the cross section. In the present experiment, the effective width of the electron beam as a sampling function is taken to be somewhat larger than the width at 1/2 maximum, probably about 2 eV. Therefore, any sudden discontinuity in the cross section would be observed over about a 2 eV interval. Thus the rise in the present measured cross section from 1.94×10^{-16} cm^2 at 15.5 eV to 3.76×10^{-16} cm^2 at 18 eV is consistent with the onset of the abrupt process of autoionization.

Ion Beam Energy Error. The estimated systematic error in the ion beam energy is the sum of the error in the ion beam acceleration power supply and the voltage drop across the ionizing filament. This results in an ion beam energy error of less than one percent. Since the

measured cross section varies with the ion velocity and hence as the square root of the ion energy, the systematic error in the cross section measurement due to this cause is less than 0.5 percent. As the estimate of the instrumentation error is thought to be conservative, the small component of systematic error due to the ion beam energy is not included in the total systematic error.

Instrumentation Error. The instruments used, their nominal accuracies and their calibration procedures have been described in Chapter III. The accuracies of these instruments are combined to yield the worst-case estimate of the overall accuracy. This figure of ± 7.0 percent is taken to be the systematic error of the instrumentation and the total systematic error.

Random Errors

The task of assigning meaningful random error limits is more difficult than that of evaluating the systematic error. This is because a subjective judgement is required to determine what constitutes the best estimate of the random error after consideration of both the experimental apparatus and the ultimate objective of the research.

Over a short period of time, cross section measurements made where the signal-to-noise ratio is nominal exhibit little scatter, typically on the order of one or two percent. This degree of scatter is representative of the best that could be expected from the experiment. Over a period of several weeks, however, the scatter increases to several percent. This increase in scatter is correlated to some extent with a deterioration of the apparatus' performance as monitored by the consistency checks. It was also noted that some runs deteriorated faster

than others presumably due to initial differences in the ion beam profiles and how these changed with the ageing of the ionizing filament. Oil backstreaming from the diffusion pump was also found to have some detrimental effect on the electron beam but was not observable until after about three weeks of operation. The typical operating period during which data were taken was about two weeks.

The question now arises as to what constitutes the best estimate of the random error. Clearly, the most conservative estimate of the random error is the extreme limits of the experimental scatter. This formulation however, suffers from the serious defect of producing an error that is likely to increase with the number of measurements (samples) at a given electron energy. However, the standard deviation of the samples will decrease with an increasing number of samples, if as expected, the sample mean converges to the population mean.

Since a primary purpose of the present research is to examine the cross sections for possible structure, it was deemed necessary to use some statistical estimate of how closely the sample mean approaches the population mean. Such an estimate facilitates meaningful analysis of the relative shape of the cross section curve. The 90 percent confidence limits[54] were adopted as the appropriate statistical parameter. The 90 percent confidence limits are given in Table 3 for all incident electron energies and graphically in Figure 13 for all incident electron energies below 100 eV.

When considering the absolute magnitude of the cross sections, the more conservative approach of setting the maximum total error equal to the maximum experimental scatter plus the systematic error was

adopted. Values of the maximum experimental scatter are given in Table 3 for all experimental points. The maximum total error is given in tabular form (Table 3) for all experimental points, and in graphical form (Figure 12) for a representative sample of experimental points.

CHAPTER V

COMPARISON WITH EXPERIMENT AND THEORY

In this chapter the present Ba^+ results are compared with the previous experimental results of Peart and Dolder[31] and with some theoretical approximations. The theoretical comparisons are made using classical estimates since no quantum mechanical calculations for the ionization of Ba^+ by electron impact are as yet available. The present results are compared with classically scaled Cs cross sections and with ionization cross sections calculated using the classical method due to Gryzinski.[19,41,42] Since the excitation energies of the possible autoionizing states are unavailable, the Gryzinski calculation includes only those contributions to the total ionization cross section due to direct ionization.

Comparison with Previous Experimental Results

Before comparing the two sets of experimental data it is appropriate to discuss the experimental apparatus used by Peart and Dolder[31] particularly with respect as to how it differed from the apparatus employed in the present research.

The apparatus used by Peart and Dolder was of modular construction and consisted of several stainless steel tanks bolted together. The first tank housed the water cooled surface ionization ion source and was differentially pumped by a two inch diffusion pump. Upon emerging from the ion source, the ion beam was passed through a magnetic analyzer

which removed any impurities present from the ion beam. The analyzed and collimated ion beam passed into another tank which contained the interaction region and the electron gun. A slit scanner was also provided with which to measure the beam profiles. After the interaction region, a second magnet performed an e/m analysis of the emerging beam and directed the various charge-state components into their appropriate collection cups. The beam modulation technique developed by Dolder et al.[34] was used to obtain the measured data. The pressure in the interaction region was approximately 2×10^{-8} Torr.

Aside from the constructional techniques, the major differences between the apparatus used by Peart and Dolder[31] and that used in the present research is the method of charge-state separation and the operating pressure in the interaction region. An electrostatic analyzer was used to separate the various charge states and the operating pressure was approximately 5×10^{-9} Torr in the present experimental apparatus. Peart and Dolder operated their experiment using modulated beams, but both continuous and moduated beam methods were used in the present research.

A meaningful comparison with the experimental results of Peart and Dolder is complicated by certain ambiguities which appear in their paper. Their presentation of data is inconsistent and leads to several possible conclusions depending upon one's interpretation of the text and its tabulated and graphical data. For reference purposes, the authors' tabulated data and several figures are identified and briefly discussed below.

(1) Figure 3,* page 875, gives their measured ionization cross sections in graphical form as a function of electron energy from zero to 2000 eV. An inset is included which shows the cross sections in greater detail for energies below 50 eV.

(2) Figure 4, page 876, gives a family of recorder traces showing the variation of the cross section as a function of electron energy with the electron current as a parameter. These curves are apparently considered to be qualitative since the ordinate is not scaled. The abscissa is scaled in 2 eV intervals out to about 30 eV. This figure also includes an inset which shows the energy spread of their electron beam.

(3) Table 1, page 877, lists the Ba^+ ionization cross sections and their attendent maximum total error at selected electron energies from 15 to 2000 eV.

In the abstract of their paper, in at least two places in the text and in the caption of Figure 3, the authors state that the measured cross section increases abruptly by a factor of almost three at 18 eV of electron energy. The authors also indicate in the text that the interval of rapid rise is from 18 to 20 eV of incident electron energy. An analysis of the inset in Figure 3 or of Figure 4 shows that the cross section is, respectively, slightly increasing or decreasing from 18 to 20 eV of electron energy. However, if one assumes that the 18 to 20 eV interval quoted in the text represents the uncorrected electron energies,

---

*To avoid confusion with figures and tables in the present work, all figure and table numbers referring to the paper by Peart and Dolder (Ref. 31) are underlined.

then the increase is occurring between 16 and 18 eV actual electron energy and is consistent with the graphical data. This interpretation, however, is not consistent with the statement made at the bottom of page 876 where the authors note; "A correction of 2 eV has been applied to the electron energies quoted in this paper."

If one shifts the graphical data rather than the values quoted in the text, then the cross sections given in Figure 3 would show a zero value at 12 eV and the 20 eV value would still not equal the value of 4.25×10^{-16} cm^2 quoted in the abstract. Were the graphical recorder plots in Figure 4 shifted they would qualitatively agree with the text. However, if this shift were made, the 15 eV value of the cross section given in Table 1 would no longer agree with the graphical data of Figure 3.

Another point of disagreement concerns the value of the 17 eV cross section as given in Table 1. The 17 eV cross section does not agree with either Figure 3 or Figure 4 if their respective energy scales are correct. However, the tabulated 15 eV electron energy cross section does agree well with the data presented in Figure 3, but appears to be larger than the value estimated from Figure 4. It should be recalled, however, that Figure 4 is of qualitative significance only.

There appear to be at least two possible interpretations of the authors' data that can be deduced from the above discussion. These possible interpretations are listed below.

(1) The 18 to 20 eV interval of rapid rise quoted in the text actually represents uncorrected electron energy values and

should be 16 to 18 eV actual electron energy.* Also the 17 eV cross section value given in Table 1 is probably incorrect and should be about 3 x 10^{-16} cm^2 as scaled from Figure 3.

(2) The 18 to 20 eV interval of rapid rise quoted in the text represents the actual electron energy, the 17 eV cross section value tabulated in Table 1 is correct, and all of the graphical data must be shifted in the direction of increasing energy by 2 eV to agree with the text. However, the graphical data will still not agree with all of the tabulated data.

Above about 25 eV of incident electron energy, the cross section is relatively flat and the two eV discrepancy discussed above is of little significance.

Figure 14 gives a graphical comparison between the present experimental results and those of Peart and Dolder. The results of Peart and Dolder[31] are taken from Table 1 of their paper. The data are presented on a semi-logarithmic plot and the maximum total error limits are indicated for a representative sample of data points. As can be seen from the figure, the agreement between the two sets of data is generally good and is well within the combined experimental error. There appears to be a slight disagreement near 17 eV of incident electron energy.

---

*This interpretation seems to be reinforced by information given by Dolder in Ref. 48. In this reference, Dolder gives a figure (Figure 5-3-7) that appears to be a duplicate of Figure 3. However, in the text of this reference as well as in the caption of Figure 5-3-7, Dolder indicates that the cross section increase occurs between 16 and 18 eV due to the onset of autoionization. No reference or other statement is given as to why the 16 to 18 eV interval is quoted in Ref. 48, but an 18 to 20 eV value is given in Ref. 31. The tabulated cross sections given in Ref. 48 are the same as those given in Ref. 31.

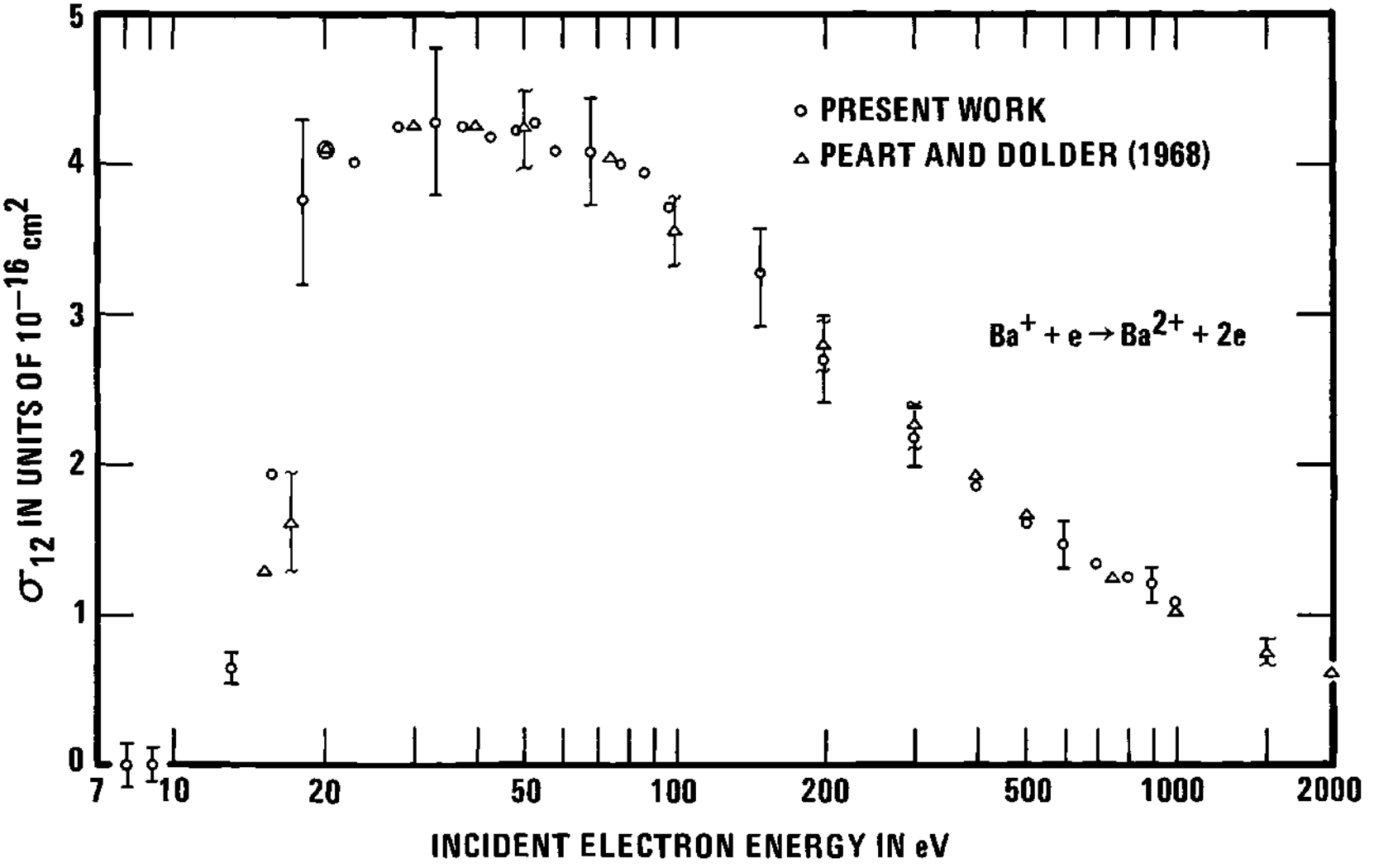

Figure 14. Comparison with Previous Experimental Results.

The cross section measured by Peart and Dolder has the value of 1.6×10^{-16} cm^2 at that point while the result of the present research is about 3.0×10^{-16} cm^2. This may indicate that the first interpretation of the aforementioned authors' results is correct. However, if one includes the combined uncertainty in the electron energy of ±3.0 eV, then the experimental agreement is satisfactory under either interpretation. In the region of rapid rise of the cross section, which according to the present data is from about 15.5 to 18 eV of incident electron energy, the cross section increases from 1.94×10^{-16} cm^2 to about 3.76×10^{-16} cm^2. This value is comparable to that scaled from Figure 3 of the previous results, but does not agree with the abstract or with other statements within the paper. Once again, the electron energy spread and energy offset are of considerable importance in these comparisons. In addition, the experimental scatter is not reflected in the above figures.

The overall agreement with the experimental results of Peart and Dolder[31] is thus seen to be quite good throughout the entire range of incident electron energy. No comparisons can be made as to possible structure away from the threshold region since Peart and Dolder apparently obtained their tabulated data from a smooth curve drawn as some "best fit" through the experimental points. The slight dip at 19 eV recorded by Peart and Dolder in Figure 4 of their paper was either not observed in the present work or was lost in averaging the data. The experimental scatter at the 18 and 20 eV points is sufficient to mask such structure. Additional comments regarding possible structure in the

cross section curve are given elsewhere in this chapter and in the next chapter.

Comparison with Theory

The present results are first compared with classically scaled Cs ionization cross sections. The method of classical scaling is based upon Thomson's[39] classical model for ionization previously discussed in Chapter I. If one knows a particular cross section $\sigma_1(x)$, where x is the reduced incident electron energy as defined by Equation (8), then any other cross section $\sigma_2(x)$ can be written as

$$\sigma_2(x) = \sigma_1(x)\left[\frac{I_1}{I_2}\right]^2 \frac{N_2}{N_1} \tag{26}$$

where I_1 and N_1 are, respectively, the ionization energy and the number of electrons having that energy for target number one; I_2 and N_2 are similarly defined for target number two. For members of an isoelectronic sequence $N_1 = N_2$ and thus

$$\sigma_2(x) = \left[\frac{I_1}{I_2}\right]^2 \sigma_1(x) \tag{27}$$

which is a particularly simple result. Since Equation (26) is based upon Thomson's theory, it is strictly valid only for neutral atoms, but holds reasonably well for ions in the limit of large incident electron energies where the effects of the different nuclear Coulomb fields become insignificant. The simple law given by Equation (27) holds quite well for the isoelectronic pairs, $H(He^+)$; $He(Li^+)$ and

$A(K^+)$. It holds to within about 15 percent for $Na^+(Mg^{2+})$ but fails for $Ne(Na^+)$.

Figure 15 presents the classically scaled cross section for the ionization of Cs by electron impact compared with the present experimental results for the ionization of Ba^+. The Cs cross sections were obtained from the absolute measurements of McFarland and Kinney,[11] with the low energy measurements of Heil and Scott[12] normalized to those of McFarland and Kinney at 50 eV. One notes that the apparent structure in the Ba^+ cross section is only about two percent in relative magnitude and is thus smaller than the total error in the measurement, such structure cannot conclusively be regarded as being present. Study of Figure 15 also indicates that the experimental results could possibly be converging to the scaled Cs values. However, extrapolation to $x = 200$ shows that the scaled cross section is then only about 60 percent of the measured value thus indicating a very slow convergence. It therefore must be concluded that classical scaling provides a poor estimate of the cross section for this particular process. A possible explanation for this discrepancy could be the failure of the scaling process to properly account for the presence of autoionization and inner shell ionization.

The present results are also compared with calculations made using the classical method due to Gryzinski.[19,41,42] This calculation was made to demonstrate the qualitative influence of inner shell ionization upon the shape of the cross section curve. The Gryzinski method was chosen over other classical approximations because it gives the correct asymptotic dependence for the cross section and it has been

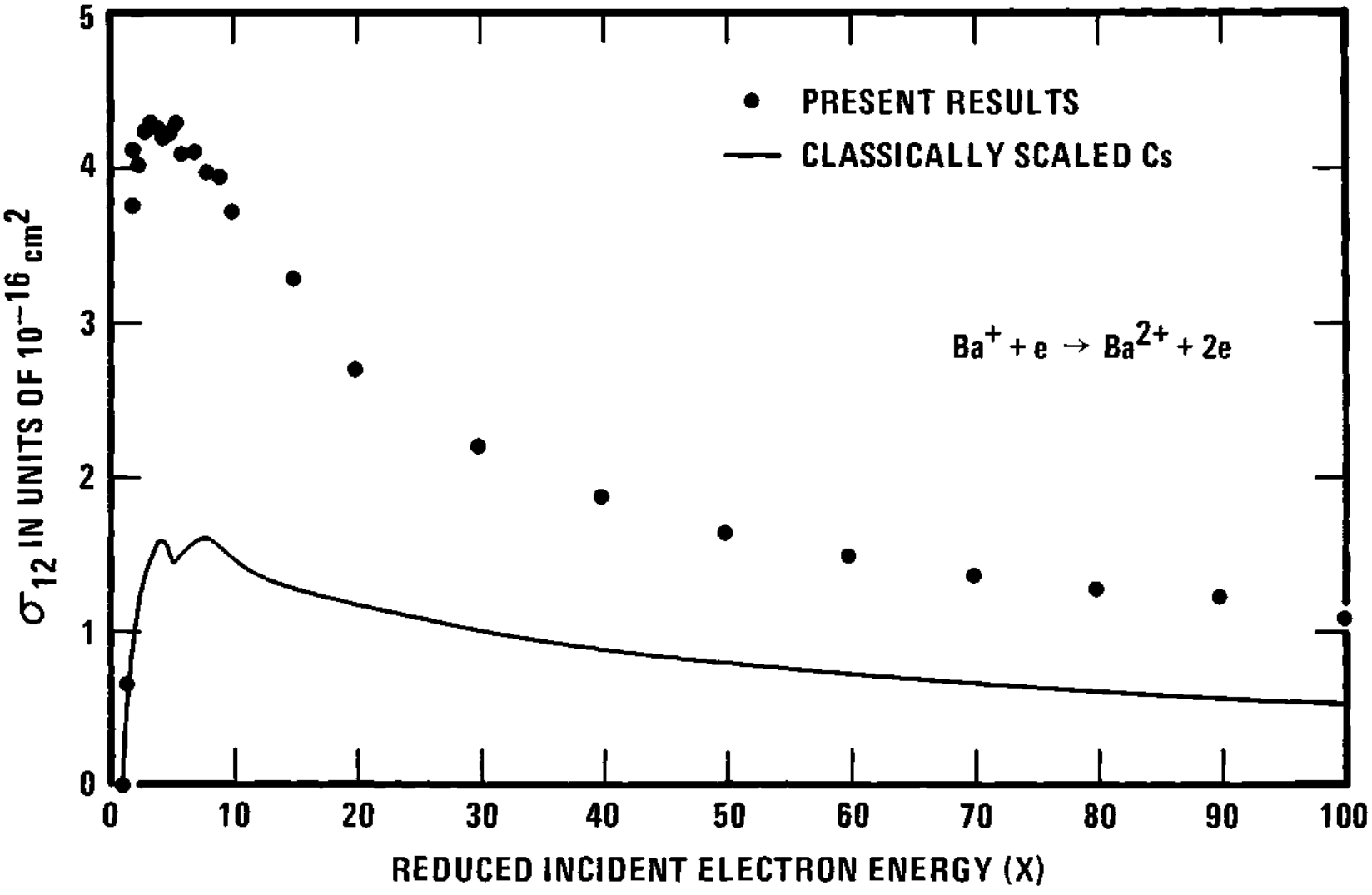

Figure 15. Comparison with Classically Scaled Cs.

demonstrated to give reasonably good results for the alkali metal atoms which are isoelectronic to the alkaline earth ions. Before giving the results of the Gryzinski-type calculations, a few of the most basic ideas involved in the method are discussed.

While Thomson's early theory assumed that the target electrons were initially at rest, Gryzinski (and also others[36,37]) has taken the more realistic approach of considering the motion of the atomic electrons. Gryzinski started with the classical results of Chandrasekhar[55] and Chandrasekhar and Williamson[56] who calculated the energy transfer between two particles moving with respect to one another and interacting through an inverse square law force. Gryzinski assumed the collision process to be a binary encounter between the target electron and the incident electron. Under this simplification the electrons interact with each other only and not with the nucleus. Gryzinski then removes the explicit dependence on the velocity of the atomic electrons by integrating over an assumed velocity distribution. His velocity distribution, which was empirically chosen to give the correct asymptotic dependence to the cross section, can be shown to be physically incorrect. Next, Gryzinski makes the assumption that the average atomic velocity can be expressed in terms of the electronic binding energy by the simple kinetic energy relationship

$$I = 1/2\ mv_0^2 \tag{28}$$

where I is the binding energy, m is the electronic mass and v_0 is the average velocity of an atomic electron. This assumption is good for hydrogen, but is likely to be rather crude in other cases.

However, if one adopts a pragmatic attitude and accepts the above approximations used by Gryzinski, the expression for the total cross section for ionization by electron impact is given by

$$\sigma(x) = 6.56 \times 10^{-14}\ eV^2\ cm^2 \sum_k \frac{1}{I_k^2} \frac{1}{x}\left[\frac{x-1}{x+1}\right]^{3/2} \left\{1 + \frac{2}{3}\left(1 - \frac{1}{2x}\right) \ln\left[2.7 + (x-1)^{1/2}\right]\right\} \tag{29}$$

where k is the number of shells, N_k is the number of electrons in the k^{th} shell and I_k is the ionization potential in eV for an electron in the k^{th} shell. The reduced incident electron energy x takes the usual form for each shell.

Figure 16 shows the present experimental results compared with cross sections calculated using Equation (29). Contributions from the 5s, 5p and 6s shells are included in the total ionization cross section. Since the total calculated cross section is only about 50 percent of the experimentally determined value at 1000 eV electron energy, the quantitative agreement between the experimental and theoretical values is poor. However, one will note that the shape of the Gryzinski calculation agrees in general with the measured cross sections except that the peaks do not occur at the same electron energy and the threshold behavior of the two cross sections is different. If the calculated cross section is normalized to the measured cross section at 500 eV, this relative agreement is more apparent. The normalized Gryzinski calculation is found to be about 15 percent low at 50 eV electron energy and about 3.5 percent high at 100 eV electron energy.

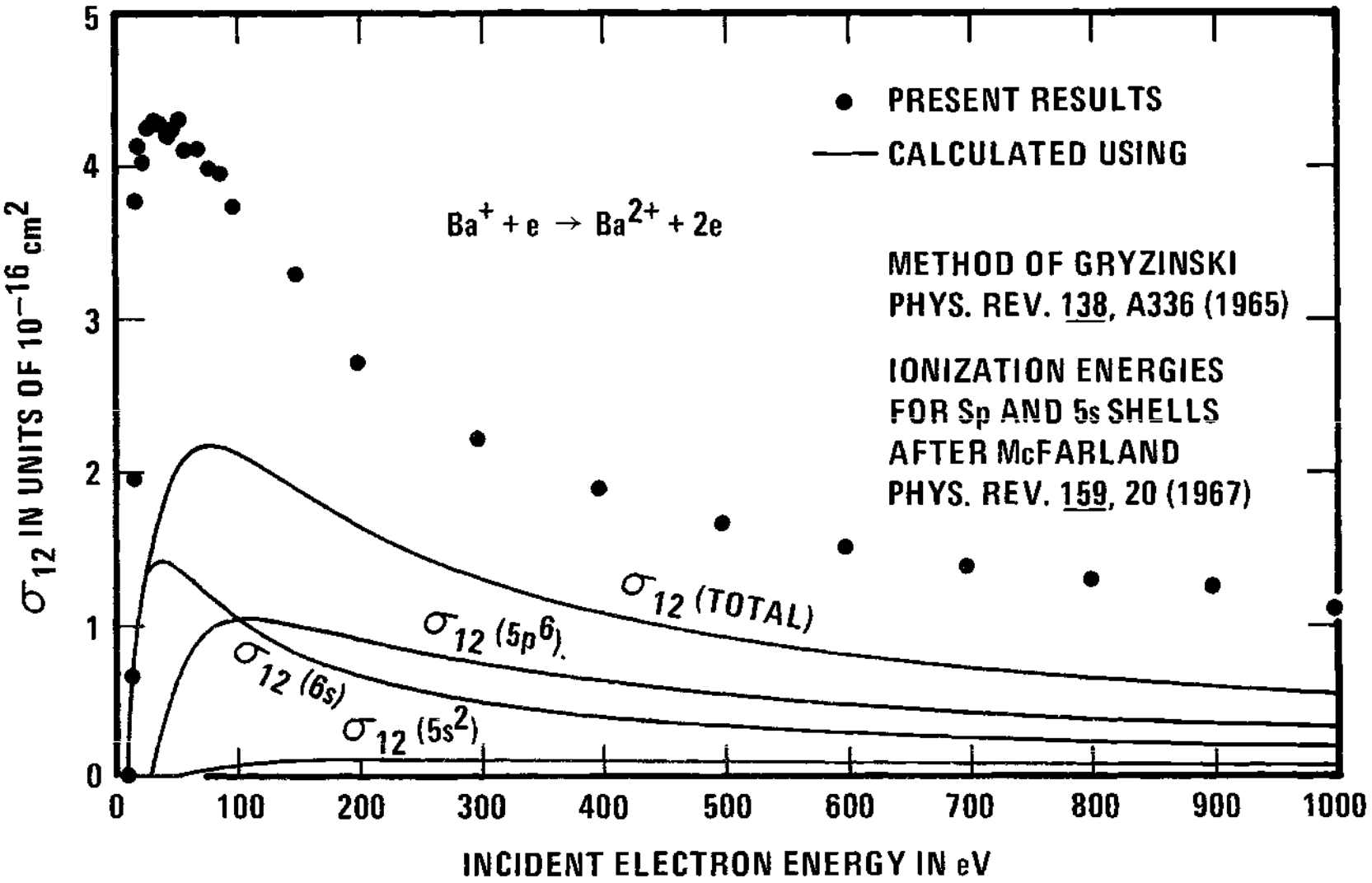

Figure 16. Comparison with Cross Sections Calculated Using the Classical Method Due to Gryzinski.

This represents a reasonable degree of relative agreement. If for example, only the ionization of the 6s valence electron had been included in the calculation, the normalized cross section at 50 eV electron energy would be 170 percent of the measured value and that at 100 eV, 150 percent of the measured value. It thus appears that the shape of the experimentally determined cross sections can be adequately explained only if contributions from the closed shells are included in the total cross section. One should note that the inner shell ionization energies estimated by McFarland[43] could be slightly in error and better estimates would either improve or worsen the quantitative agreement with the experimental results. The qualitative conclusion that the inner shell contributions are required to adequately explain the shape of the cross section curve would not be affected.

CHAPTER VI

CONCLUSIONS

The absolute cross sections for the single ionization of Ba^+ ions by electron impact have been measured for incident electron energies from below threshold (10.001 eV) to approximately 1000 eV. These measurements were performed under both continuous and pulsed beam conditions in a crossed beam apparatus operating at a residual gas pressure of approximately 5×10^{-9} Torr. The apparatus used was a modified version of that developed by Lineberger.[46]

The experimental results are presented graphically in Figures 12 and 13 as well as in tabular form in Table 3. Careful consistency checks were performed to ensure that the experimental data are free from systematic error arising from such causes as pressure modulation of the background gas, focusing of the ion beam by the electron beam, and errors in the profile determination.

The experimental results as shown in Figure 13 indicate that the slope of the cross section curve increases sharply at about 15 eV incident electron energy. The cross section then rapidly rises from 1.94×10^{-16} cm^2 to 3.78×10^{-16} cm^2 between 15.5 and 18 eV. This rapid rise is consistent with the onset of autoionization when the energy spread of the electron beam is considered. The cross section also appears to have some variation of apparently systematic nature between about 20 and 100 eV. This apparent structure can be seen with a compressed energy scale in Figures 15 and 16. The relative magnitude of these variations is of the order of the 90 percent confidence limits of

the random error. Thus while the maximum total error is substantially greater than the magnitude of these variations, the size of the variations as compared with the confidence limits, which better reflect the short term error of the data, indicate that there is some possibility of structure existing in the cross sections below about 100 eV. An additional point to note is that the experimental measurements were made at randomly selected energies and it is thus unlikely that the apparent structure is the result of the particular experimental procedure. It is impossible at the present time to deduce any specific cause of the apparent structure. If it is indeed present, the structure is probably due to a combination of both inner shell ionization and autoionization. Additional theoretical work will be required to definitely establish the existence, and if it is present the origin of this apparent structure. The present experimental results should provide an excellent incentive for such a theoretical investigation.

As seen in Figure 14 the present results are in good agreement with the previous results of Peart and Dolder.[31] Certain inconsistencies in their paper prevent a definitive comparison of results near threshold where the rapid rise apparently due to autoionization occurs. However, if it is assumed that the graphical data given by Peart and Dolder are correct, then the threshold of autoionization and the magnitude of the change in the cross section as given by them is in good agreement with the present results. At energies where the 2 eV inconsistency in their data is unimportant, the present results agree with those of the above authors to well within the combined experimental

error. No experimental comparison as to structure (other than the autoionization near threshold) can be made, since apparently the data of Peart and Dolder are taken from a smooth curve drawn as some "best fit" through their experimental points.

The present results are quantitatively in poor agreement with classically scaled Cs ionization cross sections. There is, however, some apparent similarity in the behavior of the cross sections near their peak values. The existence of this similarity, which can be seen in Figure 15, is based on the assumption that the structure near the peak of the Ba^+ experimental cross sections is real. This point, as discussed above, has not been conclusively demonstrated.

Calculations made using the classical method of Gryzinski[19] with the ionization energies estimated by McFarland[43] are in poor absolute agreement with the present results. This comparison is presented in Figure 16. The qualitative shape of the cross section curve obtained by using Gryzinski's method suggests that inner shell ionization is of definite significance in the ionization of Ba^+ by electron impact.

A P P E N D I C E S

APPENDIX I

DERIVATION OF σ_{12} IN TERMS OF EXPERIMENTAL PARAMETERS

From the definition of a cross section, the number of ionizing events R' per unit volume per second is given by

$$R' = n_i n_e V_r \sigma_{12} \tag{A-1}$$

where n_i and n_e are the number densities of the ions and electrons, respectively, V_r is the relative velocity of the colliding particles and σ_{12} is the cross section for the ionization process. If the ions and electrons move in mutually perpendicular, well colimated beams parallel to the X and Y axes respectively, their number densities and relative velocity can be obtained from

$$n_i(y, z) = \frac{S_i(y, z)}{e V_i} \tag{A-2}$$

$$n_e(x, z) = \frac{S_e(x, z)}{e V_e} \tag{A-3}$$

$$V_r = (V_i^2 + V_e^2)^{1/2} \tag{A-4}$$

Here S_i and S_e are the two electric current densities, which are in general nonuniform, e is the electronic charge and V_i and V_e are the particle velocities.

Substitution into Equation (A-1) and multiplications by the differential volume element gives as the number of ionizing events per second

$$R'(x,y,z)dx\,dy\,dz = \frac{(V_i^2 + V_e^2)^{1/2}}{e^2 V_i V_e}\,\sigma_{12} S_i(y,\ z) S_e(x,z)dx\,dy\,dz\ . \quad \text{(A-5)}$$

Physical arguments lead directly to a simplification of Equation (A-5). The expressions $S_i(y,z)$ and $S_e(x,z)$ indicate that the ion and electron current densities depend upon all position coordinates. Actually, electron motion in the y-direction averages out any ion density variations in the y-direction. Similarly, the ions traveling in the x-direction average out possible electron beam nonuniformities in that direction. Thus the only density variation that needs to be considered is in the z-direction. Equation (A-5) may now be rewritten as

$$R'(z)dz = \frac{(V_i^2 + V_e^2)^{1/2}}{e^2\ V_i V_e}\ \sigma_{12}\ i(z)\ j(z)\ dz \quad \text{(A-6)}$$

where $i(z)$ and $j(z)$ are, respectively, the one-dimensional ion and electron current densities. Upon integration, the expression for the number of ionizing events per second becomes

$$R = \frac{(V_i^2 + V_e^2)^{1/2}}{e^2\ V_i V_e}\ \sigma_{12} \int_{z_{ie}} i(z)\ j(z)\,dz \quad \text{(A-7)}$$

where z_{ie} is that region along the z axis where nonvanishing current densities exist simultaneously. It is convenient to write Equation

(A-7) in such a manner as to include the total currents, ion and electron, in the expression. Now,

$$I = \int_{z_i} i(z)\, dz \tag{A-8}$$

and

$$J = \int_{z_e} j(z)\, dz \tag{A-9}$$

where J is the total electron current, I is the total ion current, z_i and z_e are, respectively, the linear extent of the ion and electron beams on the z axis. By simultaneously multiplying and dividing Equation (A-7) by the product of the two currents, one obtains

$$R = \frac{(V_i^2 + V_e^2)^{1/2}}{e^2 V_i V_e}\, \sigma_{12}\, I\, J\, \frac{\int_{z_{ie}} i(z)\, j(z)\, dz}{\int_{z_i} i(z)\, dz \int_{z_e} j(z)\, dz} \cdot \tag{A-10}$$

Equation (A-10) can now be solved for the cross section to yield

$$\sigma_{12} = \frac{e^2 V_i V_e}{(V_i^2 + V_e^2)^{1/2}}\, \frac{F}{I\, J}\, R \tag{A-11}$$

where the form factor F is given by

$$F = \frac{\int_{z_i} i(z)\,dz \int_{z_e} j(z)\,dz}{\int_{z_{ie}} i(z)\,j(z)\,dz} \cdot \qquad \text{(A-12)}$$

In the present experiment, the number of ionizing events per second is not counted, but is obtained indirectly from the measured I_{SIG}^{2+} current. Therefore,

$$R = \frac{I_{SIG}^{2+}}{2e} \cdot \qquad \text{(A-13)}$$

The factor of two in the denominator arises because of the doubly charged ions. Finally, the expression for the electron impact cross section in terms of the experimental parameters becomes

$$\sigma_{12} = \frac{e\,V_i V_e}{(V_i^2 + V_e^2)^{1/2}} \frac{I_{SIG}^{2+}}{IJ} F \cdot \qquad \text{(A-14)}$$

To obtain a finite approximation for F, let the range of integration in Equation (A-12) be uniformly partitioned into segments of length Δz. Then F may be approximated by

$$F \approx \frac{\Delta z \sum_k i_k \sum_k j_k}{\sum_k i_k j_k} \qquad \text{(A-15)}$$

where i_k is the average ion current density in the k^{th} partition and j_k is the average electron current density in the k^{th} partition.

If a movable slit scanner, with ion slit height h_i and electron slit height h_e were positioned such that the slits were centered on the k^{th} partitions, then,

$$i_k = \frac{\Delta I_k}{h_i} \tag{A-16}$$

and

$$j_k = \frac{\Delta J_k}{h_e} \tag{A-17}$$

where ΔI_k is the positive ion current passing through the ion slit in the k^{th} position and ΔJ_k is the electron current passing through the electron slit in the k^{th} position. Upon substitution, the slit heights cancel and there results,

$$F \cong \frac{\Delta z \sum_k \Delta I_k \sum_k \Delta J_k}{\sum_k \Delta I_k \Delta J_k} . \tag{A-18}$$

Thus if the slit scanner is moved across the beams in uniform steps of length Δz, the resulting ion and electron currents, measured as a function of slit position can be used in Equation (A-18) to calculate F. This last expression is the desired approximation to F. It is important to note that the only relevant dimension in this expression is the spacing between slit positions, Δz; other dimensions, such as the overall height of the ion beam and the heights of the scanning slits, cancel out.

APPENDIX II

TYPICAL EXPERIMENTAL PARAMETERS AND DATA

Typical experimental parameters and data are presented in Tables 5, 6, and 7. Table 5 gives the operating parameters of the experimental apparatus as recorded before data series 65-C. All electrode voltages and other experimental parameters were recorded on this sheet together with the results of the preliminary adjustments of the experimental apparatus. A new sheet was begun and the preliminary adjustments were repeated either when some parameter of the ion beam was changed, or at the start of a new measurement period.

Table 6 gives a typical beam profile data sheet. The calculation of the form factor with these data was carried out on this sheet. Information for the determination of the slow electron correction was also conveniently recorded here.

The result of a typical data run is given in Table 7. The measured values of the various signal components were recorded together with all other information required to evaluate the experimental cross section.

TABLE 5. TYPICAL OPERATING PARAMETERS.

PUMPDOWN NO. 65
SERIES 65–C
DATE 8 SEP 1970

ION OPTICS OPERATING VOLTAGES

F_1X_1 = +14 V	F_2X_1 = –056 DIAL
F_1X_2 = 0 V	F_2X_2 = +096 DIAL
F_1Y_1 = 0 V	F_3Y_1 = +324 DIAL
F_1Y_2 = –9 V	F_3Y_2 = –270 DIAL

ION SOURCE

NOMINAL ION CURRENT = 1.1×10^{-7} A. ION ENERGY = 1.0 keV

EXTRACTION = 270 V REPELLER = 0 V

ELECTROSTATIC ANALYZER

ANALYZER VOLTAGE = 690 V CKECK PLATEAU – OK

COLLECTION CUPS

ION CUP SUPPRESSOR = 300 V I^{2+} CUP APERTURE = –100V

ELECTRON CUP SUPPRESSOR = 90 V RETARDING = 0 V

PARTICLE LOSS IN ANALYZER

I^+ IN I^+ CUP = 1.15×10^{-7} A I^+ IN I^{2+} CUP = 1.15×10^{-7} A

I^+ SATURATES AT 1.15×10^{-7} A ION CURRENT WITH ELECTRON CURRENT OF 1.0 mA.

PERCENT FOCUS = 0

MODE

~~PULSED~~ CONTINUOUS

PULSE PERIOD = N/A

ION BEAM DUTY FRACTION = N/A

FOCUS VOLTAGES

F_1 FOCUS = 0 V F_2 FOCUS = –50 V F_3 FOCUS = –200 V

COMMENTS

MAGNETS NOT USED IN THIS SERIES

TABLE 6. TYPICAL FORM FACTOR DATA SHEET.

DIFFERENTIAL FORM FACTOR
TAKEN (BEFORE) (~~AFTER~~) RUN NO. 65–C–1

	INITIAL	FINAL
J	150×10^{-6}	148×10^{-6}
I	1.15×10^{-7}	1.15×10^{-7}

MICROMETER POSITION	ΔJ (A)	ΔI (A)	$\Delta J\ \Delta I$ (A^2)
820	0.0×10^{-6}	0.000×10^{-8}	0.000×10^{-14}
840	0.0	0.010	0.000
860	0.0	0.110	0.000
880	0.0	0.395	0.000
900	0.0	0.750	0.000
920	0.0	0.980	0.000
940	0.4	1.060	0.424
960	2.4	1.060	2.544
980	13.5	1.030	13.905
1000	35.0	0.980	34.300
1020	49.0	0.955	46.795
1040	38.0	0.945	35.910
1060	15.0	0.930	13.950
1080	2.6	0.880	2.288
1100	0.0	0.740	0.000
1120	0.0	0.490	0.000
1140	0.0	0.235	0.000
1160	0.0	0.075	0.000
1180	0.0	0.010	0.000
1200	0.0	0.000	0.000
0.020 INCH	155.9×10^{-6}	11.635×10^{-8}	150.116×10^{-14}
ΔM	$\Sigma\ (\Delta J)$	$\Sigma\ (\Delta I)$	$\Sigma\ (\Delta J\ \Delta I)$

SEC DATA

$J = 150 \times 10^{-6}$

$J' = 148 \times 10^{-6}$

$SEC = \frac{J}{J'} = 1.01$

PRESSURE

2.7×10^{-9} TORR

$$F = \frac{2.54\ \Delta M\ \Sigma\ (\Delta J)\ \Sigma\ (\Delta I)}{\Sigma\ (\Delta J\ \Delta I)} = \frac{(5.08 \times 10^{-2})\ (1.559 \times 10^{-4})\ (11.635 \times 10^{-8})}{(150.116 \times 10^{-14})} = 0.614\ cm$$

TABLE 7. TYPICAL CROSS SECTION MEASUREMENT DATA.

RUN NO. 65–C–1	ELECTRON ENERGY 50 eV		DATE 9 SEP 1970
MEASURED SIGNALS (AMPERES)			
$I^{2+}(I, J)$	$I^{2+}(I,0)$	$I^{2+}(0, J)$	$I^{2+}(0,0)$
4.400×10^{-14}	0.760×10^{-14}	-0.367×10^{-14}	-0.042×10^{-14}
4.367×10^{-14}	0.775×10^{-14}	-0.358×10^{-14}	-0.033×10^{-14}
4.380×10^{-14}	0.775×10^{-14}	——	——
AVERAGE 4.382×10^{-14}	AVERAGE 0.770×10^{-14}	AVERAGE -0.362×10^{-14}	AVERAGE -0.038×10^{-14}
$\langle I^{2+}(I, J)\rangle - \langle I^{2+}(I, 0)\rangle = 3.612 \times 10^{-14}$		$\langle I^{2+}(0, J)\rangle - \langle I^{2+}(0, 0)\rangle = -0.324 \times 10^{-14}$	
OTHER MEASURED QUANTITIES			
ION ENERGY = 1.0 keV		ION CURRENT = 1.15×10^{-7} A	
ELECTRON CURRENT = 150 μA	ELECTRON APERTURE CURRENT = 0.1 μA	SLOW ELECTRON CORRECTION SEC = 1.01	
ION BEAM CONVER GENCE = 0% WITH 1.0 mA ELECTRON BEAM		FORM FACTOR F = 0.614 cm	
CALCULATIONS			

$$I^{2+}_{SIG} = [\langle I^{2+}(I, J)\rangle - \langle I^{2+}(I, 0)\rangle] - [\langle I^{2+}(0, J)\rangle - \langle I^{2+}(0, 0)\rangle]$$

$$I^{2+}_{SIG} = 3.936 \times 10^{-14} \text{ A.}$$

$$\sigma_{12} = \frac{ev_i}{2} \times \frac{I^{2+}_{SIG}}{I \times J} \times F \times SEC = \frac{(3.003 \times 10^{-13})(3.936 \times 10^{-14})(.614)(1.01)}{(1.15 \times 10^{-7})(1.50 \times 10^{-4})}$$

$$\sigma_{12} = \frac{7.3299 \times 10^{-27}}{1.725 \times 10^{-11}} = 4.25 \times 10^{-16} \text{ cm}^2$$

BIBLIOGRAPHY*

1. E. H. S. Burhop, The Auger Effect and Other Radiationless Transitions (Cambridge University Press, New York, 1952), Chapter 1.

2. Ibid., pp. 171-174.

3. E. U. Condon and G. H. Shortley, The Theory of Atomic Spectra (Cambridge University Press, New York, 1967), p. 371.

4. A. Temkin, editor, Autoionization, Astrophysical, Theoretical, and Laboratory Experimental Aspects (Mono Book Corp., Baltimore, 1966).

5. M. O. Krause and T. A. Carlson, Phys. Rev. 158, 18 (1967).

6. I. Bergstrom, Beta- and Gamma-Ray Spectroscopy, edited by K. Siegbahn (North-Holland Pub. Co., Amsterdam, 1955), p. 628.

7. J. P. Tate and P. T. Smith, Phys. Rev. 46, 733 (1934).

8. Y. Yaneko, J. Phys. Soc. Japan 16, 2288 (1961).

9. G. O. Brink, Phys. Rev. 127, 1204 (1962).

10. G. O. Brink, Phys. Rev. 134, A345 (1964).

11. R. H. McFarland and J. D. Kinney, Phys. Rev. 137, A1058 (1965).

12. H. Heil and B. Scott, Phys. Rev. 145, 279 (1966).

13. K. J. Nygaard, J. Chem. Phys. 49, 1995 (1968).

14. R. H. McFarland, Phys. Rev. 139, A40 (1965).

15. J. D. Garcia, J. Chem. Phys. 47, 3679 (1967).

16. S. S. Prasad, Proc. Phys. Soc. (London) 92, 871 (1967).

17. C. E. Moore, Natl. Bur. Std. (U. S.), Circ. No. 467, Vol. I, 1949; Vol. II, 1952; Vol. III, 1958.

18. H. Beutler and K. Guggenheimer, Z. Phys. 88, 25 (1934).

---

*Abbreviations used herein conform to those found in the American Institute of Physics Style Manual (1969).

BIBLIOGRAPHY (Continued)

19. M. Gryzinski, Phys. Rev. 138, A336 (1965).

20. H. W. Drawin, Z. Phys. 164, 513 (1961).

21. P. Feldman and R. Novick, Phys. Rev. 160, 143 (1967).

22. S. S. Prasad and K. Prasad, Proc. Phys. Soc. (London) 82, 655 (1963).

23. M. R. C. McDowell, Case Studies in Atomic Collision Physics, Vol. I, edited by E. W. McDaniel and M. R. C. McDowell (North Holland Pub. Co., Amsterdam, 1969), Chapter 2.

24. M. R. H. Rudge, Rev. Mod. Phys. 40, 564 (1968).

25. S. Geltman, Topics in Atomic Collision Theory (Academic Press, New York, 1969), pp. 152-167.

26. O. Bely and H. Van Regemorter, Ann. Rev. Astron. Astrophys. 8, 329 (1970).

27. B. L. Moiseiwitsch and S. J. Smith, Rev. Mod. Phys. 40, 238 (1968).

28. M. O. Pace, Absolute Experimental Cross Sections for the Excitation of Barium Ions by Electron Impact, Ph.D. thesis, Georgia Institute of Technology, Atlanta, Georgia, 1970.

29. E. Hinnov, T. K. Chu, H. Hendel, and L. C. Johnston, Phys. Rev. 185, 207 (1969).

30. S. O. Martin, B. Peart, and K. T. Dolder, J. Phys. B 1, 537 (1968).

31. B. Peart and K. T. Dolder, J. Phys. B 1, 872 (1968).

32. O. Bely, J. Phys. B 1, 23 (1968).

33. D. L. Moores and H. Nussbaumer, J. Phys. B 3, 161 (1970).

34. K. T. Dolder, M. F. A. Harrison, and P. C. Thonemann, Proc. Roy. Soc. (London) A-264, 367 (1961).

35. J. B. Wareing and K. T. Dolder, Proc. Phys. Soc. (London) 91, 887 (1967).

36. A. Burgess and I. C. Percival, Adv. At. Mol. Phys. 4, 109 (1968).

37. L. Vriens, Case Studies in Atomic Collision Physics, Vol. I, edited by E. W. McDaniel and M. R. C. McDowell (North Holland Pub. Co., Amsterdam, 1969), Chapter 6.

BIBLIOGRAPHY (Concluded)

38. M. J. Seaton, Atomic and Molecular Processes, edited by D. R. Bates (Academic Press Inc., New York, 1962), Chapter 11.

39. J. J. Thomson, Phil. Mag. 23, 449 (1912).

40. M. Gryzinski, Phys. Rev. 115, 374 (1959).

41. M. Gryzinski, Phys. Rev. 138, A305 (1965).

42. M. Gryzinski, Phys. Rev. 138, A322 (1965).

43. R. H. McFarland, Phys. Rev. 159, 20 (1967).

44. H. Funk, Ann. Physik 4, 149 (1930).

45. G. H. Dunn, Atomic Physics, edited by B. Bederson, V. W. Cohen, and F. M. J. Pichanick (Plenum Press, New York, 1969), pp. 417-433.

46. W. C. Lineberger, The Ionization of Lithium Ions by Electron Impact, Ph. D. thesis, Georgia Institute of Technology, Atlanta, Georgia, 1965; Phys. Rev. 141, 151 (1966).

47. M. F. A. Harrison, Brit. J. Appl. Phys. 17, 371 (1966).

48. K. T. Dolder, Case Studies in Atomic Collision Physics, Vol. I, edited by E. W. McDaniel and M. R. C. McDowell (North Holland Pub. Co., Amsterdam, 1969), Chapter 5.

49. J. W. Hooper, W. C. Lineberger, and F. M. Bacon, Phys. Rev. 141, 165 (1966).

50. G. H. Dunn and B. Van Zyl, Phys. Rev. 154, 40 (1967).

51. F. M. Bacon, The Excitation of Barium Ions by Electron Impact Ph. D. thesis, Georgia Institute of Technology, Atlanta, Georgia, 1968; Phys. Rev. 178, 182 (1969).

52. G. D. Yarnold and H. C. Bolton, J. Sci. Instr. 26, 38 (1949).

53. G. A. Harrower, Rev. Sci. Instr. 26, 850 (1955).

54. R. S. Burington and D. C. May, Jr., Handbook of Probability and Statistics with Tables, Second Edition (McGraw-Hill Book Co., New York, 1970), pp. 241-245.

55. S. Chandrasekhar, Astrophys. J. 93, 285 (1941).

56. S. Chandrasekhar and R. E. Williamson, Astrophys. J. 93, 308 (1941).

VITA

Robert King Feeney was born in Albany, Georgia on 6 July 1938. He is the son of Mr. and Mrs. E. W. Feeney, Jr.

Mr. Feeney attended public schools in Miami, Florida, where he was graduated from Miami Edison High School in 1956. He received the degree of Bachelor of Electrical Engineering (Co-operative Plan) from the Georgia Institute of Technology in 1961. Mr. Feeney then worked for the Convair Division of General Dynamics Corporation in San Diego, California for a short time before entering the U. S. Army. He served for two years as a platoon leader in the 123rd Maintenance Battalion, 1st Armored Division, Fort Hood, Texas.

In 1963, he began graduate study in electrical engineering at the Georgia Institute of Technology and was employed as a graduate research and teaching assistant. Mr. Feeney received the degree of Master of Science in Electrical Engineering from the Georgia Institute of Technology in the summer of 1964.

Mr. Feeney is a member of Eta Kappa Nu, Sigma Xi, the Institute of Electrical and Electronic Engineers and the American Physical Society.